

Wind farm control strategies for structural load management and energy efficiency

Gonzalez Silva, J.

DOI

[10.4233/uuid:6dccdf8a-2ef7-4105-b6bb-85938eaf3c1e](https://doi.org/10.4233/uuid:6dccdf8a-2ef7-4105-b6bb-85938eaf3c1e)

Publication date

2025

Document Version

Final published version

Citation (APA)

Gonzalez Silva, J. (2025). *Wind farm control strategies for structural load management and energy efficiency*. [Dissertation (TU Delft), Delft University of Technology]. <https://doi.org/10.4233/uuid:6dccdf8a-2ef7-4105-b6bb-85938eaf3c1e>

Important note

To cite this publication, please use the final published version (if applicable). Please check the document version above.

Copyright

Other than for strictly personal use, it is not permitted to download, forward or distribute the text or part of it, without the consent of the author(s) and/or copyright holder(s), unless the work is under an open content license such as Creative Commons.

Takedown policy

Please contact us and provide details if you believe this document breaches copyrights. We will remove access to the work immediately and investigate your claim.

WIND FARM CONTROL STRATEGIES

**FOR STRUCTURAL LOAD MANAGEMENT
AND ENERGY EFFICIENCY**

WIND FARM CONTROL STRATEGIES

FOR STRUCTURAL LOAD MANAGEMENT
AND ENERGY EFFICIENCY

Dissertation

for the purpose of obtaining the degree of doctor
at Delft University of Technology
by the authority of the Rector Magnificus prof. dr. ir. T.H.J.J. van der Hagen,
chair of the Board of Doctorates,
to be defended publicly on Monday 17 March 2025 at 5:30 pm

by

Jean GONZALEZ SILVA

Master of Science in Mechatronic Systems
Universidade de Brasília, Brazil,
born in Macaé, Brazil.

This dissertation has been approved by the promotor.

Composition of the doctoral committee:

Rector Magnificus,	chairperson
Dr. ing. R. Ferrari,	Delft University of Technology, promotor
Prof. dr. ir. J.W. van Wingerden,	Delft University of Technology, promotor

Independent members:

Prof. dr. ir. Tamas Keviczky,	Delft University of Technology
Dr. ir. José Rueda Torres,	Delft University of Technology
Dr. Nikolay Dimitrov,	Technical University of Denmark
Prof. dr. Simon Watson,	Delft University of Technology
Dr. Paula Chanfreut,	Technical University of Eindhoven



Keywords: active power control, thrust balance, load-limiting control, wake effects, reliability, energy security, wind tunnel, distributed control

Printed by: Gildeprint

Cover by: J. Gonzalez Silva

Funding: The work presented in this thesis was supported by the European Commission through the WATEREYE project, Grand No. 851207.

Copyright © 2025 by J. Gonzalez Silva

ISBN 978-94-6496-351-9

An electronic version of this dissertation is available at
<http://repository.tudelft.nl/>.

To Jayne, my beloved wife.

CONTENTS

Summary	xi
Samenvatting	xiii
Acknowledgements	xv
1 Introduction	1
1.1 Motivation	2
1.2 Background and state-of-the-art	5
1.2.1 Wind turbine control	5
1.2.2 Wind farm control	7
1.2.3 Wind farm modelling	10
1.3 Research gap	12
1.4 The goals and contributions of this thesis	12
1.5 Thesis organization	16
2 Wind farm control for compensating power losses, thrust balancing, and load-limiting	19
2.1 Introduction	20
2.2 Control strategies	22
2.2.1 Power tracking control	22
2.2.2 Wind farm control for compensating power losses	24
2.2.3 Wind farm control for thrust force balancing	25
2.2.4 Wind turbine control for load-limiting	27
2.3 Simulation example	28
2.3.1 Simulation setup	28
2.4 Results	30
2.4.1 Statistical calculations	31
2.4.2 Mechanical calculations	33
2.4.3 Simulation results	34
2.4.4 Quantitative results and discussions	37
2.5 Conclusions	39
3 Load limiting wind turbine control	43
3.1 A switching thrust tracking controller	44
3.1.1 Introduction	44
3.1.2 Control architecture	46
3.1.3 Simulation	50
3.1.4 Conclusions and discussion	52

3.2	Convex model predictive control	55
3.2.1	Introduction	55
3.2.2	Control architecture	56
3.2.3	The degree of freedom on kinetic energy	59
3.2.4	Flow stability.	60
3.2.5	The use of kinetic energy	61
3.2.6	Convex model predictive control formulation	61
3.2.7	Simulation	63
3.2.8	Conclusions and discussion.	65
4	Distributed wind farm control	67
4.1	Introduction	68
4.1.1	A centralized approach and its reliance on wake modeling	68
4.1.2	The shift from centralized to distributed controllers	69
4.1.3	Our contributions.	70
4.1.4	Outline of the remainder of the chapter	71
4.2	Problem formulation	71
4.2.1	Wind farm model.	71
4.2.2	Wind farm control	73
4.3	Multi-rate consensus-based distributed control.	75
4.3.1	Graph notation and wind farm communication network	75
4.3.2	Average consensus between WF control samplings	76
4.3.3	Distributed power compensation	78
4.3.4	Power distribution	80
4.3.5	Thrust force balance control	81
4.3.6	Stability of the proposed control scheme	83
4.4	Results and discussion	90
4.5	Conclusion.	94
5	Wind tunnel testing of wind farm controllers	95
5.1	Introduction	96
5.2	Experimental setup	98
5.3	Adopted strategies	99
5.3.1	Derating control strategies	99
5.3.2	Wind farm control strategies	104
5.4	Experimental results	107
5.4.1	Derating control performance.	107
5.4.2	Thrust force balance	111
5.4.3	Wind farm control performance.	112
5.5	Discussion and conclusion	115
6	Conclusions and recommendations	119
6.1	Conclusions	120
6.2	Limitations.	122
6.3	Recommendations	123
6.4	Society impact	124

Curriculum Vitæ	141
List of publications	143

SUMMARY

WIND turbines have been deployed worldwide to address the growing energy demand while also targeting ambitious plans for the energy transition to renewable sources. Although wind energy is a key renewable energy source, it still faces unsolved challenges and offers ample room for innovation. One major concern is its variability, with the maximum power available fluctuating over time. Importantly, wakes from upstream turbines also contribute to reducing the power availability for downstream turbines. These wake effects are magnified by the construction of large wind farms with densely spaced wind turbines, aiming to efficiently use the allocated space.

Wind farm control strategies can be implemented to mitigate these wake effects and optimize wind farm power generation. In scenarios requiring *on-demand* response, such as those explored in this thesis, wind turbines are leveraged to provide flexibility, constrained by their maximum power availability. The power delivery of wind power plants upon request is facilitated by a closed-loop wind farm controller, providing active power control at fast timescales. Active power control involves adjusting the resource's active power to assist power grid operators in balancing energy supply and demand, thereby improving energy security. Our proposed closed-loop control solution provides superior response capabilities by compensating for reduced power availability, ultimately enhancing the reliability of on-demand power generation.

The wind variability across turbines, intensified by wake effects, contributes not only to attaining fluctuations in power generation but also to fluctuations in structural loads on the turbines. Amplified by wake-induced turbulence, this structural load variability across turbines leads to uneven degradation of turbine components over the long term. In offshore scenarios, where accessibility is limited and maintenance operations must be minimized due to higher costs compared to onshore counterparts, controlling turbines to prolong their lifetime is of significant interest. In this thesis, this aspect is addressed at both the wind farm and wind turbine levels.

At the farm level, we propose that farms fulfilling grid energy demands must also balance the aerodynamic forces of their turbines to evenly distribute structural degradation among them. This can be achieved without compromising the power generation when the turbines operate below their maximum energy extraction capacity. We have demonstrated that by implementing a real-time feedback loop, it is feasible to balance aerodynamic loads while meeting wind farm energy demands, albeit limited by wind availability. Moreover, we have demonstrated that balancing aerodynamic forces is advantageous for active power control in a wind farm affected by wake effects, compared to simply distributing power requests uniformly.

At the wind turbine level, we introduced two wind turbine controllers designed to individually restrict real-time aerodynamic loads as a surrogate of structural loads in turbine components. These controllers are referred to as load-limiting controllers. The first load-limiting controller employs an optimal control approach. The operator can impose struc-

tural load constraints, using a convex model predictive control for power tracking. The second controller, which is more practical, utilizes a switching mechanism with integral control that allows the operator to prioritize a structural load setpoint over a power demand setpoint. This prioritization aims to reinforce structural safety in situations where turbines are compromised from their design conditions. This could be a consequence of numerous factors, such as unpredictable degradation, installation issues, vessel collisions, and others.

As wind turbines prove to be a viable, reliable, and eco-friendly energy source, new wind farm projects are becoming more ambitious, incorporating a larger number of turbines than ever before. Additionally, there is a substantial growth in wind turbine installations within existing wind farms. This growth in the number of turbines poses an implementation challenge for wind farm control systems. Similar challenges have been encountered in controlling other large-scale systems with collective goals, where agents must instead make decisions based on partial information due to communication limitations in processing or transmission.

Anticipating this implementation challenge, we transition from a centralized to a distributed wind farm control solution. Taking advantage of the time scale inherent in typical wind farm controller implementations, we exchange information with neighboring turbines rather than a central workstation. Our aim, in particular, is not to gather partial information but to achieve consensus across the entire farm. However, our control methodology has a negative implication - the addition of delays - which is carefully examined by the derived stability condition for the design and is assessed through simulations. Notwithstanding these delays, the proposed solution is fully distributed and has been demonstrated to be both simple and effective, facilitating the application of our control solutions in large-scale wind farms.

Lastly, we validate our wind farm control solutions through experiments conducted with scaled wind turbines in full-wake conditions. In this way, we verify the benefits of our control solutions not only through high-fidelity simulations but also through real-world experimentation.

The work presented in this thesis emphasizes the importance of wind turbine controllers capable of offering demanded power to the grid while enhancing reliability in power delivery and addressing structural and maintenance concerns. We introduce closed-loop wind farm controllers designed to handle these challenges. Furthermore, we expand the implementation through a distributed approach on one front, while on the other front, we validate the solutions by means of experiments. The findings from this research contribute to the efficient operation of future wind farms by employing feedback control strategies across clusters of wind turbines.

SAMENVATTING

WINDTURBINES worden wereldwijd ingezet om aan de groeiende energievraag te voldoen en tegelijkertijd ambitieuze plannen te realiseren voor de overgang naar hernieuwbare energie. Hoewel windenergie een belangrijke hernieuwbare energiebron is kampt het nog steeds met onopgeloste uitdagingen en biedt het voldoende ruimte voor innovatie. Een belangrijke zorg is de variabiliteit ervan, waarbij de maximale beschikbare energie in de loop van de tijd fluctueert. Belangrijk is ook dat het zog van stroomopwaartse turbines bijdragen aan het verminderen van de beschikbare energie voor stroomafwaartse turbines. Dit zogeffect wordt versterkt door de bouw van grote windparken met dicht op elkaar geplaatste windturbines, met als doel om de toegewezen ruimte efficiënt te gebruiken.

Windparkbesturingsstrategieën kunnen worden geïmplementeerd om deze zogeffecten te verminderen en de stroomopwekking van windparken te optimaliseren. In scenario's waarbij een on-demand respons nodig is, zoals in de scenario's die worden onderzocht in deze scriptie, worden windturbines geüpdatet om over flexibiliteit te beschikken te leveren dat beperkt wordt door het maximaal beschikbare windvermogen. De opvraagbare stroomlevering van windturbineparken wordt gefaciliteerd door een gesloten-lus-windparkbesturing, die actieve vermogensregeling biedt op snelle tijdschalen. Actieve vermogensregeling omvat het aanpassen van het actieve vermogen van de energiebron om netbeheerders te helpen leveringszekerheid te borgen middels het balanceren van vraag en aanbod. Onze voorgestelde gesloten-lus regeling biedt superieure responsmogelijkheden door het compenseren van verminderde energiebeschikbaarheid, en verbetert daarmee de betrouwbaarheid van de opvraagbare stroomvoorziening.

De variabiliteit van wind, versterkt door zogeffecten, draagt niet alleen bij aan fluctuaties in de stroomopwekking, maar ook aan structurele belastingen op de turbines. Deze structurele belastingsvariabiliteit over turbines leidt op de lange termijn tot ongelijke degradatie van turbineonderdelen. In offshore scenario's, waar de toegankelijkheid beperkt is en onderhoudsactiviteiten moeten worden geminimaliseerd vanwege hogere kosten in vergelijking met onshore tegenhangers, is het regelen van turbines om hun levensduur te verlengen van groot belang. In deze scriptie wordt dit aspect behandeld op zowel windpark- als windturbine-niveau.

Op het niveau van het windpark stellen we voor dat windparken die voldoen aan de vraag naar netstroom ook de aerodynamische krachten van hun turbines moeten balanceren om de structurele degradatie gelijkmatig te verdelen. Dit kan worden bereikt zonder de stroomopwekking in gevaar te brengen indien de turbines minder dan het maximaal beschikbare vermogen leveren. We hebben aangetoond dat het middels een real-time feedback-lus mogelijk is om aerodynamische belastingen in balans te brengen terwijl aan de vraag naar windparkstroom wordt voldaan, mits er voldoende wind is. Voorts hebben we aangetoond dat het balanceren van aerodynamische krachten voordelig is voor de actieve vermogensregeling in een windpark dat wordt beïnvloed door zogeffecten, vergeleken met het gelijkmatig verdelen van het opgevraagde vermogen.

Op het niveau van de windturbine hebben we twee windturbinebesturingsregelaars ontworpen die real-time aerodynamische belastingen individueel beperken als vervanging voor structurele belastingen van turbineonderdelen. Deze regelaars worden belasting-limiterende regelaars genoemd. De eerste belasting-limiterende regelaar maakt gebruik van een optimaal regelalgoritme. De beheerder kan structurele belastingsbeperkingen opleggen met behulp van een convex modelvoorspellende regelmethode voor vermogensopvolging. De tweede controller, die praktischer is, maakt gebruik van een schakelmechanisme met integrator-regeling dat de beheerder in staat stelt een structurele belastings-setpoint boven een vermogens-setpoint te prioriteren. Deze prioritering is bedoeld om de structurele veiligheid te verbeteren in situaties waarin turbines worden beïnvloed door externe factoren zoals onvoorspelbare degradatie, installatieproblemen, aanvaringen door vaartuigen, enzovoort.

Omdat windturbines een rendabele, betrouwbare en milieuvriendelijke energiebron blijven te zijn, worden nieuwe windparkprojecten steeds ambitieuzer, met een groter aantal turbines dan ooit tevoren. Bovendien is er een aanzienlijke groei in het aantal windturbine-installaties binnen bestaande windparken. Deze groei in het aantal turbines vormt een implementatie-uitdaging voor windparkbesturingssystemen. Vergelijkbare uitdagingen zijn geconstateerd bij de besturing van andere grootschalige systemen met collectieve doelstellingen, waarbij individuele actoren beslissingen moeten nemen op basis van een onvolledige informatievoorziening ten gevolge van communicatiebeperkingen in verwerking of transmissie.

Anticiperende op deze implementatie-uitdagingen maken we de overgang van een centrale naar een gedistribueerde windparkbesturingsoplossing. Door gebruik te maken van de tijdschaal die inherent is aan typische windparkbesturingsimplementaties, wisselen we informatie uit met naburige turbines in plaats van een centraal werkstation. Ons doel is nadrukkelijk niet om onvolledige informatie te verzamelen, maar om consensus te bereiken onder alle windturbines in het windpark. Onze besturingsmethodologie heeft echter een negatieve implicatie - de toevoeging van vertragingen - die zorgvuldig wordt onderzocht door de afgeleide stabiliteitsvoorwaarde voor het ontwerp en wordt beoordeeld aan de hand van simulaties. Ondanks deze vertragingen is de voorgestelde oplossing volledig gedistribueerd en tonen wij aan dat deze zowel eenvoudig als effectief is, hetgeen de toepassing van onze besturingsoplossingen in grootschalige windparken vergemakkelijkt.

Ten slotte valideren we onze windparkbesturingsoplossingen door middel van experimenten uitgevoerd met geschaalde windturbines in volle-zog-omstandigheden. Op deze manier verifiëren we de voordelen van onze besturingsoplossingen niet alleen via hoogwaardige simulaties, maar ook via experimenten in de echte wereld.

Het werk in deze scriptie benadrukt het belang van windturbinebesturingsregelaars die in staat zijn om de gevraagde energie aan het net te leveren terwijl ze de betrouwbaarheid van energielevering waarborgen en structurele en onderhoudsproblemen adresseren. We introduceren gesloten-lus windturbinebesturingsregelaars die zijn ontworpen om deze uitdagingen aan te gaan. Daarnaast breiden we de implementatie uit met een gedistribueerde aanpak en valideren we de oplossingen middels experimenten. De bevindingen uit dit onderzoek dragen bij aan de efficiënte werking van toekomstige windparken door gebruik te maken van gesloten-lus regelstrategieën voor groepen van meerdere windturbines.

ACKNOWLEDGEMENTS

RESEARCH is akin to an enthusiastic voyage into the realms of the unknown. Doctoral researchers embark on solo journeys to explore uncharted fields. An insatiable thirst for knowledge and unwavering perseverance have always been requisite qualities to pursue a doctoral degree. These characteristics are essential when doing half of your doctorate during the pandemic, working mostly from home. The talks in academic corridors were replaced by the silence of isolated home offices; the vibrant exchange of ideas gave way to the solitary sound of keystrokes against screens; and researchers were challenged to rediscover the essence of autonomy in their scholarly pursuit. Then, the question arises: to what extent can an aspiring scientist progress without support from colleagues and predecessors? The Ph.D. journey revealed itself, not merely as a quest for knowledge, but as a demonstration of resilience in the face of adversity. These challenges are further pronounced when one is immersed in a foreign culture, encountering distinct languages and relationship behaviors.

First of all, I would like to acknowledge my wife Jayne, to whom I dedicate this work. She chose to be on my side by embracing the plan of moving abroad to a country halfway across the globe. She arrived in the Netherlands and endured a difficult period, even lonelier than my own. Nevertheless, she always supports me to persist and give my best in the pursuit of the doctorate. Although facing even greater obstacles in a tough job market for immigrants, she not only persevered but flourished, which makes me extremely proud.

Also, I would like to acknowledge my family, in particular, my mother, Sueli. She always encouraged me to study abroad and pursue my dreams. As my foremost model of determination, my mother skillfully balanced working as the primary provider for our home, advancing her own education, and raising both me and my sister. Talking about her, I also thank my sister, Eliana, for her support and encouragement, letting me to believe further in myself. Lastly, special thanks to my father Ademil who was consistently there for us, raising me with a sense of creativity and autonomy in problem-solving.

However, none of this would be possible without the trust given by my promoters, Riccardo Ferrari and Jan-Willem van Wingerden. I immensely thank you for all your support and guidance throughout my doctoral program. To Riccardo, thank you for being a fundamental player on this journey. Your ability to understand complex problems and make effective decisions was invaluable to me. Additionally, your attentiveness to even the minutest details doesn't go unnoticed and truly sets you apart. I appreciate your comprehensive approach as a leader and the immense dedication you show as a supervisor. I have learned a lot from your mentorship. To Jan-Willem, thank you for your decisive leadership. Your capability to manage a large team, your deep know-how in wind farm control, and your keen interest in new technologies and collaborations have been inspiring. To both of you, I owe a debt of gratitude for allowing me to delve into fascinating topics on control theory and beyond. I appreciate the opportunity to gain valuable experience with wind farm simulators and coding, which I have thoroughly enjoyed.

In my Ph.D. I had the opportunity to meet many colleagues and have a wonderful time

at TU Delft. Gabriel Albuquerque was one of the first people I met at TU Delft. More experienced in the house, he introduced me to the department and shared important hints as a new immigrant. Then, I met Zhixin Feng who shared the workload on the European project, working together extra hours to finish the project demands and deliverables on time. Further, I want to thank Twan Keizer who was very receptive and supportive from technical to daily life issues, such as from deep discussion contributing to this work to reflecting on the best Dutch beer. Starting my research in wind energy, Yichao Liu was the one always willing to discuss, humble, and enthusiastic about new ideas. However, Sebastiaan Mulders took the cake for enthusiasm, attentive but multiple times more excited to try out new controllers. My ideas would not become a reality without the work of Bart Doekemeijer on the complete wind farm simulation setting. Bart was very attentive, willing to share his work, and most importantly to help debug any small problem that might appear. Moreover, I would like to thank Daan van der Hoek for his collaboration, support, and patience in sharing how to operate the scale turbines in the experimental laboratory. Also, a special thanks go to Alex Galo. With a quick mindset, Alex was always up to discussions contributing a lot to this work, and as a friend brightened up the gray days. Another special thanks goes to Rogier Dinkla, who shared special moments at conferences and contributed greatly with the Dutch abstract.

Nevertheless, I would like to thank all the other colleagues I had the opportunity to meet in the Delft Center for System and Control (DCSC) department. Starting with the Fault Tolerant Control group, there were Tushar Desai, Atindriyo, Wolfram Martens, Yang Wang, Lucca Ballotta, Ivo van Straalen, and Bart Wolleswinkel. Then, in the Wind Energy group, there were David Domingos, Maarten van den Broek, Marcus Becker, Claudia Muscari, Livia Brandetti, Amr Hegazy, Bert Van den Abbeele, Mees van Vondelen, Jonas Gurtknecht, Joeri Frederik, Unai Santiago, Daniel Van Den Berg, Emanuel Taschner, Uwe Fechner, and Marion Coquelet. Additionally, I had the pleasure of meeting Cees, Giannis, Mathias, Barbara, Abhimanyu, Emilio, Tian, Lotfi, Frida, Coen, Clara, Sander, Roger, Jacques, Frederik, Max, Pedro, Maarten, Steven, Eva, Pascal, Giorgos, and Elias. I am deeply appreciative of all the enjoyable moments we shared.

I would like to thank all the DCSC Ph.D. candidates, professors, and secretaries for the great times in and outside the office. Special recognition goes to the secretaries and support staff - Erica, Heleen, Francy, Bo, Anna, Martha, and Sandra; that was always very attentive and did not forget the organization of Christmas dinners and Pub quizzes! I would like to acknowledge the technicians Wim, Will, and Ralph for the assistance that made the experiments in this work possible. Also, to the professors Dimitris, Manon, Kim, Bart, and Manuel for their short but meaningful discussions and insights in research and living as a foreign researcher. I am also indebted to all the great educators that I had the luck to participate in their classes, from online courses to physical ones.

To conclude, I am greatly indebted to the European society to have funded my research as a Ph.D., to the Brazilian society to have funded my education before that, and to TU Delft and the Dutch society to have received me so well.

*Jean Gonzalez Silva
Delft, April 2024*

1

INTRODUCTION

Large-scale wind energy production plays a crucial role in combating climate change. The concept of extracting energy out of wind has been adopted by many in the past for several purposes but has never achieved the maturity and scale of today. Nowadays, wind energy technology has evolved to megawatts-producing wind turbines situated in demanding locations, such as offshore sites. However, the control of wind turbines is a challenging task due to the non-linear nature of wind flow around structures and the complexities of flow stability. Additionally, the proximity of turbines in a wind power plant introduces dynamic interactions affecting overall power production and structural integrity.

Currently, the main attention is on maximizing energy extraction by exploring techniques such as wake steering and wake mixing. However, as wind has become the predominant source of energy, a shift in the control paradigm to active power regulation is expected. Controlling wind turbines to produce on-demand power requires taking turbine interactions into account and addressing concerns about turbine degradation and possible failures, as highlighted in the citations below.

"A future wind power plant will need to comply to stricter grid code requirements and providing ancillary services to ensure safe and reliable operation of the power system."

Eguinoa et al. [1]

"The existence of wakes further complicates the process of understanding both the overall plant performance and the loads experienced by the turbines."

Paul Veers et al. [2]

This thesis delves into these concerns and challenges. We develop novel wind farm control algorithms and we validate them through high-fidelity simulators and experiments. The goal of this chapter is to relate these contributions to state-of-the-art control and align them with the long-term perspectives in the wind energy community.

1.1. MOTIVATION

ENSURING energy security is essential for developing a sustainable society. In renewable energy, a key challenge lies in ensuring reliable energy generation, primarily due to their inherent volatility, particularly in solar and wind power. Committing to energy security fortifies our resilience against diverse challenges, from energy availability fluctuations to geopolitical tensions, withstanding equipment failures and natural disasters. This dedication promotes grid stability and fosters economic prosperity. Embracing energy security sets the stage for a future where reliance on renewable energy sources (RES) can increase, mitigating environmental impacts, and cultivating resilience against uncertainties.

In recent years, the rapid development of wind energy has been driven by concerns over global warming and the exhaustion of fossil fuels. Pushed by ambitious climate targets, for instance, the 1.5°C pathway [3] and the net zero commitment by 2050 [4], the new installations of wind power plants in 2020 and 2021 accounted for an impressive 23% of all installations made before 2021 [5]. In 2022, the total global wind power capacity was up to 906 GW, helping the world avoid over 1.2 billion tonnes of CO₂ annually [6] - equivalent to the annual carbon emissions of South America. Furthermore, the growth of wind energy is associated with political and economic advantages, for instance, empowered by the achievement of self-sufficiency in energy generation.

Wind energy has transitioned from being an innovative alternative to a well-established and viable solution for energy generation. The viability of wind energy has seen a remarkable surge, attributed to the significant 69% reduction in the levelized cost of elec-

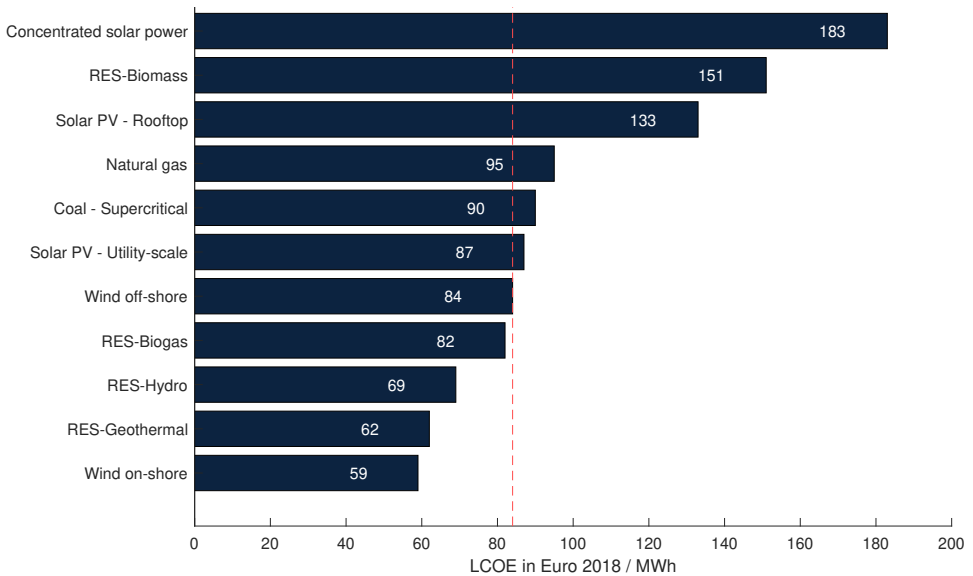


Figure 1.1: Levelized cost of energy by source in Europe in 2018 [7].

tricity (LCOE)¹ from 2010 to 2022 [8]. This cost reduction is a result of advancements in manufacturing, installation, and support services within the wind energy sector. While wind energy has become increasingly competitive, without subsidies, with traditional sources of energy [9], there is still a lot of potential for further reducing the LCOE [10]. For example, Figure 1.1 illustrates that offshore wind already presents lower costs compared to non-renewable sources, like coal and natural gas. Still, offshore wind costs are higher than those of other renewable sources, such as biogas, hydro, and geothermal.

According to a more recent IRENA report [11], in 2022, onshore wind achieved an LCOE of 33 USD/MWh, while solar photovoltaics (PV) significantly reduced its LCOE to an impressive 49 USD/MWh, outshining offshore wind at 81 USD/MWh. However, offshore wind remains with great potential to be competitive through ongoing reductions in manufacturing, installation and operational costs.

Increasing the density of turbines in wind power plants reduces the required area and cuts down on equipment and maintenance costs. However, a downside of placing wind turbines near each other is that the aerodynamic interaction between turbines may have a critical effect on the total electrical power generation and the structural loads experienced by the turbines [12]. As a wind turbine extracts energy from the wind, it reduces the downstream wind velocity and adds turbulence to the flow. The altered flow is called the wake of a wind turbine (cf. in Figure 1.2). This adverse effect can be alleviated by strategically placing turbines based on the prevailing wind direction, i.e. through the wind farm layout design, and/or by employing wind farm control techniques. In this thesis, we concentrated on the latter approach.



Figure 1.2: A photograph of an offshore wind farm in Denmark in foggy conditions, which clearly shows the wakes behind the turbines. The downstream rows of turbines experience lower wind speeds and higher turbulence intensities as a result of the operation of the upstream turbines. Source: Bel Air Aviation Denmark.

¹The LCOE is a crucial metric that indicates the average net present cost of electricity over the operation lifetime of a generator.

The concept of wind farm control, which has been extensively studied [13, 14, 15], aims to optimize overall performance of wind power plants by addressing wake effects and maximizing energy generation. With the increasing penetration of wind energy into the electricity grid, wind farms are transitioning their focus from maximizing energy generation to regulating their operation to meet grid demands. Wind turbine controllers originally designed for maximum power extraction must also offer flexibility. This is enforced by new grid codes, such as those implemented in Ireland [16] and England [17]. Flexibility in energy generation allows for adjusting the electrical production of a plant. This adjustment in wind farms can be performed in response to factors such as a price signal, grid frequency, or an activation signal from the grid operator.

As we transition to on-demand energy generation, wake effects also present a critical challenge for wind farm controllers [12, 18]. The interaction between each turbine's ability to generate on-demand power and the wind flow varies with different derating control strategies. These strategies determine how generator torque and blade pitching angles combine to influence aerodynamic forces [19, 20], resulting in different wake characteristics. From the perspective of wind farms, the flexibility in each turbine offers various options for distributing power references across the farm while maintaining overall power output. Effectively managing this distribution, while considering turbine wake interactions, enhances the reliability of power delivery. Furthermore, incorporating turbine structural loads into this power distribution can prolong operational lifespan, a topic explored further in this dissertation.

Lately, offshore sites have been successfully explored by several countries, with France and Italy each commissioning their first commercial offshore wind projects in 2022. Although the offshore sites have advantages compared to onshore in terms of steadier and stronger wind speeds, the complex and dynamic marine environment has brought great challenges to the transportation, installation, and operation of equipment [21]. Notably, the operation and maintenance costs, influenced by the difficult accessibility and environmental conditions, can constitute as much as 30% of the LCOE [22]. The occurrence of faults is intensified by the harsh environmental conditions and the maintenance access is restricted to the crew and boat availability. Therefore, the offshore wind power plant should operate with measures in place to ensure resilience and handle potential faults.

Both industry experts and researchers acknowledge the importance of enhancing the operational reliability of wind farms [2]. Reliability, defined as the ability to sustain energy generation over time, is based on four key pillars: availability; quality over time; durability; and dependability. In the context of wind energy, depicted in Figure 1.3, these pillars translate to the following: the availability of wind resources, quality of wind energy generation and services, longevity of turbine functionality, and reliance on alternative energy sources to meet the grid demands. Essentially, wind farm control plays a crucial

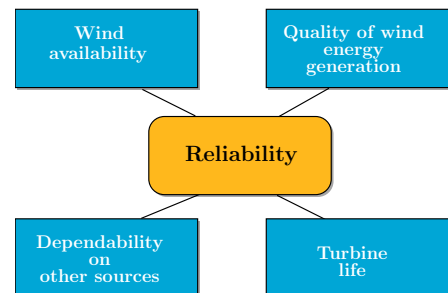


Figure 1.3: Four pillars of wind energy reliability.

role in influencing all four aspects of the reliable operation of wind turbines.

Collaborators from both industry and academia, participating in the European research program WATEREYE [23], have dedicated their efforts to developing smart solutions aimed at diminishing operation & maintenance expenses for offshore applications. The focus lies in empowering wind farm operators with the capability to accurately forecast the necessity for future maintenance through sensing & monitoring systems [24]. Our contribution directs attention to developing wind farm control algorithms that consider structural loading in the turbine operation, drawing from collaborative work efforts in the WATEREYE project.

This thesis centers on enhancing energy security by developing wind farm control strategies that fortifies the reliability of wind energy. Our goal is to promote flexibility in wind energy by regulating the power output of wind farms with designated set points, establishing a harmonious equilibrium between electricity generation and grid demand. However, wakes reduce wind availability for downstream turbines and potentially saturate their power generation. We investigate a compensation control framework designed to boost power generation by using real-time feedback to address these wake effects. Additionally, our efforts extend to improving structural safety by factoring in the operational structural loads and health status of turbines. We advocate for wind farms to operate by distributing structural loads, therefore contributing to the longevity of wind turbines. Furthermore, we propose the adoption of wind turbine controllers that limit structural loads to guarantee safety in specific turbines. As a culmination of our research, we have broadened the application of wind farm control approaches to a distributed framework and substantiated their effectiveness through scaled experiments. In summary, our aim is to advance both short-term wind energy security through improved power tracking strategies and the long-term sustainability of wind power systems by addressing structural loads, thereby fostering economic benefits.

1.2. BACKGROUND AND STATE-OF-THE-ART

THE technology and science of control of wind turbines can be divided into two categories: wind turbine control and wind farm control. In this section, we start with a brief introduction to the state-of-the-art control of individual industrial wind turbines, then we extend it to power tracking control methodologies; followed by a short discussion on the wind farm control strategies from literature. Finally, we introduce the simulation tools used for the development and first validation of the strategies in this thesis.

1.2.1. WIND TURBINE CONTROL

To effectively explore wind farm control strategies, it is essential to first delve deeper into the specifics of wind turbines. The wind turbine technology has gradually matured over the past forty years. The predominant type of installed wind turbines is horizontal-axis wind turbines as illustrated in Figure 1.4. These turbines operate based on three key degrees of freedom available for actuation: the pitch angle of each blade, the generator torque, and the nacelle yaw angle. The methodology used to operate these turbines dictates the control strategy, which can be classified into two distinct methods: greedy control and power tracking control. Our discussion of these control strategies will provide a foundation for the exploration of the control strategies proposed in this thesis.

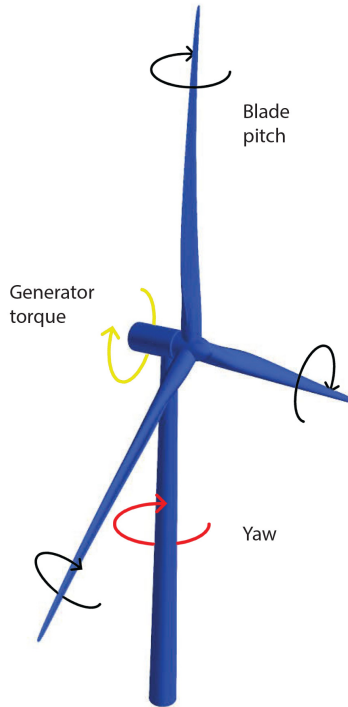


Figure 1.4: Degrees of freedom available for actuation: blade pitch, generator torque, and yaw.

Greedy control: At an individual wind turbine level, the intuitive approach to decrease the cost of wind energy is to maximize energy capture. The majority of industrial wind turbines utilize variable speed control technology, combined with the adjustment of the collective blade pitch angles [25]. This state-of-the-art wind turbine control, so-called greedy control, is divided into two operation conditions: above-rated wind speed and below-rated wind speed. At the above-rated conditions, the objective is to produce a fixed amount of power that aligns with the operational limits of the turbine. This is achieved by pitching the blades to keep the rotor speed constant at its rated value. The rated rotor speed and corresponding generator torque guarantee the safe operation of the electric generator and rotating components. At the below-rated conditions, the wind does not contain sufficient energy to fully exploit the capacity of the generator. Therefore, the turbine is set to extract the maximum energy quantity possible. This is achieved by keeping the blade pitch angles constant at the optimal angle, while the generator torque is designed to maximize its aerodynamic efficiency in power generation. Furthermore, the yaw actuator, controlled by a yaw controller, adjusts the orientation of the wind turbine's rotor plane perpendicular to the measured wind direction.

At a wind farm level, greedy control remains widely employed in industry, where individual turbines maximize their own power generation without accounting for wake effects. However, the drawback of greedy control is its non-cooperative nature, which leads to a

substantial disparity in power generation and aerodynamic loads. As a consequence of the wakes generated by the turbines, those situated in the front rows generate a greater amount of power and may endure the highest mean structural loads, resulting in a difference in life-time across turbines and increased likelihood of faults and failures. In contrast to greedy control, power tracking controllers show promise in fulfilling energy needs while also reducing aerodynamic loads.

Power tracking control: Power tracking control is an important feature for wind turbines that allows flexibility in energy generation, thereby generating energy on demand and offering support to the stability of the power grid. This control method involves adjusting the generator torque and blade pitch angles of a wind turbine to regulate its power output. In this work, as typically, we exclude yawing for power tracking purposes. With two control inputs to achieve a power output set-point, there is a degree of freedom. Therefore, several strategies can be adopted, for instance, the power tracking strategies with constant rotor speed, constant tip-speed ratio, or minimum thrust coefficient [20, 26]. Each strategy has different moment of inertia associated with the rotational components, influencing the power tracking performance and structural loading. Additionally, each strategy produces a distinct flow stream due to the associated aerodynamic forces, influencing the energy density within the flow and captured by downstream turbines.

A limitation of power tracking controllers is that they are constrained by the available power in the wind. When the power demand exceeds this limit, turbine saturation is reached and the turbine operates in a greedy manner, producing less power than demand. Additionally, wakes reduce the available wind power, thereby lowering the upper limit in downstream turbines. By regulating the power output of individual turbines, it becomes possible to coordinate the operation of all turbines within the wind power plant while considering the wake effects. This coordination is provided by wind farm control strategies that properly distribute power references to optimize energy generation and ensure structural integrity.

1.2.2. WIND FARM CONTROL

Over the past decade, the industry and academy have shifted their focus from wind turbines to wind farms. The main challenge at the wind farm level is the formation of wind wakes, which are slower, more turbulent streams of air that emerge behind a turbine rotor during operation. These wakes often persist for several kilometers, causing efficiency losses on downstream turbines. To further promote the financial competitiveness of wind as a renewable energy source, these wake losses must be addressed. Most commonly, the wake effects are mitigated through wind farm control.

Wind farm control involves a set of operation strategies wherein the control settings of each turbine are coordinated considering the behavior of the other turbines within the farm and the energy requirements. Essentially, wind farm control is designed to operate turbines in a coordinated manner to achieve a common objective, which is to reduce the LCOE of the wind power plant.

At the beginning of wind energy, and often still today, reducing the LCOE entails maximizing energy output while minimizing the manufacturing, installation, operation & maintenance, and decommissioning costs. In this initial scenario, the share of energy generated by wind turbines is lower compared with fossil fuel-based energy production and other

alternatives in the electrical grid. Therefore, wind farms mostly operate by maximizing energy generation while the grid is regulated by non-renewable energy and other sources.

The main explored wind farm control methodologies include *wake steering*, *axial induction control*, and *wake mixing* [27]. These methodologies have demonstrated significant potential for enhancing energy generation and transitioned from academic concepts to industrial products. For instance, axial induction control has been explored with incremental gains reported in [28]. Extensive experimentation at a commercial wind farm with wake steering, achieved by yawing wind turbines, is detailed in [29], demonstrating increased power generation. Similarly, field experiments conducted in [30] have shown overall improvements in power generation through wake steering. Ultimately, wake mixing, also known as dynamic induction control, enhances wake recovery by dynamically adjusting the turbine blade pitch to create a changing boundary condition in the wake, thus increasing downstream energy capture. An example of this methodology is the *helix* approach [31]. Figure 1.5 depicts wake steering and wake mixing control strategies typically aimed at maximizing power output.

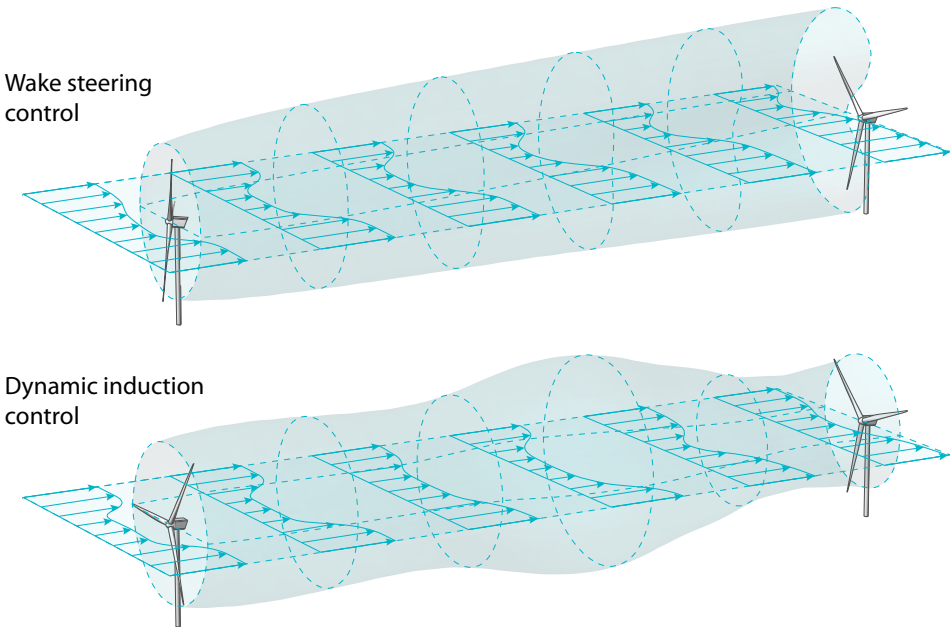


Figure 1.5: Wind farm control methodologies designed to maximize power. Source: van der Hoek [32].

However, this perspective of maximizing power generation is poised for a significant transformation as wind energy capacity surpasses that of non-renewable and other sources. Wind farms will therefore be required to aim at meeting the energy demand from the grid, which is the primary goal of the wind farm controllers in this dissertation. This transition is starting to be noticed through different indicators: derating features now being required by regulations in highly developed countries [16, 17], future trends of European regulations [33], and discussions among researchers about the integration of wind energy with the

electricity grid [2, 34, 35].

The ability to regulate the active power output of the turbines, for instance by providing secondary frequency regulation [36], has relevant economic implications for wind farm operation. Enhancing system frequency stability through the turbines eradicates support mechanisms utilized for frequency regulation [37]. Moreover, the greater wind energy flexibility the better the association with the current energy markets [1]. As a novel approach, *active power control* raises numerous questions from different perspectives as illustrated in Figure 1.6. In addition to the raised questions, the integration of power tracking controllers as a new feature in wind turbines presents novel technical challenges in operation that warrant additional research.

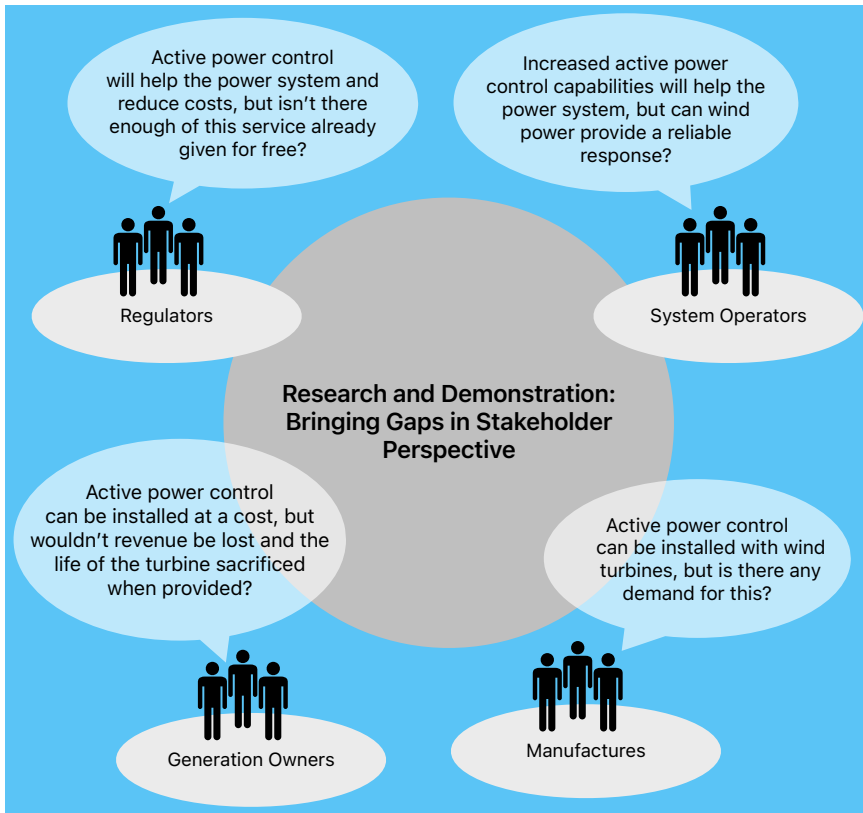


Figure 1.6: Perspectives of various stakeholders on active power control provided by wind farms. Adapted from Ela et al. [34]

Additionally, turbines are becoming increasingly slender and flexible due to the continuous growth in size and industry trends leaning towards material efficiency for cost-effectiveness. Given a target operational lifespan of approximately 20-30 years, it is essential to address the aerodynamic loads and structural degradation of turbines by wind turbine and farm controllers. Notably, wakes do not only impact available power but also affect aerodynamic loads by altering the flow structure.

Several studies have focused on mitigating structural loads, such as those discussed in [38, 39]. Enabling active power control and incorporating derating capabilities can significantly extend the lifetime of these turbines [40, 41], driven by the reduction of turbine loads [20]. Moreover, integrating structural load considerations into wind farm control systems further enhances the long-term performance of wind power parks.

Foreseeing the installation of large-scale wind farms, this thesis also addresses the scalability of wind farm control for practical implementation and applicability of wind farm controllers in such scenarios. As wind farms can be comprised of a substantial number of turbines, deploying centralized controllers might present challenges due to the increased complexity of the network, including network topology constraints and communication overhead. In contrast, distributed control approaches can excel in performance while considering restrictions in communication and control. Researchers have explored decentralized controllers for wind farms, as demonstrated in [42, 43, 44].

1.2.3. WIND FARM MODELLING

To understand how wind turbine interactions behave, engineering models are constructed to describe the important characteristics necessary for control. To that end, wind farm models vary in their correspondence to the effects of real-world scenarios. On one hand, low-fidelity models, e.g. FLOW Redirection and Induction in Steady State (FLORIS) [45], are based on parametric flow models that leverage engineering physical assumptions, resulting in a low computational cost. They are typically used for control synthesis and wind farm analysis, e.g. annual energy production predictions.

On the other hand, high-fidelity models have higher accuracy. These models simulate turbine behavior and detail the flow in wind farms by resolving the governing equations in three-dimensional space. The main limitation of such a detailed model, that includes the atmospheric boundary layer, is the substantial computation cost. Therefore, they are commonly used for offline applications. Exploring the viability of employing high-fidelity models in real-time applications is a recent subject of investigation, as exemplified by [46].

In this thesis, high-fidelity simulations, containing accurate physical models, are computed offline aiming at the validation of wind farm control concepts. Below, we will discuss about OpenFAST and SOWFA in more detail, as they are used in different parts of this thesis to evaluate the proposed wind farm control concepts.

OPENFAST

As a wind turbine engineering tool for simulating the coupled dynamic response of wind turbines, OpenFAST [47] is one of the most utilized simulation models in wind energy research. It couples aerodynamics models, hydrodynamics models for offshore structures, control and electrical system (servo) dynamics models, and structural (elastic) dynamics models. OpenFAST relies on these advanced engineering models that stem from fundamental laws, yet incorporate appropriate simplifications and assumptions. In the course of its development, OpenFAST was enhanced with computational solutions and tuned with empirical data.

FAST.Farm The extension of the capabilities of OpenFAST for multi-turbine wind farms is identified by the name of the Fatigue, Aerodynamics, Structures and Turbulent Farm

tool (FAST.Farm) [47]. FAST.Farm is a medium-fidelity multiphysics engineering tool that aims to balance the need for accurate modeling of the relevant physics while maintaining low computational costs. This tool uses a simplified (two-dimensional) version of the governing equations [48]. The Navier- Stokes (NS) equations are approximated using a thin shear layer approach, which is computationally less expensive than high-fidelity tools. FAST.Farm demonstrates great promise as a tool for designing wind farm controllers and simulating wind farm behavior [49]. Therefore, it was also explored during the development of this thesis, in which we have contributed to an implementation of a MATLAB/Simulink interface [50].

SOWFA

One of the most comprehensive wind plant models available is the Simulator for Wind Farm Application (SOWFA) [51]. As a computation fluid dynamic modeling (CFD) tool based on OpenFOAM [52], SOWFA is employed to model the atmospheric boundary layer interaction with wind turbines based on the principles of fluid mechanics. The modeling approach is a large eddy simulation (LES), an advanced numerical method that accounts for unsteady flow and incorporates turbulent effects in three-dimensional space. Realistic ambient atmospheric turbulence intensity, induced by varying inflow and atmospheric thermal stability conditions, is reproduced by using precursor simulations. The effects of Buoyancy forces due to variations in the flow density and Coriolis forces due to planetary rotation are included. Using information from OpenFAST models [47], the wind turbines can be modeled using either actuator disk models or actuator line models. Furthermore, mesh refinements can be imposed to enhance the representation of the flow interaction with the turbines. Having more detailed information on the flow interaction among wind turbines allows wind farm controllers to undergo initial validation before conducting experiments and extensive testing campaigns. A snapshot of the SOWFA output at a specific instant in time is illustrated in Figure 1.7.

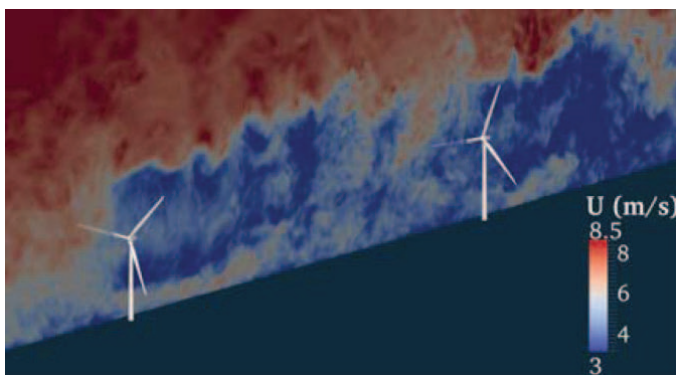


Figure 1.7: A vertical slice of the wind flow velocity field simulated in SOWFA. Source: Churchfield et al. [53]

1.3. RESEARCH GAP

AFTER considering the previous sections, we see that there are still relevant challenges for the integration of wind energy. The shift from maximizing to on-demand energy generation necessitates novel technologies in wind turbine and wind farm control. Previous works highlight the potential of wind farm control strategies to boost energy generation and mitigate low power availability caused by wake effects, thus enhancing energy safety. However, there are still gaps to address in achieving on-demand power generation. In particular, there are still uncertainties in choosing derating control strategies for wind turbines and the performance of wind farm control strategies in real-world environments.

Furthermore, structural loading is typically not considered by wind farm controllers. Wind turbines are certified by manufacturers using broad design load scenarios to ensure safe operation. However, the lifetime of turbines is tied to the structural loading they experience, which is heavily influenced by wake effects. This emphasizes the impact of wind farm control strategies accounting for wake effects in the durability of turbines. Previously considered as conflicting objective with power maximization, the management of structural loads benefits from the flexibility of on-demanded energy generation. Operating wind farms below their maximum capacity allows for distributing different power references across turbines, this freedom is used to distribute them in order to alleviate variations in structural loads. This approach to structural load management would prolong the life of turbines, thereby enhancing the reliability of wind power plants.

Moreover, technological advancements in digitalization and real-time monitoring of turbine structures enable the assessment of structural loads and health conditions. Integrating these assessments into wind turbine control helps manage turbine effectively and ensure safety. This approach enhances the durability and reliability of turbines, which is particularly critical in challenging settings such as remote offshore locations, where it can significantly reduce the risk of premature aging and unexpected shutdowns due to failures.

Finally, wind farm controllers typically rely on frameworks that are challenging to scale due to high computation costs and require full communication across turbines. These factors complicate the implementation of wind farm controllers, limiting their applicability. This thesis also explores distributed frameworks that offer solutions to these challenges. These advancements facilitates implementation and can further position wind energy as a cost-effective competitor to non-renewable energy sources and aid in the expansion of offshore wind energy.

1.4. THE GOALS AND CONTRIBUTIONS OF THIS THESIS

THE aim of this Ph.D. dissertation is to address the four key scientific gaps: evaluating the effectiveness of wind farm controllers for on-demand power generation, exploring the distribution of structural loads, integrating health status and structural loads with turbine operation, and scaling wind farm controllers. Our contribution is in the development and testing of wind farm controllers that prioritize active power regulation while addressing structural loading considerations. In short, the goal of this thesis is formalized as:

Thesis Objective

To design wind farm control strategies that can allow on-demand energy generation while taking into account structural loads.

More specifically, we aim to address the reliability challenges in wind energy arising from wake effects. This dissertation begins with the investigation of the following question:

Research Question 1

How can wind farm control enhance reliability in on-demand energy generation in the presence of wake effects?

Power tracking controllers enable direct regulation through the turbines, but the available power can be significantly reduced due to low incoming wind speeds and wake effects. In dense wind farms, which are increasingly common, turbine wakes notably affect overall power availability. Therefore, we have the following contribution:

C 1. We implement a closed-loop control architecture in high-fidelity simulations to counteract power losses. In our control architecture, turbines collaborate to compensate for power losses caused by low wind speeds, albeit limited by their own power availability. This architecture reduces offsets and oscillations associated to wake effects in the overall wind farm power output, integrating wind energy more efficiently into the grid.

This architecture ensures resilience in dealing with not only low wind speeds in parts of the farm but also promises to compensate for potential faults and failures. Once wind farms are configured to meet a total energy demand, there is a freedom in distributing individual power references across the turbines. This offers an opportunity for structural load management explored by the next research question.

Research Question 2

How can wind farm control balance structural loads across turbines, while not compromising power delivery?

Numerous researchers have studied the reduction of structural loads, recognizing it as a necessary trade-off with power generation at single wind turbines. In contrast, at a wind farm, balancing structural loads while tracking a wind farm power reference can be accomplished in a non-competitive manner. Our forthcoming contribution focuses on designing controllers to ensure this balance:

C 2. We developed a closed-loop thrust force balancing control to operate alongside with wind farm power tracking. This control reduces uneven wear of components across the farm, primarily influenced by the prevailing wind direction and their wakes, while ensuring the wind farm continues to meet grid requirements. To maintain the on-demand energy

generation without compromise, thrust force balancing must prioritize turbines with available power. This approach avoids competing with power delivery and inevitably allows variations in structural loads during periods of low wind availability.

While efforts are made to balance the structural loads, turbines can still exhibit a probability of developing system faults and display uneven degradation from other causes, such as environment conditions and deviations in manufacturing and installation. This prompts our third research question.

Research Question 3

Given the health condition of a wind turbine, how can wind turbine control be formulated to reduce structural loading?

Assuming the knowledge of the health status of a turbine, structural safety must be prioritized to avoid substantial costs related to failures. Turbine controllers can offer derating capabilities, but typically they do not related in real-time with the current structural loads. To reduce the stress on the component, the operation should be altered accordingly. An advanced controller would allow turbines to operate at reduced levels according to the current structural loads rather than resorting to complete shutdown, a conventional practice. Then, our next contributions are the followings:

C 3.a We developed a novel switching control algorithm aimed at lowering the aerodynamic loads in a closed-loop manner. This algorithm switches from tracking a power reference to tracking a thrust force reference as a surrogate for structural loading. This approach enables continuous production under safe operational conditions, thereby eliminating the necessity for a complete turbine shutdown.

C 3.b We explore the application of a convex Model Predictive Control (MPC) for power tracking, in which a constraint on aerodynamic loads can be integrated into its formulation. We assess different derating methods with the MPC formulation and their performance in relation to the kinetic energy associated with the rotating components during operation.

Limiting aerodynamic loads reduces the probability of mechanical failures and enhances safety levels. In specific scenarios, prioritizing safety over power generation is crucial to maintain long-term sustainability while waiting for maintenance events. From the wind farm perspective, any resulting power losses incurred due to reduced operation can be compensated by the neighboring turbines. Moreover, wind farms are expected to be installed considering overplanting², preparing for potential faults and periods of low wind availability.

Accounting for the considerable number of turbines in wind power plants, several challenges arise to apply wind farm controllers. These challenges include issues related to communication and computation, which often require a central point of communication

²Overplanting is the installation of a larger wind power capacity than stipulated.

through which all turbines are connected. Consequently, the fourth research question is posed.

Research Question 4

How can wind farm controllers be designed to suit large-scale wind farms?

To answer this research question, we explored distributed control approaches and adapted our wind farm control strategies. Distributed control offers modularity, reduces communication costs and eases computational demands. However, it may sacrifice performance due to incomplete farm-wide information. To reach performance similar to centralized controllers, we explored consensus theory to acquire full information with limited communication among neighboring turbines. Our contribution is a distributed control strategy described as follows:

C 4. We derived a distributed control strategy designed to achieve scalability in wind farm control while maintaining performance levels equivalent to centralized approaches. We leverage a multi-rate strategy and utilize consensus theory to collectively respond to information about the entire wind farm.

The proposed distributed controller facilitates the implementation of our previous wind farm control strategies and performs comparably to the centralized one. In this dissertation, we derived the stability conditions for its design and assessed its performance using high-fidelity simulations.

Finally, we tested our wind farm control strategies using scaled turbine models to bridge the gap between theoretical simulations and practical application. Laboratory experiments is a cost-effective alternative to direct validating using MW-scale turbines. Experimental results provide crucial insights that complement high-fidelity simulations and address the following research question:

Research Question 5

How do novel wind farm control concepts, specifically power compensation and thrust force balancing, perform when subjected to experimental validation?

The experimental findings confirmed the effectiveness and applicability of power compensation and thrust force balancing proposed in this research, yielding positive outcomes and contributing as follows:

C 5. The control architectures outlined in contributions **C 1.** and **C 2.** were implemented and validated in a scaled experimental setup, extending our results beyond the simulation environment. The results mirrored those observed in simulations, demonstrating positive outcomes and indicating potential benefits for wind farms using the proposed controllers.

1.5. THESIS ORGANIZATION

THE outline of the thesis and the connections between chapters, as depicted in Figure 1.8, serve to guide the reader through the content of this dissertation.

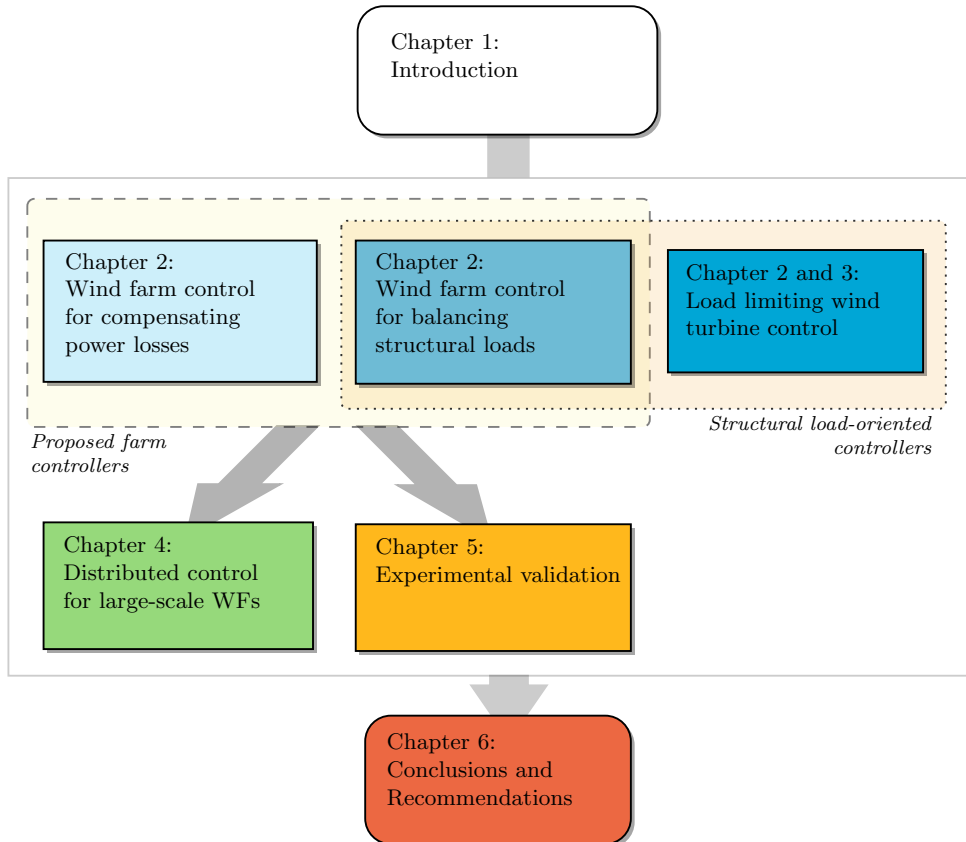


Figure 1.8: Visualization of the outline of this thesis.

Moreover, the subsequent bullet points comprise an introductory summary of each chapter.

- **Chapter 2:** Traditionally, wind farm control aims to distribute power set-points to individual turbines to maximize energy extraction and, thus, their usage as assets. Yet, grid balance and frequency support are fundamental in the presence of high renewable penetration and volatility of energy prices and demand. This requires a shift from power maximization to revenue maximization. Acknowledged by industry and researchers, a significant hurdle for wind farms lies in managing turbine wakes. In this chapter, three active power control strategies pushing this paradigm shift are investigated, namely: wake-loss compensation, thrust balancing, and load-limiting control. The findings of large eddy simulations of a reference wind farm show that wake-loss

compensation indeed improves the power generation on waked wind farms, but at the price of increased structural loads on certain turbines. The addition of a thrust balancing can equalize the stresses of individual turbines and their wear in the long term, while still attaining the required power output at the farm level. Furthermore, load-limiting controllers could potentially aid by allowing maintenance to be scheduled in a single time window, thus reducing operation and maintenance costs.

- **Chapter 3:** This chapter details the closed-loop switching control architecture aimed at reducing thrust force in individual turbines. By taking inspiration from developments in the field of reference governors, an existing demanded power tracking controller is extended by a thrust tracking controller. The activation of the thrust tracking controller occurs only when a user-defined constraint on fore-aft thrust force is exceeded, which can be set based on the actual damage status of the turbine. Additionally, a convex MPC is formulated to track a power demand while considering aerodynamic loads and flow instability. This latter control approach enables the incorporation of load constraints directly into its formulation. Unlike typical implementations of MPC for wind turbines, is oriented to power tracking, delving into the effects associated with the kinetic energy of the rotational components across different derating methods.
- **Chapter 4:** The implementation of a centralized control architecture in large-scale wind farms can raise numerous issues due to the large number of turbines and its required communication network. In this chapter, we derive a distributed control approach for active power tracking of wind farms, namely multi-rate consensus-based distributed control (MCDC). The MCDC is designed to ensure that tracking errors caused by turbine saturation are equally compensated *throughout the wind farm*, while only requiring local information exchanges between turbines. Furthermore, the proposed controller ensures that aerodynamic loading is balanced across the wind farm in a distributed manner. Finally, the overall power reference is distributed via a leader-follower consensus algorithm, resulting in a fully distributed approach. Our control approach facilitates the wind farm *modularity* and *sparsity*, which reduces the costs associated with control design and its applicability. We establish stability conditions of the underlying distributed algorithms. Finally, we demonstrate the effectiveness of the proposed MCDC through high-fidelity simulations by comparing it to the centralized approach, with WTs regulating their total active power output on demand in the presence of wakes, and at the same time ensuring that structural loads are evenly spread.
- **Chapter 5:** The results from wind tunnel experiments are presented aimed at evaluating the potential of different wind turbine and wind farm control strategies for active power regulation, therefore enhancing wind farm reliability and integration with the grid. The experiments are conducted in a wind tunnel at Delft University of Technology, using three servo-actuated and sensorized wind turbine scaled models. Two derating control strategies based on blade-pitch actuation are considered at the wind turbine level: constant tip speed ratio and optimal generator torque-based strategy. These derating control strategies are evaluated based on their ability to achieve the desired response, their undergoing aerodynamic loading, and the downstream power

availability. At the wind farm level, the wind farm control approaches are considered: thrust balance and power compensation. The impacts on wind farm power generation and aerodynamic loading are discussed, highlighting the achieved improvements.

The final chapter of this thesis labeled Chapter 6, presents concluding remarks regarding the main goal of this thesis, highlights our limitations, includes potential avenues for future work and discuss the societal impact of our research. A complete list of published articles, including those not featured in this dissertation, is provided at the end of this thesis.

2

WIND FARM CONTROL FOR COMPENSATING POWER LOSSES, THRUST BALANCING, AND LOAD-LIMITING

No individual can win a game by himself.

Pelé

*We must indeed all hang together, or,
most assuredly, we shall all hang separately.*

Benjamin Franklin

In this chapter, the main challenges related to the densification of wind farms are exposed: the low energy availability in the flow inside wind parks and variation in structural loading. Have you ever wondered how wind farm control could be utilized to face these challenges? Let's delve further to reveal the potential of wind farm control. Our proposed wind farm controllers utilize a combination of feedforward and feedback loops to compensate for disturbances and power losses. They also evenly distribute aerodynamic loads throughout the wind park and restrict structural loads to values that can be adjusted in real time by the operator. As a result, we enhance flexibility and reliability, key concerns in the realm of renewable energy.

This chapter has been published in Silva, Ferrari, and van Wingerden [54].

2.1. INTRODUCTION

According to the Global Wind Energy Council, 93.6 GW of new wind power was installed in 2021, which accounts for a 12.5% growth compared to 2020 [5]. Still, to meet the ambitious global plans for decarbonization, a growth of 180 GW per year would be required. The integration of wind power into the grid is becoming more relevant than ever as additional wind power capacity is commissioned each year across the globe. Future wind power plants will need to provide operational characteristics similar to those of conventional power plants, that comply with stricter grid code requirements and provide ancillary services to ensure safe and reliable operation of the power system [55, 56]. As an example for other countries, the United Kingdom has laid out its “Net-zero” plan for 2050, which aims to increase offshore wind energy from around 7 GW today to 75 GW by 2050. Note that the peak demand for the United Kingdom in 2020 was about 48.76 GW [57]. Such a substantial increase in the volume of wind energy connected to the grid will require that wind farms no longer operate in a “greedy” manner, whereby the wind farms aim at maximizing energy capture. Another drawback of the current concept of maximum power generation is the variance of aerodynamic loading across a dense farm due to the turbine interactions. Instead, it is likely that wind farms will be required to participate in a more meaningful manner in the grid balance, and consider the impact of their strategy on the structural loading of individual turbines.

Rapid penetration of renewable energy sources, with their inherently fluctuating power availability, is still challenging for electric power systems. This raises questions about how the systems would operate when renewable generation becomes the dominant technology. The wind availability further reduces with farm densification due to turbine interactions, leading to overplanting as a trivial solution. In *overplanting*, the wind farm is conservatively designed and is expected to operate in derated conditions [58, 34]. Balancing the wind farm production with the demanded grid loads can be provided by the so-called *Active Power Control* (APC), as demonstrated by Fleming et al. [12] in high-fidelity simulations. A centralized APC was introduced by an author [18], where a closed-loop controller is proposed to mitigate the oscillations of power generation caused by the wake effects, mainly the induced turbulence.

The ability to control the individual power output may lead to improvements in the provision of ancillary services [59, 60, 61]. The potential to regulate the active power, such as secondary frequency regulation, has relevant economic implications for wind farm operators [37]. As a result, turbines that directly participate in the system frequency stability significantly enhance their cost-effectiveness by eliminating support mechanisms and improving the integration grid system. In addition, turbines under a power tracking controller, which does not operate to extract the maximum amount of power, are subjected to lower aerodynamic loads compared to those regulated by traditional controllers. This can lead to the extension of their service life [41, 20, 40]. Recently, new regulations have been pushing the wind industry towards the development of such technologies, with the Irish and the British grid codes being the first examples of the participation of wind power plants in frequency control [16, 17]. These regulations require the provision of frequency control services directly from the wind turbines. Future trends for European regulations, like the European Network Code developed by the ENTSO-E, indicate the need for down-regulated wind turbines to participate in primary frequency control [33]. In literature, APC has been

widely used for single wind turbines, where examples of wind turbine APC algorithms can be found in Aho et al. [36], Zhu et al. [62], Lio et al. [26], and Kim et al. [63]. Still, APC results are less explored in a wind power plant context where realistic flow interactions should also be taken into account.

Still providing the required power output, wind farm control can be leveraged to reduce turbine loads [42, 64]. As a strong driver of fatigue loading, wakes are known to induce turbulence due to both wake meandering and wake-added turbulence [15]. Reducing wake effects on downstream turbines could alleviate fatigue damage, especially on the blades. Recent research in this area can be found in [38, 39, 43, 65]. In Vali et al. [39], tower base fore–aft bending moments are balanced while the wind farm power production follows a reference signal evaluated in a mid-fidelity model. In Stock et al. [65], the wind farm control dispatches power commands aiming to favor the loads in the turbines. A joint pitch-based and yaw-based control based on optimization algorithms is investigated by Kanev et al. [38] and, finally, the work in Baros et al. [43] implements a decentralized load control, where turbines can communicate with neighboring ones. All the above-mentioned works are either based on mid-fidelity simulations or real-time optimization algorithms whose computational costs are still high for practical implementation. These notions lead to a shifting paradigm whereby wind farm control can support better asset management under time-varying demand and electricity prices [1, 35]. In the zero-subsidy era, maximizing revenue is likely to be prioritized over annual energy production gains. This can be achieved by reducing the active power during periods of low grid loads demand and low electricity prices, as well as the optimization of loads for potential extension of the service life.

Recently, at an individual turbine level, condition-based control making use of down-regulation has become the focus of several publications, where turbines are down-regulated to reduce loading on specific components [66, 67, 20, 40]. These strategies in the offshore environment are of great value since accessibility is the major barrier to offshore wind implementation. Long down periods and expensive maintenance events as results of faults are more prone to happen due to the harsh offshore environment, which includes wave loads and accelerated corrosion [68]. As an alternative to shutdown, down-regulation can have a significant cost-effective impact on production by safely operating damaged turbines [69]. The Levelized cost of electricity can be reduced by avoiding unexpected maintenance costs in long term with preventive methods. Turbine operations can be constrained to provide more structural reliability by being self-aware of possible non-designed conditions [70, 71].

The main contribution of this chapter is the extended evaluation of three APC strategies for wind farm control, namely wake-loss compensation, thrust balancing, and load-limiting control. This evaluation is conducted in terms of power generation and mechanical loads across the entire wind farm. First, the active power compensation of wake losses uses the current turbine power output to enhance the tracking of defined power demand. Therefore, the power system's reliability is increased by maintaining the electrical frequency close to nominal. Moreover, depending on the weather conditions, i.e. the wind power availability, a thrust balancer uses estimations of aerodynamic forces to equalize thrust forces in all possible turbines in the farm. This leads to a uniform distribution of structural loads across the turbines. As consequence, the degradation of high-loaded turbines is reduced together with their associated maintenance costs. In addition, the total farm available power can be

increased by the cooperative farm operation, as seen in [72]. Lastly, a load-limiting strategy using the instantaneous thrust estimations derived from regular turbine measurements, i.e. rotor speed, generator torque, and blade pitch angles, switches its feedback loop between tracking the power reference signal and limiting the instantaneous thrust force based on a user-defined thrust force threshold. As a prevention measure of structural faults, the threshold should be defined by the operator or health monitoring systems due to unexpected or accumulated damage to the turbine structure. This load-limiting strategy based on a power tracking controller is explored at the wind farm level in contrast to the existing literature.

A reference wind farm layout is simulated in a high-fidelity environment. Results compare the APC strategies in terms of root mean squared, mean absolute, and peak errors; as well as, time-averaged means, standard deviations, and damage-equivalent loads. The damage-equivalent loads are computed for the turbine rotor shaft, tower base, and blade root. The findings show that the proposed wake-loss compensation exhibits a simple and effective concept that significantly improves wind farm power tracking in waked conditions. As the wake-loss compensation does not consider wake models for simplicity, the variance of loads is an undesirable side effect. Then, when thrust force balancing is added the aerodynamic loads are equalized and the standard deviations from damages in distinct turbine components are reduced. This effectively mitigates the variance of loads on the farm. Furthermore, specific turbines had their structural damages drastically reduced using the load-limiting control based on the instantaneous load estimations while the effects on the wind farm power generation are minor.

2.2. CONTROL STRATEGIES

2.2.1. POWER TRACKING CONTROL

In variable-speed, variable-pitch machines, the rotational speed, and the grid frequency are decoupled due to an indirect connection between generator and grid, which is carried out, nowadays, by the so-called back-to-back converters [73]. This concept is about 25 years old and allows wind turbines to down-regulate by reducing their speed while the grid frequency is maintained.

Herein, the wind turbine controller is synthesized to track a reference power signal whenever possible. Down-regulation based on blade pitch is considered. The controller shows a resemblance with the pitch-reserve controller described in Aho et al. [36] and the KNU2 algorithm in Kim et al. [63]. The choice based on blade pitch is justified by the following characteristics: a monotonic thrust reduction in response to monotonic demanded power reduction is achieved; operation close to the min- C_T method [62]; ensuring a stability margin w.r.t. stall regions [74].

The turbines are down-regulated by applying both the blade pitch and generator torque. The blade pitch controller consists of a gain-scheduled PI control law, where the blade pitch command θ is defined as

$$\theta(s) = \bar{K}_P(\theta_{\text{meas}}) [\omega_{\text{gen, meas}} - \omega_{\text{gen, ref}}(P_{\text{dem}})] + \frac{\bar{K}_I(\theta_{\text{meas}})}{s} [\omega_{\text{gen, meas}} - \omega_{\text{gen, ref}}(P_{\text{dem}})], \quad (2.1)$$

in which $\omega_{\text{gen, meas}}$ and θ_{meas} , respectively, are the measured generator speed and the mea-

sured collective blade pitch angle. The reference generator speed, $\omega_{\text{gen,ref}}$, is a function of the demanded power P_{dem} . $\bar{K}_P(\theta_{\text{meas}})$ and $\bar{K}_I(\theta_{\text{meas}})$ are the gain-scheduled proportional and integral gains [75].

The blade pitch controller, as a feedback loop, seeks to regulate the generator speed to the desired reference speed and it is similar to the controller used for generator speed regulation in above-rated conditions, traditionally. However, the generator speed setpoint depends on the demanded power rather than a rated value, $\omega_{\text{gen,rated}}$, as depicted in Figure 2.2. The relation in Figure 2.2 is obtained by the traditional generator torque-speed curve from Figure 2.1. The generator speed setpoint is selected by the same amount of power that the turbine would generate by *greedy control* in different wind conditions and it is upper-bounded by the rated value. The literature standard for wind turbine control is referred to as *greedy control*. The reader is referred to [76, 77] for more information on *greedy control* and [75, 78] for practical implementation of such a controller.

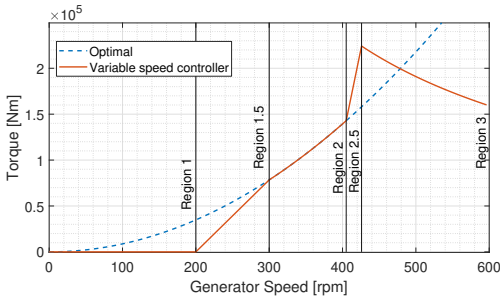


Figure 2.1: Generator torque as a function of the rotor speed for the DTU 10MW Reference Wind Turbine

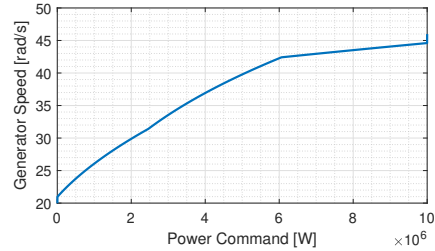


Figure 2.2: Generator speed reference as a function of the demanded power for the DTU 10MW Reference Wind Turbine

Together with the blade pitch controller, the generator torque controller is usually applied to track the demanded power by multiplying it by the inverse of the measured generator speed as

$$\tau_{\text{gen,tracking}} = \frac{P_{\text{dem}}}{\eta_{\text{eff}}\omega_{\text{gen,meas}}}, \quad (2.2)$$

where η_{eff} is the generator efficiency. This controller would provide near-perfect tracking by meeting the generated with the demanded power. However, this generator torque control law can be problematic as a certain increase in demanded power might lead to undesirable lower rotor speed and shut-off. In the *greedy control*, the generator torque is known to be stable for $\omega_{\text{gen}} \geq 0$, and globally converges to the optimal power coefficient C_p to maximize the turbine's power generation (in region 2). The greedy torque control law¹, which is composed of the traditional regions, is represented by $\tau_{\text{gen,greedy}}$ and depicted in Figure 2.1. Therefore, combining the greedy torque with the power tracking control law yields

$$\tau_{\text{gen,combined}} = \min(\tau_{\text{gen,greedy}}, \tau_{\text{gen,tracking}}). \quad (2.3)$$

¹In the industry, the optimal torque law in region 2 is often replaced with a PID-controller-based tip-speed-ratio tracking algorithm in combination with a wind speed estimator. Such an algorithm does not sufficiently add to the relevance of this work and therefore is outside the scope of this chapter.

The generator torque control law in Equation (2.3) ensures that the turbine does not operate at a lower tip-speed ratio than expected due to fast transients. As a result, imminent shutdowns are prevented and the turbine operates conservatively to avoid stalling. Near-perfect power tracking is achieved whenever $\tau_{\text{gen, tracking}}$ is not constrained by $\tau_{\text{gen, greedy}}$ and $P_{\text{dem}} \leq P_{\text{greedy}}$, where P_{greedy} is the hypothetical power produced by greedy control with the current wind inflow. At low available power in the wind, the turbine controller completely switches to *greedy control* whenever the collective blade pitch angle reaches the switch value θ_{switch} , and the generator speed becomes lower than the reference speed. This keeps the turbine producing the maximum power while the turbine is saturated.

Also presented and further detailed in [79], the derived power tracking controller at individual turbine level is extended to the control of the wind farm in the following Sections.

2.2.2. WIND FARM CONTROL FOR COMPENSATING POWER LOSSES

Whenever a wind farm rather than the individual wind turbines are to track a reference power signal, the power setpoint distribution over the turbines must be decided on. The power that a turbine can produce is directly correlated to the local wind speed and varies within the farm due to wake interactions. This leads to a non-trivial problem of distributing a wind-farm-wide power reference signal over individual turbines. In this subsection, a model-free and closed-loop controller is synthesized to distribute the power setpoints among the turbines and to minimize the wind-farm-wide reference tracking error as shown in Figure 2.3.

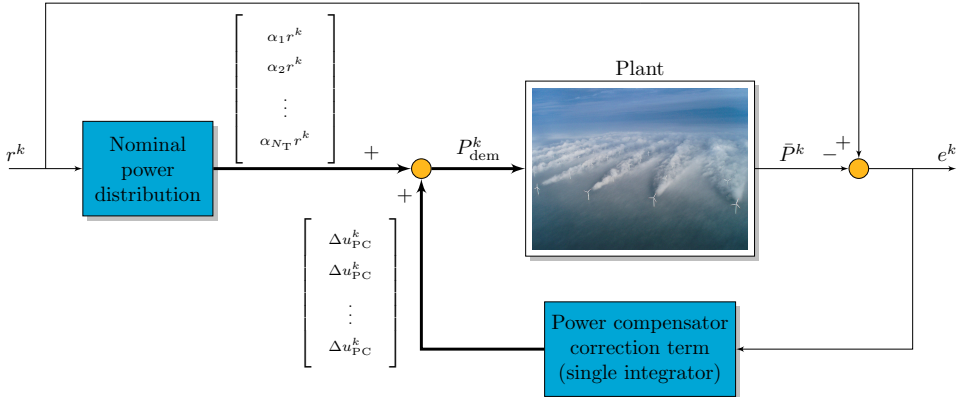


Figure 2.3: Block diagram of the wake-loss compensator.

The input signal of a single turbine is the demanded power P_{dem} , and the actual power produced P_{gen} is its output. In the situation that the turbine saturation does not occur, i.e. $P_{\text{dem}} < P_{\text{greedy}}$, and at near-perfect tracking, the input-output relationship is

$$P_{\text{gen}}^k = \tau_{\text{gen, tracking}}^k \omega_{\text{gen}}^k \eta_{\text{gen}} = P_{\text{dem}}^{k-1} (\omega_{\text{gen, meas}}^{k-1} \eta_{\text{gen}})^{-1} \omega_{\text{gen}}^k \eta_{\text{gen}}, \quad (2.4)$$

where k is the discrete-time index of the simulation and controller. With a sufficiently high sampling rate about 1–10 Hz, we can assume $\omega_{\text{gen}}^k \approx \omega_{\text{gen, meas}}^{k-1}$ and therefore, $P_{\text{gen}}^k \approx P_{\text{dem}}^{k-1}$.

Thus, the wind turbines can be approximated as pure time-delay systems² with their time delay equal to the simulation sampling time Δt , where the time $t^k = t^{k-1} + \Delta t$. Now, consider power track at the farm scale. The wind-farm-wide power reference $r^k \in \mathbb{R}$ is to be divided among the turbines. Mathematically, the demanded power signal for each turbine $P_{\text{dem},i}^k \in \mathbb{R}$ is

$$P_{\text{dem},i}^k = \alpha_i r^k + \Delta u_{\text{PC}}^k, \quad \text{with} \quad \sum_{i=1}^{N_T} \alpha_i = 1. \quad (2.5)$$

The term α_i divides the total wind farm power over the N_T turbines, defined as the nominal active power distribution, here assumed to be time-invariant and uniform for simplicity, i.e. $\alpha_i = \alpha_j, \forall i, j$. Still the target of further research, a smart nominal power distribution would benefit the operation of turbines. The global correction term $\Delta u_{\text{PC}}^k \in \mathbb{R}$, as in van Wingerden et al. [18], is the output of a pure integral controller defined as

$$u_{\text{PC}}^k = u_{\text{PC}}^{k-1} + K_{\text{I,PC}} e^k \Delta t, \quad \text{with} \quad e^k = r^k - \bar{p}^k, \quad (2.6)$$

where $K_{\text{I,PC}}$ is the integrator gain for the power compensator. The pure integrator controller is designed to compensate for the instantaneous wind-farm-wide tracking error e^k , which is obtained from the wind-farm-wide reference r^k to the sum of all individual active power generation $\bar{p}^k \in \mathbb{R}$. Although the proportional action might lead to faster responses, it is not included because turbine saturation can lead to undesirable aggressive behaviors, as well as the simplicity of the proposed control design can be kept. The integrator gain is chosen as $K_{\text{I}} = N_T^{-1} \Delta t^{-1}$, which is by definition the optimal controller for time-delay systems without turbine saturation³. The error e^k would therefore be eliminated on the next time-step, whenever all turbines are not saturated.

Using the integrator, the wind farm power tracking stability is assured, where the accumulated error tends to be eliminated in a steady state. Integrator anti-windup is implemented when all turbines are saturated. Moreover, the integrator state resets whenever all turbines are not saturated. This controller should achieve near-perfect tracking limited by the time delay and overall power availability.

2.2.3. WIND FARM CONTROL FOR THRUST FORCE BALANCING

The thrust force balancer is developed to reduce high thrust forces encountered inside the farm due to wake effects. The thrust forces, considered as the mean of the aerodynamic loads in the rotor, are reduced in these turbines, consequently, reducing their fatigue. Reducing the variation of thrust forces across the farm extends the aggregated turbine life. The main idea of the thrust force balance controller is to balance the thrust forces of all turbines to their mean value while the wind farm power tracking is maintained [72]. Hence, in addition to the power compensator feedback, a thrust control loop is synthesized by using each of the estimated instantaneous thrust forces $\hat{F}_{T,i}^k$. At each step-time, all $\hat{F}_{T,i}^k \in \mathbb{R}$ are sub-

²Pure time-delay systems have their response delayed by a time period. Time-delay systems inherently limit controller design due to right-half-plane zero (nonminimum-phase) behavior.

³Gain-scheduling due to turbine saturation are not considered and increases undesirable significant transients. Therefore, whenever saturation occurs, the wind farm control operates sub-optimally but with smother transients.

tracted by their mean thrust force $\bar{F}_T^k \in \mathbb{R}$ to obtain the thrust force error vector $e_{TB}^k \in \mathbb{R}^{N_T}$.

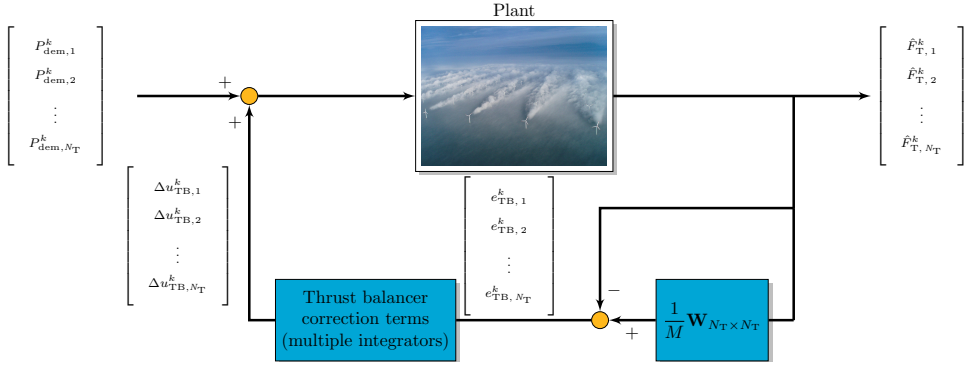


Figure 2.4: Block diagram of the thrust balancer.

In the control development, we noticed that the additional loop, depicted in Figure 2.4, would unsuccessfully try to boost the generated power of saturated turbines. In addition, the loop would reduce the demanded power of the unsaturated turbines which might be used for compensation purposes. Consequently, both loops compete with each other. Therefore, to make sure that the feedback loops will not compete, turbines that are saturated, which usually have lower thrust forces, are removed from the mean thrust force computation through the balance weight matrix

$$\mathbf{W}_{N_T \times N_T} = \begin{bmatrix} s_1 & s_2 & \dots & s_{N_T} \\ s_1 & s_2 & \dots & s_{N_T} \\ \vdots & \vdots & \ddots & \vdots \\ s_1 & s_2 & \dots & s_{N_T} \end{bmatrix}, \text{ where } \begin{cases} s_i = 1, & \text{if turbine is} \\ & \text{not saturated;} \\ s_i = 0, & \text{if turbine is} \\ & \text{saturated.} \end{cases} \quad (2.7)$$

Also, the corresponding instantaneous thrust force errors are reset as

$$e_{TB,i}^k = 0, \text{ if turbine is saturated.} \quad (2.8)$$

Then, the instantaneous thrust force error vector, e_{TB}^k , is computed as

$$e_{TB}^k = \left(\frac{1}{M} \mathbf{W}_{N_T \times N_T} - \mathbf{I} \right) \hat{F}_T^k, \quad (2.9)$$

in which M is the number of turbines that are not yet saturated, \mathbf{I} the identity matrix, and $\hat{F}_T^k \in \mathbb{R}^{N_T}$ the vector containing all of the estimated instantaneous thrust forces. Analogous to the wake-loss compensation, pure integral controllers are designed to eliminate the individual instantaneous thrust force errors with respect to the overall mean of the unsaturated turbines, as

$$u_{TB,i}^k = u_{TB,i}^{k-1} + K_{I,TB} e_{TB,i}^k \Delta t, \quad (2.10)$$

where $K_{I,TB}$ is the integrator gain for the thrust balancing, chosen to be the same value for the multiple integrators. The tuning procedure relies on the identification of the model dynamics from the demanded power to the thrust force of the defined down-regulator in Subsection 2.2.1. For brevity, the reader is referred to [72] for more details. Finally, the corresponding correction terms in $\Delta u_{TB}^k \in \mathbb{R}^{N_T}$ are added to demanded powers $P_{dem}^k \in \mathbb{R}^{N_T}$ to balance all thrust forces of unsaturated turbines.

THRUST ESTIMATION

The estimated instantaneous thrust force \hat{F}_T , which represents the main aerodynamic load, is obtained from the steady state model and the regular turbine measurements as

$$\hat{F}_T = 0.5\rho\pi R^2 \hat{v}_w^2 C_T \left(\frac{R\omega_{r,meas}}{\hat{v}_w}, \theta_{meas} \right), \quad (2.11)$$

in which \hat{v}_w is the estimated effective wind speed [80], ρ the air density, R the rotor radius and C_T the thrust coefficient from pre-computed mapping with the measured rotor speed $\omega_{r,meas}$ and collective blade pitch angle θ_{meas} . In this work, the estimation of the effective wind speed is obtained from an I&I estimator [81] through measurements of rotor speed, generator torque, and blade pitch angles. Note that \hat{F}_T is therefore a mean of the inflow loads over the rotor, where the inflow is inherently not constant by shear, wake, and other effects.

2.2.4. WIND TURBINE CONTROL FOR LOAD-LIMITING

For damaged turbines, the balance of thrust force might not be enough to guarantee safety. Such turbines require lower instantaneous loads to keep high safety levels/factors. Lastly, health monitoring systems are increasingly becoming a feasible technology for wind turbines [22, 82]. Therefore, the operation of those turbines should be appropriately constrained in real-time by the controller while still producing energy.

The down-regulation method in Subsection 2.2.1 reduces the structural stresses when reducing power demand. Thus, the turbine would be able to continue operating by down-regulating accordingly with the current loads as opposed to shutting down, until maintenance is fully performed. Although this results in sub-optimal power generation in the damaged turbines, the turbines' structural reliability is improved, where fatigue damage is alleviated and lifetime extended [69]. Also, as seen in Subsection 2.2.2, the power contributions from individual turbines can be redistributed among the turbines in the farm. That is, reducing the demanded power for a set of turbines can be compensated for by increasing the power generation in other turbines.

A switching control architecture for individual turbines, depicted in Figure 2.5, is therefore implemented in a wind farm setting. A user-defined constraint on the instantaneous thrust force is to be satisfied while the reduction in power generation is compensated by the other turbines. In the defined turbine j , the architecture allows for a demanded power profile to be tracked when the thrust force is lower than a given maximum allowed value $\bar{F}_{T,j}$. When such a value is reached, the proposed controller switches from tracking the demanded power to tracking the maximum allowed thrust force through feedback, thus satisfying the constraint on the maximum turbine instantaneous load.

The first observation is that, in order to not modify the power demand reference signal, it is sufficient for the additional local signal $\Delta u_{LL,j} \in \mathbb{R}$ to become zero. In order to do this,

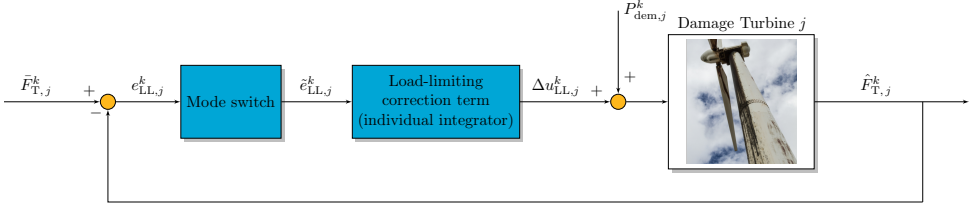


Figure 2.5: Block diagram of the load-limiting control.

a Mode Switch is designed such that the new additional local feedback loop will be open whenever the constraint on the thrust force is not exceeded. In particular, the switching will be defined by introducing the following signal

$$\tilde{e}_{LL,j} = \begin{cases} e_{LL,j}, & \text{if } e_{LL,j} < 0 \text{ or } e_{LL,I,j} < 0 \\ 0, & \text{otherwise} \end{cases} \quad (2.12)$$

where $e_{LL,j}^k = \hat{F}_{T,j}^k - \hat{F}_{T,j}^k$ and $e_{LL,I,j}^k = \int_0^{k\Delta t} e_{LL,j}(\tau) d\tau$ represent, the difference between the estimated instantaneous thrust force and its upper bound, and the time integral thereof. The rationale for this definition with the inclusion of the integral term is to avoid *chattering* when the thrust force is close to its reference, as is done for instance in the literature on Integral Sliding Mode control [83].

When the mode switch is active - that is when $\tilde{e}_{LL,j}^k \neq 0$ - the local feedback loop is closed. Using a simple pure integrator, as in previous subsections, the local correction signal $\Delta u_{LL,j}^k \in \mathbb{R}$ is obtained by

$$u_{LL,j}^k = u_{LL,j}^{k-1} + K_{I,LL} \tilde{e}_{LL,j}^k \Delta t, \quad (2.13)$$

where $K_{I,LL}$ is the integrator gain for the load-limiting loop. For further details, see [70]. As the load-limiting controller directly makes use of down-regulation, its stability is guaranteed by the down-regulation method - Subsection 2.2.1; i.e. if the down-regulation method is stable to demanded power changes, so is the controller using an integrator. This extends to all methodologies in this work.

2.3. SIMULATION EXAMPLE

2.3.1. SIMULATION SETUP

The proposed control strategies are evaluated in SOWFA [84], with wind turbines modeled using a rotating actuator disk model (ADM-R) [85]. Previous studies have been performed to validate SOWFA, for example, compared with the 48-turbine Lillgrund wind plant field data, it shows good agreement through the first five turbines in a row aligned with the wind direction [86]. In addition, SOWFA has been tested to verify that the inertial range in the turbulent energy spectra and the log-profile in the mean flow are incorporated, both of which characterize a realistic atmospheric boundary layer [53].

WIND FARM LAYOUT

The TotalControl reference wind power plant (TC-RWPP), defined in the H2020 TotalControl project, serves as a virtual test bed for wind farm control [87] and is used in this study. The TC-RWPP is a suitable reference wind farm for simulating moderate and high waked conditions depending on different inflow orientations. Figure 2.6 shows the staggered pattern of the TC-RWPP composed of 32 wind turbines. The separation between rows and columns is five rotor diameters ($5D$). This layout assumes that the prevailing wind direction is from the west in Figure 2.6. In this low wake interaction scenario, the wakes of upstream turbines hit a single turbine in the stream. In this work, we also explore a medium wake interaction scenario, where four-turbine wake interactions occur. The latter happens when the wind direction deviates 26.565° from the first scenario.

The yaw control, often implemented in a decoupled control loop, aims to align the turbine nacelle with the wind direction. Using a low-pass filtered wind direction signal from wind sensors (nacelle anemometers and/or wind vanes), a yaw angle or yaw rate is commanded to the yaw actuator to assure optimal inflow conditions. The simulations were executed with constant wind directions aiming full-waked conditions. The full-waked conditions present larger effective wind speed deficits between turbines and, consequently bigger power tracking errors. Partial-waked conditions or time-varying wind directions are supposed to be easier handled by the controllers and are not the focus herein.

The simulated turbines are DTU 10 MW Reference Wind Turbines [88], which have a rotor diameter of $D = 178.3$ m. The inflow wind direction in the simulator is from the southwest (240°), instead of the assumed prevailing wind direction from the west (270°) as in Figure 2.6. This is done to generate appropriate turbulent wind conditions by precursor simulations. Details about the positioning of the turbines in the domain for each scenario are depicted in Figures 2.7 and 2.8, where the layout is accordingly rotated -30° and -3.435° , respectively.

The distance between interacting turbines is different between the two studied scenarios. In the first scenario, the distance between the free-stream turbines and the turbines under the wake is $10.0D$, with sixteen interactions between the two turbines. In the second scenario, the distance is about $5.59D$ and there are two turbines in the free stream that are not affecting the downstream turbines, two sets of three turbines, and six sets of four turbines under wake interaction.

SIMULATION PARAMETERS

The simulation parameters are summarized in Table 2.1. The spatial discretization mesh for CFD is one step refined in a rectangular region, where the turbines are located and wakes are developed. Above 300 m of height, the mesh is coarser to reduce computation time.

In all cases, the conditions simulated in SOWFA are based on the study by Churchfield et al. [53]. The simulated atmospheric conditions consist of a neutral atmospheric boundary

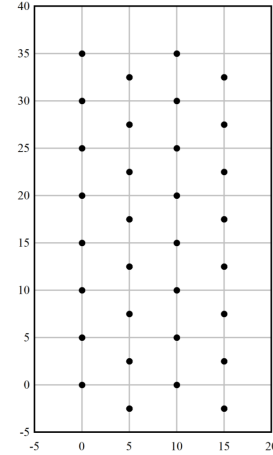


Figure 2.6: Layout of the TotalControl reference wind power plant. Units of axes are rotor diameters [87].

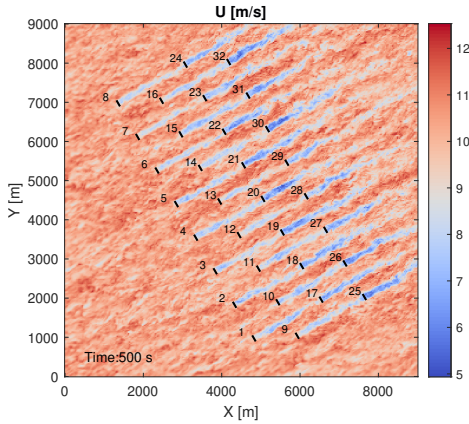


Figure 2.7: Layout of the simulated 8-by-4 wind farm rotated by -30° for the low wake interaction scenario. The background is an instantaneous horizontal slice of flow output taken from SOWFA.

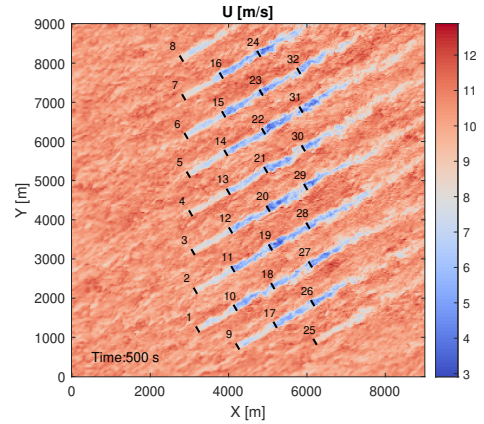


Figure 2.8: Layout of the simulated 8-by-4 wind farm rotated by -3.435° for the medium wake interaction scenario. The background is an instantaneous horizontal slice of flow output taken from a SOWFA.

layer with a low aerodynamic surface roughness value of 0.002 m - typically for offshore sites. The wind speed intensity averages 10 ms^{-1} and the turbulence intensity is around $5\text{--}6\%$ at the turbine hub height. The simulated time length of 1000 s is used to let the wakes develop through the domain. We were limited by single simulations for each controller approach because of the associated enormous computational cost due to the large simulated domain. Yet, the exact same turbulent inflow field is used.

A power tracking controller, further presented in Section 2.2.1, can follow a time-varying automatic generation control (AGC) signal. The AGC command used here is a portion of the 40-minute ‘RegD’ test signal, the most rapidly actuating test signal that is used for AGC qualification by the PJM regional transmission organization [89]. The signal is normalized and upsampled to 1 Hz . In the simulations, we assume a power command to have a persistent value of 3.5 MW , lower than half of the maximum produced power at a wind speed of 10 ms^{-1} , plus an AGC perturbation signal, which is set to have an amplitude of 1 MW . The AGC signal starts at 300 s to allow time for the wakes to develop and propagate during the simulation.

2.4. RESULTS

The key findings in this chapter are illustrated via a series of event plots and tables in this section, focusing on generated and reference power signals, turbine actuation, and mechanical loads. The results are obtained by the cumulative use of the defined controllers in Section 2.2. One of the differentiating features of this work is the analysis of full farm signals and loads. Thus, the results are broken down by quantities of interest, which encompass turbine operational parameters, such as blade pitch and generator torque, and key structural loads, including out-of-plane blade root bending moment, shaft torque, and tower-base bending moment. Time-domain histories of the quantities of interest are presented via aggregate statistics, in particular mean values, standard deviations, root mean squared er-

Table 2.1: SOWFA simulation parameters.

Property	Value
Domain size	9 km × 9 km × 1 km
Cell size outer regions	10 m × 10 m × 10 m
Cell size near rotor	5 m × 5 m × 5 m
Simulation time-step	0.5 s
Atmospheric boundary layer (ABL) stability	Neutral
Mean inflow wind speed	10 m/s
Surface roughness	0.0002 m
Turbulence intensity	5.0-6.0 %
Turbine rotor approximation	Rotational Actuator Disk Model (ADM-R) [85]
Turbine type	DTU 10 MW [88]
Turbine rotor diameter	178.3 m
Turbine hub height	119 m
Force scalar factor	1.0
Inflow velocity factor	0.94
Blade smearing factor	20.0 m
Inter-turbine interaction spacing	10.0 D and 5.59 D †

† The inter-turbine interaction spacing depends on the wind direction because of the staggered pattern defined in Subsection 2.3.1.

rors, mean absolute errors, peak errors, and short-term damage equivalent loads (DELs).

2.4.1. STATISTICAL CALCULATIONS

Root mean squared error (RMSE) is considered an excellent general-purpose error metric for tracking performance, as it is scale-dependent. It is defined as

$$\text{RMSE} = \sqrt{\frac{1}{N} \sum_{n=1}^N |x_n - x_n^{\text{ref}}|^2}, \quad (2.14)$$

where N is length of the evaluated discrete signal x , n the element variable, and x^{ref} the reference signal.

Mean absolute error (MAE), as also a widely used criterion, is defined as

$$\text{MAE} = \frac{1}{N} \sum_{n=1}^N |x_n - x_n^{\text{ref}}|. \quad (2.15)$$

This criterion is a similar measurement to the RMSE. Nevertheless, it is more robust since it is less sensitive to extreme values than RMSE. In MAE, different errors are not weighted, but the scores increase linearly with the increase in errors. Generally speaking, low values for RMSE and MAE mean that the power generation has been accurately tracking the power reference.

Table 2.2: Parameters of controllers.

Variable	Symbol	Value
Proportional gain of the pitch controller	\bar{K}_P	Gain-scheduled: 0.039 - 1.41 s [75]
Integral gain of the pitch controller	\bar{K}_I	Gain-scheduled: 0.067 - 0.28 s [75]
Derivative gain of the pitch controller	\bar{K}_D	0.0 s [75]
Corner frequency of generator speed low-pass filter	-	0.1798 Hz [75]
Generator efficiency	η_{gen}	1 [78, 75]
Generator torque constant for greedy control	K_{greedy}	79.439 N-m/(rad/s) ² [75]
Transitional generator speed bet	-	200.0 rpm [75]
Transitional generator speed - region 1.5 to 2	-	300.0 rpm [75]
Transitional generator speed - region 2 to 2.5	-	405.0 rpm [75]
Rated generator slip percentage in region 2.5	-	10.0 [77]
Rated power	P_{rated}	10 MW [88]
Transitional generator speed between regions 2.5 and 3 percent of rated generator speed	-	95.0 [77]
Rated generator speed	$\omega_{\text{gen,rated}}$	445.67 rpm [77]
Maximum generator rate	-	15,000 N-m/s [78, 75]
Maximum blade pitch rate	-	10 deg/s [78, 75]
Fine blade pitch angle	θ_{fine}	0.75 deg [75]
Switch blade pitch angle	θ_{switch}	1 deg [75]
Integral gain of the wind farm wake-loss compensator	$K_{I,PC}$	$N_T^{-1} \Delta t^{-1} *$
Integral gain of the wind farm thrust balancer	$K_{I,TB}$	0.5 [72]
Integral gain of the wind turbine load-limiting controller	$K_{I,LL}$	2.947 [70]

* Optimal gain defined in Subsection 2.2.2.

Moreover, peak error (PE) is defined by

$$\text{PE} = \max_{n \in \{1, \dots, N\}} |x_n - x_n^{\text{ref}}|. \quad (2.16)$$

Short-term fatigue DELs of quantities of interest were computed directly from the time series using the NREL postprocessing tool, MLife [90]. MLife uses rainflow counting to bin a histogram of load cycle amplitudes over the time series. A mean-value Goodman correction is also used for the histogram amplitudes. The short-term DELs are computed from the histogram bins and the material-specific Wöhler exponent, m , from classical S-N fatigue theory, as

$$\text{DEL}_{\text{short}} = \left[\frac{1}{T} \sum_k c_k f_k^m \right]^{\frac{1}{m}}, \quad (2.17)$$

in which T is the simulation time representing a 1-Hz equivalent cycle, k is the number of bins, and c is the number of cycles at load amplitude, f . As is standard practice, $m = 5$ was used for loads on the main shaft and tower made of steel, and $m = 10$ for loads on the composite blades.

2.4.2. MECHANICAL CALCULATIONS

The computation of tower-base bending moment was simplified using only the component of the fore-aft thrust force F_T and the tower height h_t as

$$M_t = F_T h_t. \quad (2.18)$$

The ultimate tower-base bending moment is derived from the ultimate stress σ_{ult} of the tower material, considered as $\sigma_{\text{ult}} = 400$ MPa, and its geometry as

$$M_{t, \text{ult}} = \frac{\sigma_{\text{ult}} I_t}{r_{o,t}}, \quad (2.19)$$

in which I_t is the moment of inertia and $r_{o,t}$ is the outside radius of the tower base. The ultimate tower-base bending moment is considered $6.0 \cdot 10^5$ kN·m. Moreover, the ultimate shaft torque is derived considering pure torque loading, i.e. $\tau_{\text{max}} = \sigma_{\text{ult}}/2$, and shaft geometry as

$$T_{\text{shaft, ult}} = \frac{J_{\text{shaft}} \tau_{\text{max}}}{r_{o, \text{shaft}}}, \quad (2.20)$$

in which J_{shaft} is the polar moment of inertial and $r_{o, \text{shaft}}$ is the outside radius of the shaft. The ultimate shaft torque is therefore considered as $3.5 \cdot 10^6$ kN·m. Lastly, the out-of-plane root-blade bending moment is computed by summing the corresponding moments due to axial forces throughout the blade span. The ultimate blade root bending moment is considered $7.0 \cdot 10^4$ kN·m [88]. Note that, with a different definition from the Standards for Certification of wind turbines, the ultimate load is herein derived from each component for the computations of short-term fatigue DEL.

2.4.3. SIMULATION RESULTS

The application of the active power control methodologies, namely wake-loss compensation, thrust force balancing, and load limitation was simulated in the low wake interaction scenario (Scenario 1) and the medium wake interaction scenario (Scenario 2). Moreover, the variability in wind energy is represented by a time-varying wind farm power reference signal, instead of varying wind conditions, as described in Section 2.3.1.

Wake-loss compensation The closed-loop wake-loss compensator boosts the individual wind turbine power references to compensate for power losses from wake effects. In Scenario 1, the power losses due to wake effects on downstream turbines are mild. The effects of oscillations due to the turbulence in the wind inflow are seen in the power output in Figure 2.9. The power compensator, denoted as PC, slightly boosts the power reference signal to deal with them. Turbines 1 and 17, an upstream and a downstream turbine respectively, are plotted for the sake of brevity, as the other turbines in the farm behave similarly.

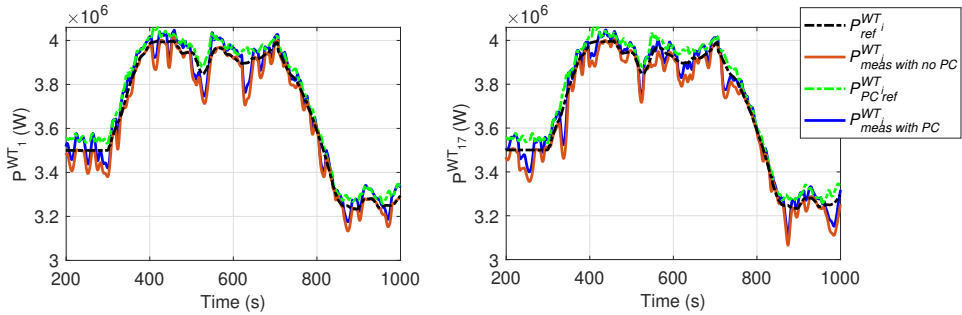


Figure 2.9: Powers of turbine 1 and 17 in Scenario 1. $P_{ref}^{WT_i}$ is the uniform dispatch power of the desired wind farm power, $P_{meas}^{WT_i}$ the obtained power with no power compensation, $P_{PC}^{WT_i}$ the new power reference given by the power compensator, and $P_{meas}^{WT_i}$ the obtained power with power compensation.

The total wind farm power signals are presented in Figure 2.10. The desired reference signal is depicted in black, the total power output signal without the proposed wake-loss compensator is in red, and the total power output signal when the PC is applied is in blue. Also, the total of the boosted power references signal in the PC simulation is plotted in green. Clearly, the PC as a wind farm closed-loop approach significantly enhances the total power trackability.

In Scenario 2, there are sets of three turbines under a consecutive full-waked flow and a lower inter-spacing distance, so the wake effects on the downstream turbines lead to a significant mismatch between the individual power generation and demand - Figure 2.11. The result is illustrated by plotting only turbines 1, 10, 18, and 27, which are ones of a four-turbine interacting set. This leads to a compromising total wind farm power generation without the PC, as seen in Figure 2.12. However, as clear evidence of the benefits of the wake-loss compensator in such a scenario, not all the boosted individual power references are being matched by their power generation, but the total wind farm power with the PC still follows the desired total power.

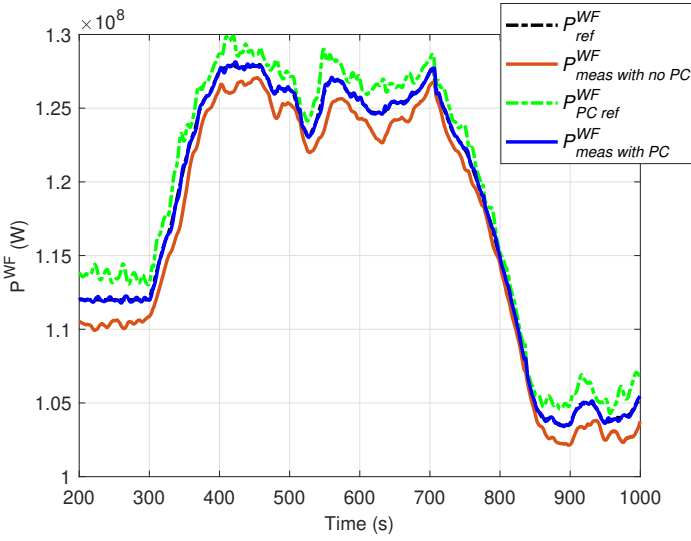


Figure 2.10: The total wind farm power in Scenario 1. P_{ref}^{WF} is the desired power for the farm, P_{meas}^{WF} the obtained power with no power compensation, $P_{PC\ ref}^{WF}$ the new power reference from the power compensator, and $P_{meas\ with\ PC}^{WF}$ the obtained power with power compensation.

The downside of this approach is that power booster as a simple strategy does not consider the wind turbine interactions in the dispatch of the additional power signals in the

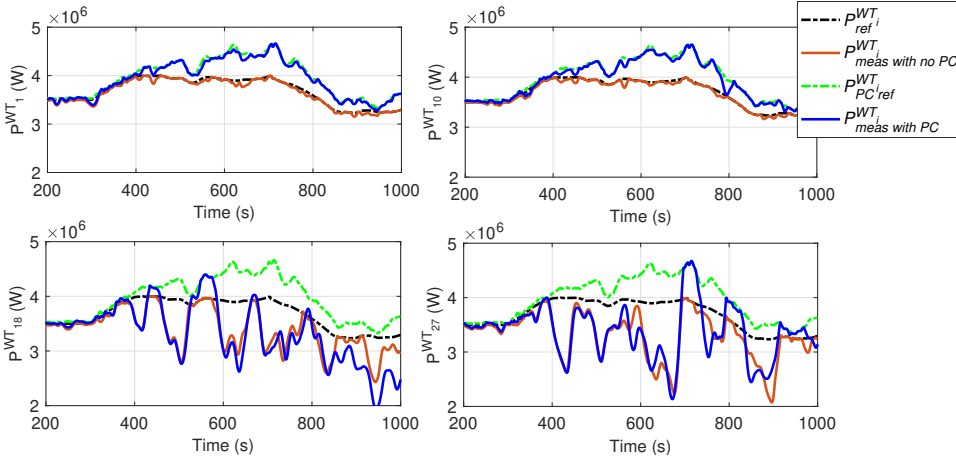


Figure 2.11: Powers of turbines 1, 10, 18 and 27 in Scenario 2. $P_{ref}^{WT_i}$ are the uniform dispatch powers of the desired wind farm power, $P_{meas}^{WT_i}$ the obtained power with no power compensation, $P_{PC\ ref}^{WT_i}$ the new power reference from the power compensator, and $P_{meas\ with\ PC}^{WT_i}$ the obtained power with power compensation.

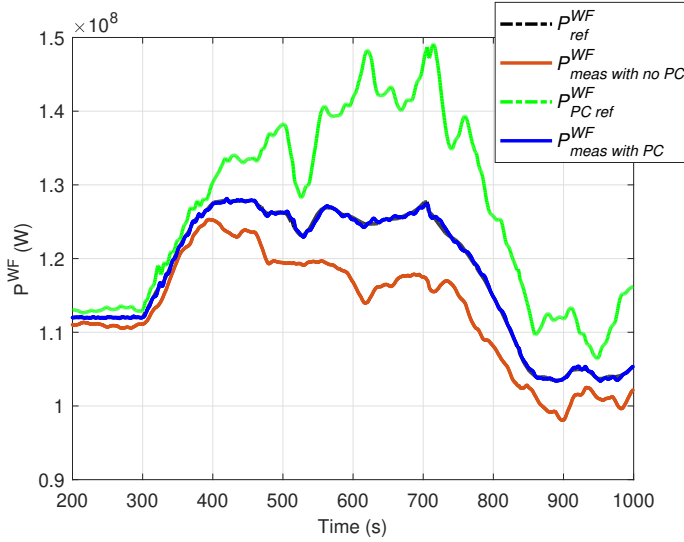


Figure 2.12: The total wind farm power from Scenario 2. P_{ref}^{WF} is the desired power for the farm, $P_{meas\ with\ no\ PC}^{WF}$ the obtained power with no power compensation, $P_{PC\ ref}^{WF}$ the new power reference from the power compensator, and $P_{meas\ with\ PC}^{WF}$ the obtained power with power compensation.

reference of each turbine. It can lead to a large variance in loads across the turbines on the farm. This variance is also seen without the PC. To convey such a downside, an additional thrust balancer is proposed and its results will be provided.

Thrust balance The thrust balancing is designed by an additional close-loop to balance loads of unsaturated turbines while the total power reference is met by the wind farm. First, the thrust balancer is activated in Scenario 1. The result is presented in Figure 2.14, where “TB” denotes thrust balancer. The difference can be seen by comparing the loads with the case with no TB in Figure 2.13. As expected due to the inflow turbulence, the thrust signals keep oscillating, but their averages are balanced. This leads to aggregated structural load alleviation in the farm and a dispatch of power references that benefits the total available power [72]. Then, for Scenario 2, the results are correspondingly depicted in Figure 2.15, Figure 2.16, and Figure 2.17.

Load limitation Accordingly to the decision of the turbine to be limited and its load threshold by the wind farm operator or health monitoring system, the turbine is derated using its estimated instantaneous loads as real-time feedback information. The load limitation is denoted as LL. The two cases were set by limiting the thrust on the turbine number eighteen (WT18), which is a waked turbine in Scenario 1 and a second downstream waked turbine in Scenario 2. In the first case, a thrust limit of 410 kN was defined, while in the second case a higher limit of 460 kN was chosen, as they are about half of the thrust variation means from previous simulations, see Figure 2.18 and Figure 2.19.

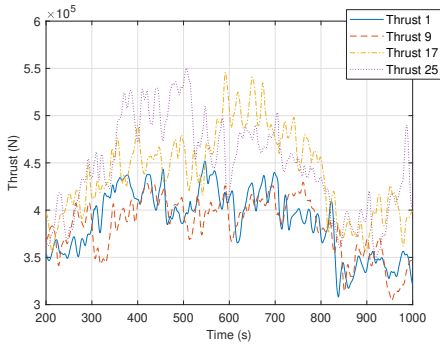


Figure 2.13: Thrust forces in Scenario 1 when PC is used and TB is not used.

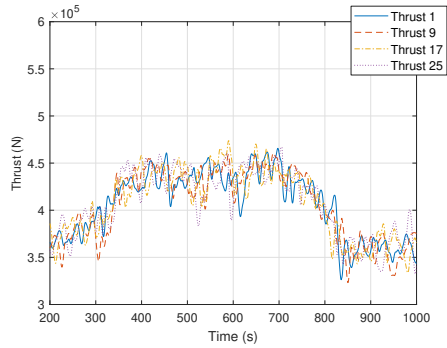


Figure 2.14: Thrust forces in Scenario 1 when both PC and TB are used.

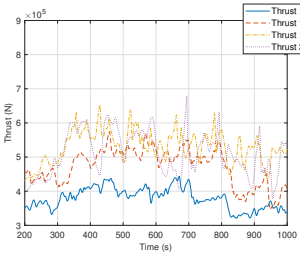


Figure 2.15: Thrust forces in Scenario 2 when both PC and TB are not used.

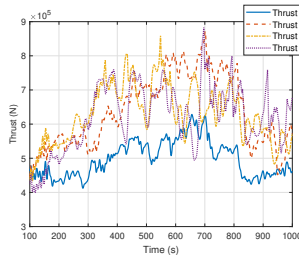


Figure 2.16: Thrust forces in Scenario 2 when PC is used and TB is not used.

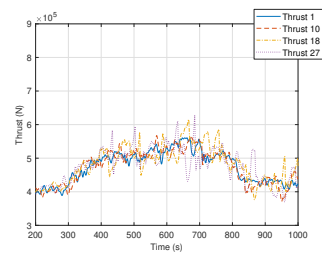


Figure 2.17: Thrust forces in Scenario 2 when both PC and TB are used.

2.4.4. QUANTITATIVE RESULTS AND DISCUSSIONS

The quantitative results are presented in three stages. All quantities are obtained after an initializing simulation time of 300 s, in which the wakes have been allowed to propagate

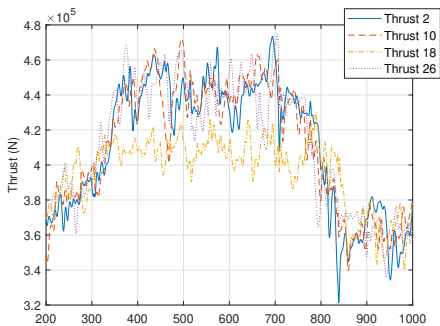


Figure 2.18: Thrust forces in Scenario 1 when both PC and TB are used. In addition, LL of 410kN in the WT 18 is applied.

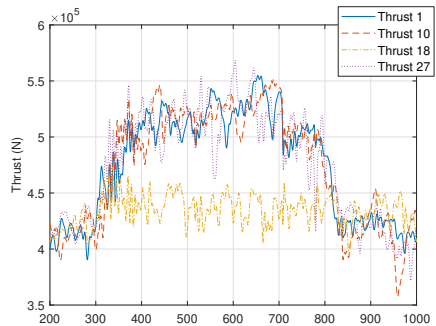


Figure 2.19: Thrust forces in Scenario 2 when both PC and TB are used. In addition, LL of 450kN in WT 18 is applied.

through the farm. First, the power tracking capability is presented in Table 2.3. It provides a quantitative comparison of reliability in terms of power generation from the entire farm from both scenarios, namely here onward as Sc1 and Sc2. The results show that the power tracking is improved with the PC based on all criteria. Furthermore, the power tracking is conserved or even improved by applying the TB on top of the PC. A slight improvement with the additional use of the LL is noticed from the RMSEs and the MAEs, although the RMSE in Sc2 and the PEs increase compared with the PC and TB together.

Table 2.3: Total Power Tracking Criteria in the Wind Farm.

Scenario	PC	TB	LL	RMSE [MW]	MAE [MW]	PE [MW]
Sc1				1.295	0.856	2.698
	✓			0.114	0.061	0.477
	✓	✓		0.114	0.060	0.461
	✓	✓	✓	0.081	0.042	0.468
Sc2				6.044	3.802	10.765
	✓			0.247	0.137	0.765
	✓	✓		0.142	0.076	0.502
	✓	✓	✓	0.167	0.071	1.316

*The colours in the cells go from green as the lowest value to yellow the highest value corresponding to the evaluated category. This colour formatting is carried along the next tables.

Next, as controllers can lead to premature degradation of actuation systems, the actuation is herein evaluated. For an overall wind farm evaluation, the averages of the time series of the operational parameters across the farm were computed and the statistics apply to them, as provided in Table 2.4. The mean of pitch actuation is reduced by applying the PC, however, the pitch and the generator torque variations are increased among turbines in the farm. This elucidates the variation in the operation of turbines due to the only use of the PC. The opposite is observed when applying the TB. The TB reduces the variance in the operation of the turbines in waked conditions. Furthermore, The LL reduces the mean of pitch actuation as a consequence of the compensation for the power losses of the load-limited turbine. However, as expected the variations increase in both pitch and generator torque due to the discrepancies in the operation of the load-limited turbine.

Finally, fatigue loads are reported in Table 2.5 through the short-term DEL of the torque in the rotor shaft, of the tower-base bending moment, and the out-of-plane blade root bending moment. These quantities directly address the central question of how closed-loop control considering structural loads could be beneficial for wind farm APC. For the addition of the TB on the PC, we derived the reduction of the standard deviations across the farm of the short-term DELs of the torque in the rotor shaft, of the tower-base bending moment, and the out-of-plane blade root bending moment. The result is a reduction of 5%, 60% and 60%, respectively, in Scenario 1; and 22%, 32% and 36% in Scenario 2. This means that the damage is distributed with the addition of the TB. Applying the LL in the defined WT18, the DELs are reduced considerably in all three loads of interest - 23%, 46% and 42%, respectively, in Scenario 1; and 60%, 64% and 68% in Scenario 2 compared with the PCTB cases

Table 2.4: Statistics of the Time-series Average of Pitch Actuation and of the Generator Torque in the Wind Farm.

Scenario	PC	TB	LL	Mean		SD		Max		Min	
				[deg]	[kN·m]	[deg]	[kN·m]	[deg]	[kN·m]	[deg]	[kN·m]
Sc1	✓			7.6	101.9	1.5	0.1	9.7	102.1	5.5	101.6
	✓	✓		4.6	99.5	3.2	3.4	9.4	102.4	1.2	93.2
	✓	✓		7.5	102.6	1.5	0.1	9.6	102.8	5.4	102.3
	✓	✓	✓	4.0	102.6	3.0	6.0	8.7	108.1	1.0	92.4
Sc2	✓			7.5	102.5	0.9	4.7	8.8	109.3	6.2	96.2
	✓	✓		4.2	102.4	2.1	11.1	7.4	119.9	2.1	90.4
	✓	✓		8.3	102.7	0.8	4.4	9.4	108.4	7.1	95.8
	✓	✓	✓	5.5	102.5	1.8	10.1	8.2	118.5	3.3	89.5

- while in the other turbines the DELs are held uniformly because of the TB. The DELs of WT18 from all simulations are depicted in Figure 2.20. According to MLife [90] and as expected, the mechanical life of the turbines for the shaft, tower, and blades in all studied cases is considered infinity, which is not suitable for the evaluation of lifetime extension from this work. This happens because the power tracking approach (derating) experiences lower loads than the traditional operation that maximizes power extraction, which is an outstanding advantage.

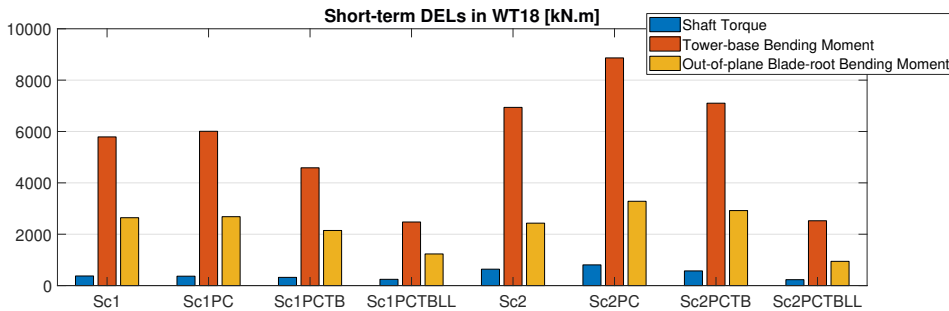


Figure 2.20: Short-term damage equivalent loads for the different controllers and scenarios.

2.5. CONCLUSIONS

Under increased wind energy penetration in the grid, APC services are essential to the reliability of power grids. An APC objective is to have the wind farm’s power generation track a power reference signal generated by transmission system operators. Due to the uncertain wake dynamics, a closed-loop control solution is proposed to provide power tracking. Since dynamical wake models are generally complex, approximations are proposed such that the closed loop can be employed with a low computational cost to work in a real-time application. In addition, induced loads are considered to prevent turbines from quick degradation and to keep them safe in damaging conditions.

Table 2.5: Short-term DELs of the Shaft Torque, Tower-base Bending Moment, and Out-of-plane Blade-root Bending Moment [kN·m].

Case	WT1			WT2			WT3			WT4		
Sc1	421	3767	1525	394	4526	1975	351	4055	1789	397	4502	1891
Sc1PC	416	3973	1654	395	4617	2021	345	4037	1780	384	4472	1869
Sc2	288	3508	1487	323	3626	1629	291	2999	1269	293	4358	2008
Sc2PC	414	5019	2132	371	5105	2234	369	4616	1804	395	6524	2950
Case	WT5			WT6			WT7			WT8		
Sc1	358	4261	1935	303	3181	1383	328	3583	1563	545	4639	1885
Sc1PC	360	4308	1941	307	3198	1407	328	3645	1611	320	3999	1875
Sc2	310	3890	1734	298	4769	2200	279	3648	1567	279	3754	1824
Sc2PC	410	5479	2234	387	6060	2698	371	5035	2114	403	4883	2049
WT9			WT10			WT11			WT12			
Sc1	359	3505	1530	325	4184	1868	324	4500	2027	337	4699	2087
Sc1PC	365	3520	1542	320	4302	1886	314	4467	2009	335	4665	2086
Sc2	248	3639	1623	318	6393	2781	267	5278	2163	260	5444	2309
Sc2PC	369	5133	2072	455	9869	4269	461	8431	3544	417	8423	3562
WT13			WT14			WT15			WT16			
Sc1	326	3870	1659	352	3976	1691	327	4966	2278	389	4176	1794
Sc1PC	328	3929	1704	344	3894	1636	321	4945	2280	379	4124	1776
Sc2	266	5507	2308	270	6484	2897	348	8343	3730	240	5343	2346
Sc2PC	435	9476	4131	458	9574	4127	481	9005	3916	386	6805	2830
WT17			WT18			WT19			WT20			
Sc1	323	5182	2373	374	5789	2643	301	5066	2149	347	6907	3096
Sc1PC	335	5279	2436	366	6008	2683	298	5161	2175	360	7044	3025
Sc2	380	8334	3521	639	6939	2431	616	8124	3456	608	8239	3249
Sc2PC	459	9358	3888	806	8865	3283	685	8840	3624	715	8063	2883
WT21			WT22			WT23			WT24			
Sc1	351	5258	2188	334	5175	2450	322	5180	2320	470	6533	3000
Sc1PC	357	5329	2238	347	5236	2478	317	5266	2385	459	6520	2997
Sc2	690	7854	3054	620	6509	2600	699	7230	2961	628	7936	3233
Sc2PC	696	7835	3068	809	8364	3077	826	9133	3486	758	8985	3385
WT25			WT26			WT27			WT28			
Sc1	346	5701	2632	341	5902	2532	331	6207	2941	418	6199	2635
Sc1PC	363	5798	2700	344	6003	2569	333	6975	3240	431	6360	2701
Sc2	293	3020	1314	664	8160	3423	870	9564	3733	644	6629	2325
Sc2PC	423	4559	1863	672	7178	2785	949	10019	3912	632	7281	2570
WT29			WT30			WT31			WT32			
Sc1	376	5093	2201	337	6005	2640	328	6902	3183	327	5389	2484
Sc1PC	349	5095	2191	340	6112	2714	325	6858	3139	337	5512	2530
Sc2	656	8099	3133	661	7328	2863	666	7411	2665	718	8719	3310
Sc2PC	726	8829	3264	729	8357	3272	728	7871	2779	699	8579	3262

*The colours in the cells go from green as the lowest value to yellow the highest value corresponding to the evaluated component.

In this chapter, we showed that wind power plants exploring APC services can provide power tracking, and reduce the loading on a farm level and specific turbines by considering additional closed loops. The application of proposed closed-loop approaches is demonstrated and evaluated in a high-fidelity simulation environment by including load examination of turbine components.

The key elements addressed in this chapter are the followings: (1) wake-loss compensation, which balances the total power generated with the consumed on the grid in the presence of wake effects; (2) thrust force balancing, which balances the structural loading across the farm; (3) load-limiting control, which increases safe margins on structural-damaged turbines by limiting the instantaneous loads to user-defined ones.

Consequently, we demonstrate that power reliability is enhanced with (1). Also, damage loading is spread across the turbines due to (2), which would lead to lower maintenance costs in the long term as sporadic maintenance events would be reduced. Moreover, the damage is mitigated effectively on the defined turbine by (3). The combination of such strategies could lead to a relevant cost reduction in wind energy. However, a quantitative overall cost-benefit analysis of an integrated APC for a wind farm has not yet been performed and remains the subject of ongoing and future work.

Further research and possible test campaigns are needed to implement the closed-loop controllers successfully in real wind farms. This research direction is relevant for reductions in the Levelized cost of energy (LCoE), particularly if extended as part of an overall co-optimization framework as by Ashuri et al. [91]. Worthwhile future avenues of investigation include time-varying wind direction and yaw control strategies like wake steering for load mitigation.

3

LOAD LIMITING WIND TURBINE CONTROL

*Intellectuals solve problems,
geniuses prevent them.*

Albert Einstein

It takes leadership to improve safety.

Jackie Stewart

Even though structural loads can be effectively distributed as presented in Chapter 2, specific events may arise such that the operation of turbines must be limited. Structural integrity of a turbine is not only influenced by the imposed structural loads but also by external factors, such as corrosion, damaged structures from potential collisions with boats, and severe weather. Through the knowledge of the turbine's health, it is imperative for turbines to prioritize safety. In order to achieve a balance between energy production and safe operation, this chapter presents load-limiting controllers we have developed. These controllers are designed to ensure that turbines generate energy while operating within safe load limits.

The work of this chapter has been published in Silva et al. [70] and Silva, Ferrari, and Wingerden [92].

3.1. A SWITCHING THRUST TRACKING CONTROLLER

Wind turbines are prone to structural degradation, particularly in offshore locations. Based on the structural health condition of the tower, power de-rating strategies can be used to reduce structural loads at the cost of power losses. This first part of the chapter introduces a novel closed-loop switching control architecture to constrain the thrust in individual turbines. By taking inspiration from developments in the field of reference governors, an existing demanded power tracking controller is extended by a thrust tracking controller. The latter is activated only when a user-defined constraint on fore-aft thrust force is exceeded, which can be set based on the actual damage status of the turbine. Having a down-regulation with monotonic aerodynamic load response, a simple linear thrust tracking controller is proposed. Such a scheme can reduce aerodynamic loads while incurring acceptable losses on power production which, in a wind farm setting, can be compensated for by other turbines. Large eddy simulations demonstrate the performance of the proposed scheme on satisfying thrust constraints.

3.1.1. INTRODUCTION

To make wind energy competitive in the transition from fossil fuel-based to renewable energy sources, it is essential to reduce the Levelized Cost of Energy (LCoE). This performance indicator takes into account the costs of construction, maintenance and the energy generated by the power plant over its entire lifetime [91].

Structural degradation reduces the lifetime of turbine components as an inevitable result of alternating stresses and environmental conditions, thereby increasing the cost of maintenance. Periodic structural loading is being considered as the main cause for component failures [93, 94]. Additionally, structural degradation is accelerated by the offshore environment, including wave action and corrosion [68].

A way to reduce the damage propagation and increase reliability is by derating the turbine appropriately to reduce structural stresses. Health monitoring systems can be used to detect and to estimate high level corrosion, mechanical flaws and cracks [22, 82]. Although this results in sub-optimal power generation for individual turbines, the turbines' structural reliability is improved, where fatigue damage is alleviated and lifetime extended [69]. As a result, the turbine is able to continue operating as opposed to shutting down, until maintenance is fully performed.

When the goal of the wind farm controller is to track a power reference, and enough power is available in the wind, the power contributions from individual turbines can be redistributed among the turbines in the farm. That is, reducing the demanded power for a set of turbines, is compensated for by increasing the power reference for the other turbines. This can be accomplished by simple compensation control loops as described in [18]. For instance, power losses due to waked conditions are compensated when turbines are not able to meet their individual power reference in [72].

Recently, condition-based control making use of down-regulation has become the focus of several publications, where turbines are down-regulated to reduce loading on specific components [66, 67, 20, 40]. These strategies in the offshore environment are of great value since accessibility is the major barrier to offshore wind implementation. Long down periods and expensive maintenance events as results of faults are more prone to happen due to the harsh offshore environment, which includes wave loads and accelerated corrosion [68]. As

an alternative to shutdown, down-regulation can have a significant cost-effective impact on production by safely operating damaged turbines [69]. The levelized cost of electricity can be reduced by avoiding unexpected maintenance costs in the long term with preventive methods. Turbine operations can be constrained to provide more structural reliability by being self-aware of possible non-designed conditions [70, 71].

At an individual turbine level, the down-regulation of power can be achieved by either operating the turbine at higher rotor speeds (HRS) or lower rotor speeds (LRS), with respect to the rotor speed from conventional controllers.

HRS approaches are beneficial for power tracking because there is more kinetic energy associated with the higher rotor speed, allowing fast recovery when demanded power increases. As an HRS approach, the Max- Ω strategy [95] maximizes the rotor speed. However, the HRS approaches present limitations for our design. The aerodynamic loads do not reduce significantly when the power demand decreases and might even increase [20]. As a result of the latter, the thrust response might not be monotone to power setpoint changes. Non-monotone behaviors do not only appear in the thrust and power relation, but they can also appear in the demanded power and generated power relation [74].

LRS approaches present lower aerodynamic loads and, consequently, lower structural loads on the blades and tower. In contrast with HRS approaches, the turbine response presents a monotone behavior from power demand to thrust. As an LRS approach, the Const- Ω [26] keeps the rotor speed constant avoiding high rotor speeds, but can reach extreme tip-speed ratio values and undesirable operation regions as wind speed changes. Furthermore, there exists the so-called min- C_T method based on steady state power coefficient (C_P) and thrust coefficient (C_T) look-up tables [26, 41]. C_P and C_T represent the wind turbine power and thrust conversion efficiencies, respectively. The method ideally leads to the smallest thrust compared to all the down-regulation strategies and demonstrates benefits for waked wind farms, which allows more available power to down-stream turbines [96, 19]. However, its operation in low tip-speed ratios is close to stall conditions, where the predominant flow stability along the blades can be lost, affecting the controlled turbine response. This latter drawback is overcome in [36] and [63] with the so-called "Active Power Control (APC) pitch" and KNU2, respectively. This approach pitches the blades to follow a reference generator speed, based on the function built from the conventional generator torque law [77, 78]. Although the power tracking response is slightly worse in the LRS approaches [36], [63], they are suitable for wind farm power tracking purposes on large farms. For instance, down-regulation providing power reserves were explored in [12].

We propose a switching control architecture for wind turbines that must satisfy a user-defined constraint on the fore-aft thrust forces. This architecture allows to track a demanded power profile when the thrust forces are lower than a given maximum allowed value. When such a value is reached, the proposed controller switches from tracking the demanded power to tracking the maximum allowed thrust force, thus satisfying the constraint on the turbine maximum loading. In particular, the following contributions are presented:

1. The extension of an existing power tracking controller via a switching thrust tracking feedback law that modifies the former's reference, by taking inspiration from the *reference governor* literature [97];
2. The introduction of an integral switching law for the thrust tracking controller in order

to avoid chattering when the estimate thrust force lies on the constraint boundary;

3. A large eddy simulation (LES) study showing the effectiveness of the proposed scheme for both laminar and turbulent wind speed profiles.

The simulation study shows how the relative reduction in the thrust force results in a generated power reduction experienced by a given turbine. This allows to satisfy constraints on structural load, which can depend for instance on the current turbine state of structural health. Furthermore, the present chapter will pave the way for the design of a wind farm power allocation control scheme, where healthy turbines can be assigned a larger demanded power to compensate for reductions in turbines that operate at their maximum allowed structural load.

3.1.2. CONTROL ARCHITECTURE

This section presents the proposed switching control architecture for load constraining. First an overview of the architecture will be given. Then, the individual constituting blocks, namely the thrust estimator, the thrust tracking controller, the switching law, and the demanded power down regulator will be described.

OVERVIEW OF THE ARCHITECTURE

The overall switching control architecture is presented in Figure 3.1, where we assume that external references $P^{\text{ref}} \in \mathbb{R}^+$ and $F_T^{\text{ref}} \in \mathbb{R}^+$ are provided for, respectively, the power to be generated by the given wind turbine and the maximum allowed fore-aft thrust forces. Starting from left, we can identify the following functional blocks:

1. The *power down-regulator* \mathcal{D} , which can track a demanded power $P^{\text{dem}} \leq P^{\text{av}}$, where P^{av} is the available aerodynamic power. \mathcal{D} provides to the turbine a reference θ^{ref} and τ_g^{ref} for, respectively, the collective blade pitch and the generator torque (see Section 3.1.2).
2. The *wind turbine*, which accepts as inputs the references θ^{ref} and τ_g^{ref} and provides the output measurements $\omega_{r,\text{meas}}$, $\tau_{g,\text{meas}}$ and θ_{meas} representing the rotor speed, generator torque and the collective blade pitch angle, respectively.

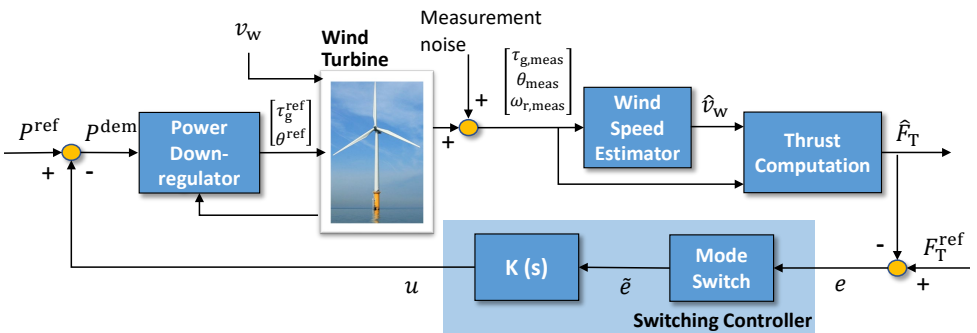


Figure 3.1: Block diagram of the proposed switching control architecture for constraining the turbine thrust forces. The novel switching controller is highlighted in light blue.

3. The *wind speed estimator*, which uses the measurements $\omega_{r,\text{meas}}$ and θ_{meas} to compute an estimate \hat{v}_w of the rotor effective wind speed v_w . As in the present work we do not assume to have a reliable wind speed measurement, so the Immersion and Invariance (I&I) wind speed estimator of [98] will be used.
4. The *thrust computation* block, which uses the wind speed estimate \hat{v}_w , $\omega_{r,\text{meas}}$ and θ_{meas} to compute an estimate of the fore-aft thrust force \hat{F}_T .
5. The *mode switch* block, which together with the transfer function $K(s)$ constitutes the novel *switching controller* for tracking the thrust force. The output of $K(s)$ is the signal u , which is subtracted from the external reference P^{ref} to obtain the demanded power $P^{\text{dem}} = P^{\text{ref}} - u$.

In order to derive the proposed switching controller, we will introduce the following

Assumption 1. *The down-regulation controller and wind speed estimator are asymptotically stable, as in [36, 63, 98].*

Assumption 2. *The dynamics from the demanded power to thrust force are represented by a first-order linear model as*

$$\frac{F_T(s)}{P^{\text{dem}}(s)} = \frac{A}{s+B} \stackrel{\text{def}}{=} G(s). \quad (3.1)$$

Remark 1. *As Assumption 1 holds, in steady conditions both generated power and thrust force will converge to a constant value. Short-term transient behaviors in the turbine operation are not the focus of our controller. This justifies the use of Assumption 2 for representing the dominant behavior.*

We are now ready to introduce the control problem addressed in this first part of the chapter:

Problem 1. *Design a feedback control law that extends, rather than replacing, the existing demanded power controller \mathcal{D} such that:*

1. *the fore-aft thrust force F_T does not exceed a user defined upper bound \bar{F}_T ;*
2. *the tracking performance of the desired power reference P^{ref} is unaltered whenever $F_T \leq \bar{F}_T$.*

The next subsection introduces the novel *switching controller* developed in this chapter.

SWITCHING CONTROLLER DESIGN

This section describes the design of the Mode Switch and the transfer function $K(s)$ introduced in previous subsection, towards solving the control problem posed in Problem 1.

The first observation is that, in order to satisfy point 2 in Problem 1, it is sufficient that the signal u becomes zero, and thus $P^{\text{dem}} = P^{\text{ref}}$. In order to do this, the Mode Switch will be designed such that the lower feedback loop in Figure 3.1 will be open whenever the

constraint on the thrust force is not exceeded. In particular, the switching will be defined by introducing the following signal

$$\tilde{e} = \begin{cases} e, & \text{if } e < 0 \text{ or } e_1 < 0 \\ 0, & \text{otherwise} \end{cases} \quad (3.2)$$

where $e = F_T^{\text{ref}} - \hat{F}_T$ and $e_1 = \int_0^t e(\tau) d\tau$ represent, the difference between the estimated thrust force and its reference, herein set as equal to the upper bound, i.e. $F_T^{\text{ref}} = \bar{F}_T$, and the time integral of that, respectively. The rationale for this definition with the inclusion of the integral term is to avoid *chattering* when the thrust force is close to its reference, as is done for instance in the literature on Integral Sliding Mode control [83].

When the mode switch is active, that is when $\tilde{e} \neq 0$, the lower feedback loop involving the transfer function $K(s)$ is closed. The design of $K(s)$, outlined in the subsequent part, will thus determine the fulfillment of requirement 1 in Problem 1.

The approach is to design $K(s)$ such that \hat{F}_T will track its reference F_T^{ref} . From this point of view, notice that variations of the power reference and wind speed also contribute to the thrust response. As such, P^{ref} and v_w are considered disturbances acting into the system. This said, the thrust response can be written in the Laplace domain as

$$F_T(s) = -G(s)u(s) + G_{d,1}(s)P^{\text{ref}}(s) + G_{d,2}(s)v_w(s), \text{ where} \quad (3.3)$$

$$u(s) = -K(s)\tilde{e}(s) = -K(s)\left(F_T^{\text{ref}}(s) - F_T(s) - n(s)\right). \quad (3.4)$$

$G(s)$ represents the transfer function of the join *power down-regulator* and *wind turbine* from the considered demanded power P^{dem} input and the thrust F_T output. $G_{d,1}(s) = G(s)$ from P^{ref} to F_T and $G_{d,2}(s)$ from v_w to F_T are the transfer functions from the considered disturbances on the down-regulated turbine. Furthermore, $n(s) = F_T(s) - \hat{F}_T(s)$ represents the estimation error between the true thrust and the estimated one (cfr. Section 3.1.2).

Substituting Eq. (3.4) into Eq. (3.3), and reorganizing the terms we have the closed-loop response as

$$\begin{aligned} F_T(s) &= \frac{K(s)G(s)}{1 + K(s)G(s)} F_T^{\text{ref}}(s) + \frac{G_{d,1}(s)}{1 + K(s)G(s)} P^{\text{ref}}(s) \\ &\quad + \frac{G_{d,2}(s)}{1 + K(s)G(s)} v_w(s) - \frac{K(s)G(s)}{1 + K(s)G(s)} n(s). \end{aligned} \quad (3.5)$$

The controller $K(s)$ should be designed to stabilize the poles of the closed-loop system, i.e. the roots of $1 + K(s)G(s) = 0$, and to guarantee steady-state convergence from changes in the reference, disturbances and estimation error. A PI controller is therefore chosen as an effective way to track the reference, to reject the disturbances and to attenuate the estimation error

$$K(s) = K_P + \frac{K_I}{s}. \quad (3.6)$$

The closed-loop characteristic equation is then equal to

$$s^2 + (B + K_P A)s + K_I A = s^2 + 2\zeta\omega_n s + \omega_n^2 = 0. \quad (3.7)$$

Proposition 1. *The steady-state thrust tracking error is bounded for steps in reference, disturbances and estimation error.*

Using Eq. (3.5), we can derive the thrust tracking error function

$$\begin{aligned} E(s) &= F_T(s) - F_T^{\text{ref}}(s) \\ &= \underbrace{(T(s) - 1) F_T^{\text{ref}}(s)}_{E_1(s)} + \underbrace{S(s) G_{d,1}(s) P^{\text{ref}}(s)}_{E_2(s)} + \underbrace{S(s) G_{d,2}(s) v_w(s)}_{E_3(s)} - \underbrace{T(s) n(s)}_{E_4(s)}, \end{aligned} \quad (3.8)$$

where $S(s) = 1/(1 + K(s)G(s))$ and $T(s) = K(s)G(s)/(1 + K(s)G(s))$ are the sensitivity and complementary sensitivity functions, respectively.

By the final value theorem, the state steady errors due to steps on F_T^{ref} , P^{ref} , v_w , and n can be computed for the proposed controller as

$$\begin{aligned} e_{ss,i} &= \lim_{t \rightarrow \infty} e_i(t) \\ &= \lim_{s \rightarrow 0} s E_i(s), \end{aligned} \quad (3.9)$$

where $i = 1, 2, 3, 4$.

By Assumption 1, $G_{d,1}(s)$ and $G_{d,2}(s)$ are stable functions, as well as the estimation error n is bounded. Therefore, the steady state error vector is $e_{ss} = [0, 0, 0, -T(0)]$ for steps on F_T^{ref} , P^{ref} , v_w , and n .

Remark 2. *The controller can be calibrated with an offset in to the thrust reference to take into account $e_{ss,4}$ if a constant bias in the thrust estimation exists. In addition, extra measurement devices can be used to improve the estimations and reduce the bias, such as the use of strain-gauges or accelerometers in the tower structure.*

Remark 3. *Deviations in the model from Assumption 2 can occur at different wind speeds given the non-linearity of the turbines, therefore it might degrade the designed controller performance. Nevertheless, as Assumption 1 and monotonicity from \mathcal{D} still hold, the tracking is kept, as well as steps from disturbances rejected and from noise attenuated, even though model uncertainties exist.*

THRUST COMPUTATION

The estimated average fore-aft thrust force, representing the aerodynamic loads, is computed by

$$\hat{F}_T = 0.5 \rho \pi R^2 \hat{v}_w^2 C_T \left(\frac{R \omega_{r,\text{meas}}}{\hat{v}_w}, \theta_{\text{meas}} \right), \quad (2.11)$$

where \hat{v}_w is the estimated effective wind speed, ρ the air density, R the rotor radius and C_T the thrust coefficient computed with the measured rotor speed $\omega_{r,\text{meas}}$ and collective blade pitch angle θ_{meas} . In this work, the estimation of the effective wind speed is obtained from the I&I estimator [98] through measurements of rotor speed, generator torque and blade pitch angles.

POWER DOWN-REGULATOR

For the down-regulator \mathcal{D} the APC pitch approach [36, 63] is adopted in this work, because of the following characteristics:

- A monotonic thrust reduction in response to monotonic demanded power reduction is achieved;
- Operation close to the min- C_T method, see Fig. 3.2;
- Stability margin for the stall region [74].

The turbine is down-regulated using the blade pitch controller, which consists of a gain-scheduled PI control law

$$\theta(s) = \bar{K}_P(\theta_{\text{meas}}) \left[\omega_{g,\text{meas}} - \omega_g^{\text{ref}}(P^{\text{dem}}) \right] + \frac{\bar{K}_I(\theta_{\text{meas}})}{s} \left[\omega_{g,\text{meas}} - \omega_g^{\text{ref}}(P^{\text{dem}}) \right], \quad (2.1)$$

where $\omega_{g,\text{meas}}$ and θ_{meas} are the measured generator speed and the measured collective blade pitch angle, respectively. The reference generator speed as function of the demanded power P^{dem} is represented by $\omega_g^{\text{ref}}(P^{\text{dem}})$. $\bar{K}_P(\theta_{\text{meas}})$ and $\bar{K}_I(\theta_{\text{meas}})$ are the gain-scheduled proportional and integral gains [75]. While the generator torque controller is applied to track the demanded power by multiplying it by the inverse of the measured generator speed as

$$\tau_g = \frac{P^{\text{dem}}}{\eta_{\text{eff}} \omega_{g,\text{meas}}}. \quad (2.2)$$

Both controllers are applied whenever the demanded power is lower than the rated power, and the measured generator speed is higher than the reference generator speed or the blade pitch angle is higher than a switch blade pitch angle. Otherwise, the turbine follows the conventional turbine controllers [75].

3.1.3. SIMULATION

The proposed control architecture is evaluated in SOWFA [53]. In this first part of the chapter, the actuator line method is implemented using the DTU 10MW reference wind turbine [88]. The control parameters of the controllers are based on the values provided

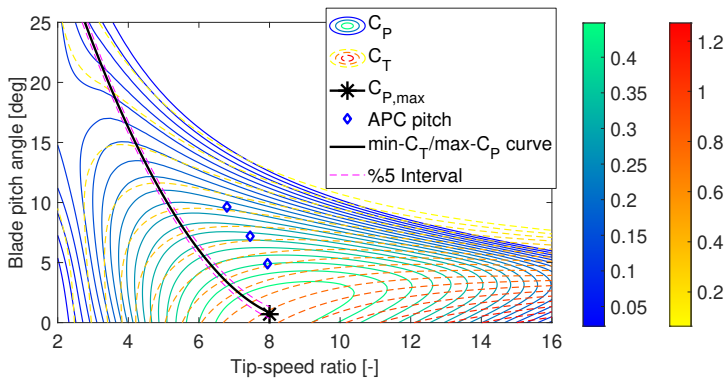


Figure 3.2: C_p and C_T of the operation points of “APC pitch” given a reduction in the demanded power (5, 4 and 3 MW) at 9 m/s wind speed and min- C_T /max- C_p curve for the DTU 10MW reference wind turbine.

Table 3.1: SOWFA simulation parameters

Property	Value
Sub-grid-scale model	One-equation eddy viscosity
Domain size	3 km × 3 km × 1 km
Cell size outer regions	10 m × 10 m × 10 m
Cell size near rotor	2.5 m × 2.5 m × 2.5 m
Simulation timestep	0.04 s
Atmospheric boundary layer stability	Neutral
Mean inflow wind speed	9 m/s
Turbulence intensity	0.0 and 5.0 %
Turbine rotor approximation	Actuator Line Model
Turbine type	DTU 10 MW
Turbine rotor diameter	178.3 m
Turbine hub height	119 m
Blade smearing factor	5.0 m

with the NREL's Reference OpenSource Controller (ROSCO) [75]. An overview of the parameters for the SOWFA simulations is shown in Table 3.1.

At a mean wind speed of 9 m/s (i.e. below rated wind speed), the first-order model from Eq. (3.1) was identified from down-regulating 3 to 4 MW of power using the thrust step response, see Fig. 3.3. The model parameters were identified as $A = 0.068$ and $B = 0.625$. By considering a simple first-order model, only the dominant dynamic behavior is captured. For the controller design, we choose $K_P = 0$ and a damping coefficient $\zeta = 0.7$, then $\omega_n = 0.446$ and $K_I = 2.947$. As is seen in Fig. 3.4, the integrator is sufficient to add tracking and robustness to the plant from G to $L = KG$, where the disturbances are reduced and the estimation error is attenuated, as shown by S and T . The controller provides an infinity gain margin and a phase margin of 65.2 degrees at a frequency of 0.047 Hz for the identified model. Up to 99% of tracking until frequencies of 0.2 Hz and at least 90.9%

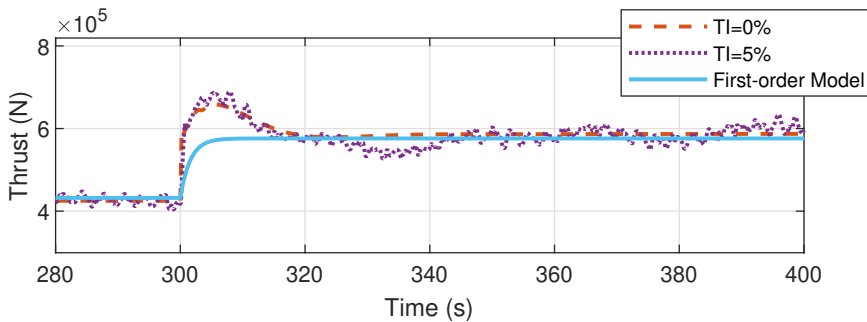


Figure 3.3: Thrust response of a step demanded power from 3 to 4 MW at 9 m/s with the down-regulator \mathcal{D} defined in Section 3.1.2.

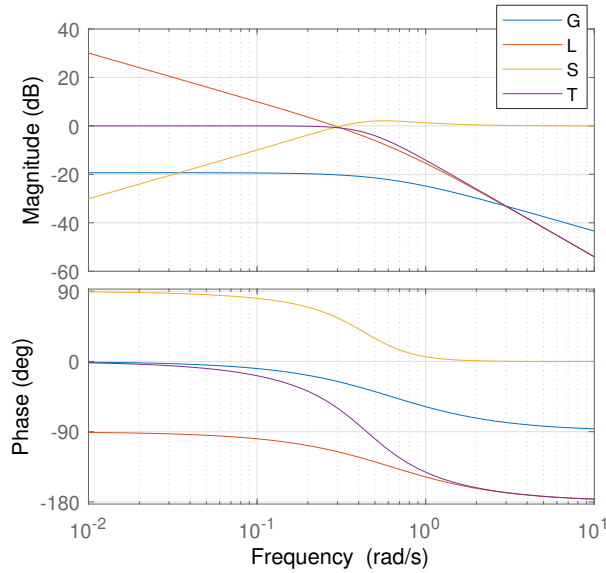


Figure 3.4: Bode magnitude and phase plots of $L(s)=G(s)K(s)$, $S(s)$ and $T(s)$ for $G(s) = 0.067625/s+0.625$ and $K(s)=2.947/s$. The crossover frequencies 0.2 Hz and 7.16 Hz of L at +20dB and -20dB are considerably high and low, respectively. Meaning high tracking robustness and disturbance rejection [99].

of reduction for frequencies greater than 7.16 Hz (from the crossover frequencies of L at ± 20 dB).

The simulations were performed by feeding a reference power signal below the available power based on the normalized standard test signal [89]. The results of the thrust tracking controller are presented in Figs. 3.5 and 3.6, using a uniform wind inflow and a turbulent one, respectively. As the maximum thrust is about 512 kN by just tracking power, the thrust references were accordingly set as 500, 475, 450, 425 kN for the uniform inflow case. The results shown in Table 3.2 present a roughly linear relation between the percentage of the maximum power loss and the percentage of reduction of thrust in the case studies.

The proposed control architecture was able to track the computed thrust sufficiently, even though oscillations appear in the thrust force. These oscillations are due to the tower effect characterized by the blade passing frequency (3P) and to the inflow wind profile reproduced by SOWFA. They are partially accommodated by the adopted wind speed estimator and thrust computation. In addition, the proposed integral switching law presents robustness against chattering and smooth transitions.

3.1.4. CONCLUSIONS AND DISCUSSION

A closed-loop switching control architecture for addressing aerodynamic load constraints on wind turbines is presented. The framework makes use of down-regulation and wind speed estimations. The proposed architecture effectively limits the aerodynamic loads,

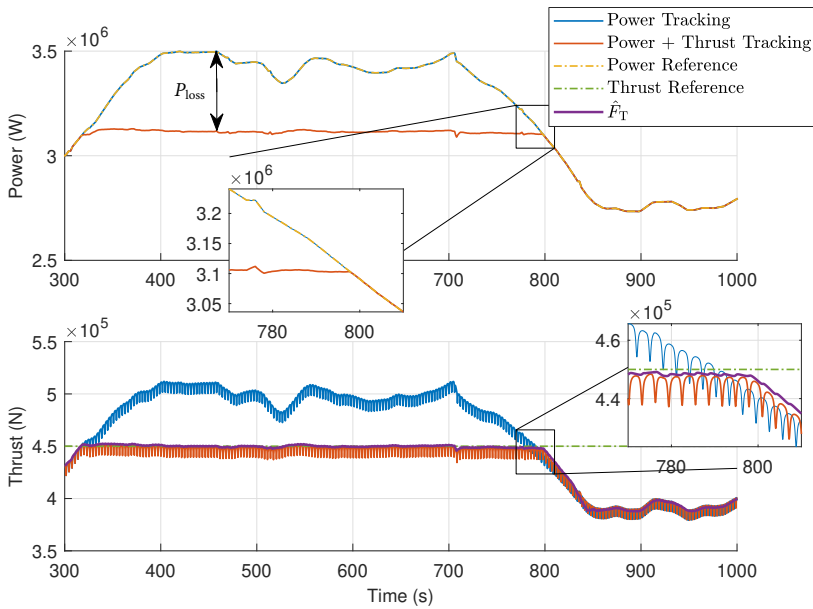


Figure 3.5: Power and thrust of the simulations with no turbulence. Thrust tracking with reference of 450 kN.

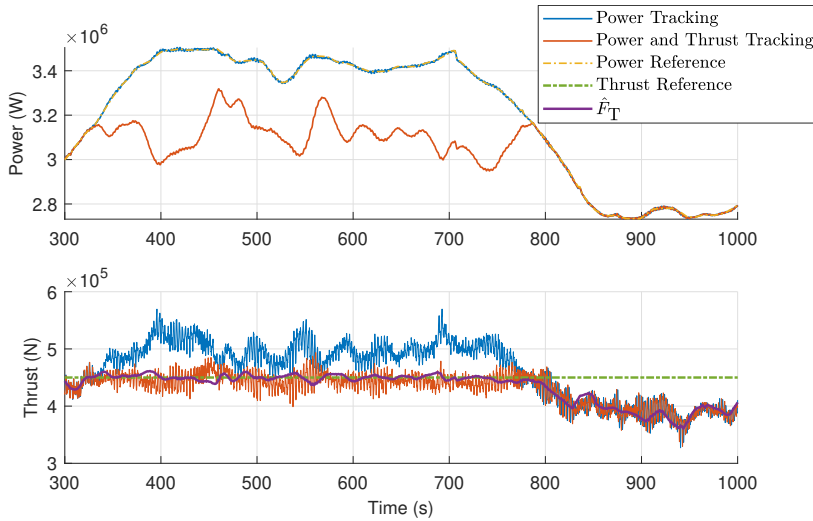


Figure 3.6: Power and thrust of the simulations with turbulence (turbulence intensity of 5%). Thrust tracking with reference of 450 kN

where the appropriate user-defined constraint would ensure the safety of the system. In fact, such approaches present an undesirable loss in power generation but they can be acceptable from a farm-wide perspective. Therefore, the proposed architecture aims to prevent me-

Table 3.2: Power loss as a function of the thrust reference

Thrust reference [kN]	Percentage of thrust reduction [%]	Maximum power loss [MW]	Percentage of power reduction [%]
500	2.35	0.0750	2.1
475	7.23	0.2175	6.2
450	12.12	0.3826	10.9
425	16.99	0.5382	15.4

chanical structures from failure and their associated costs by avoiding high stresses from the aerodynamic loads. Also, this can lead to a profit from keeping turbines operating in non-designed conditions, such as corroded structures.

Future work will focus on the development and the performance of model predictive controllers for down-regulation purposes, aiming to avoid unstable flow behaviors and oscillations in response signals and expand the present framework to farm simulations.

3.2. CONVEX MODEL PREDICTIVE CONTROL

Wind turbine (WT) controllers are often geared towards maximum power extraction, while suitable operating constraints should be guaranteed such that WT components are protected from failures. Control strategies can also be devised to reduce the generated power, for instance to track a power reference provided by the grid operator. They are called down-regulation strategies and allow to balance power generation and grid loads, as well as to provide ancillary grid services, such as frequency regulation. Although this balance is limited by the wind availability and grid demand, the quality of wind energy can be improved by introducing down-regulation strategies that make use of the kinetic energy of the turbine dynamics. This second part of the chapter shows how the kinetic energy in the rotating components of turbines can be used as an additional degree-of-freedom by different down-regulation strategies. In particular we explore the power tracking problem based on convex MPC at a single wind turbine. The use of MPC allows us to introduce a further constraint that guarantees flow stability and avoids stall conditions. Simulation results are used to illustrate the performance of the developed down-regulation strategies. Notably, by maximizing rotor speeds, and thus kinetic energy, the turbine can still temporarily guarantee tracking of a given power reference even when occasional saturation of the available wind power occurs. In the study case we proved that our approach can guarantee power tracking in saturated conditions for 10 times longer than with traditional down-regulation strategies.

3.2.1. INTRODUCTION

In the transition to renewable energy sources, several countries reached a penetration level of renewable generation of more than 15% of their overall power-generation mix. Many of them (e.g., Spain, Portugal, Ireland, Germany, Denmark and the United States) have already crossed this threshold significantly, and experienced instantaneous penetration levels higher than 50% [100]. Due to such significant contribution of renewable energy sources, including wind power, grid operators are increasing their demand for ancillary services to be provided by wind turbines (WTs).

In particular, grid operators can make use of so-called *Active Power Control (APC)* to request turbines to provide a given reference power output [12]. The power reference command sent to all generators will guarantee that, at grid level, supply and demand are balanced and grid frequency is stabilized. As the power that a WT can generate is upper bounded by the available power in the incoming wind flow, WTs can only be *down-regulated*, that is operate in a way to track a power reference that is lower than the theoretical available maximum. Due to the nonlinearities present in the dynamics of WTs, several down-regulation methodologies that achieve power tracking are possible [20, 26, 41].

Still, existing down-regulation strategies were developed for steady state conditions only, and cannot directly take into account available information on changing wind conditions, such as those provided by short time weather forecasts or LIDAR measurements. Furthermore, they do not accommodate directly the need to minimize structural loads on the WT, which on the long period can lead to premature failures.

In order to address these challenges, in this chapter we propose a down-regulation approach based on convex MPC. We will show how all the major down-regulation strategies present in the literature can be implemented with the proposed MPC approach. Furthermore, we will introduce a novel down-regulation strategy based on the maximization of

kinetic energy, and show its benefits in guaranteeing power tracking also during occasional periods of saturation, when the reference power from the grid is larger than the available power in the wind flow.

MPC approaches have already demonstrated their potential in several works on wind turbine and wind farm [101] control. An MPC formulation based on power flow and energy was presented in [102], while [103] and [104] have extended it by including the tower flexural model and by considering the presence of faults, respectively. By assuming the knowledge of future demanded power and wind variations, in [105] the authors are able to damp grid frequency oscillations by storing and releasing the WT kinetic energy. The use of kinetic energy as an energy reserve for grid stabilization is also explored in [106], where power generation can be increased by temporarily supplying kinetic energy from the rotor. To the best of the authors' knowledge, anyway, no work did consider the problem of promoting flow stability on the WT blades during down regulation. Indeed operating in low flow stability regions can lead to rotor speed oscillations, undesirable turbine responses and ultimately cause stall conditions [26].

The contribution of this second part of the chapter is three fold.

- We develop a general convex MPC framework for power tracking on wind turbines which includes the kinetic energy as a degree of freedom;
- We extend the cost function in order to minimize aerodynamic loads, and add a constraint that enforces flow stability;
- We present a simulation study based on the NREL 5 MW WT [77] and compare different down-regulation strategies under saturated conditions in OpenFAST [47].

A key ingredient for obtaining a convex MPC formulation in the present case is to use a linear model of the WT dynamics, expressed in energy form. Such form allows to remove the non-linear relationship among rotor speed, blade pitch angles, and wind speed from the optimization problem. The aerodynamic rotor power is then chosen as an optimisation variable, which is constrained by a piecewise affine approximation of the available wind power. This formulation allows naturally to include the kinetic energy as a degree of freedom and leads to a linear optimization problem. Due to this freedom, an extra objective can be added to the optimization problem and thus recover the different existing down-regulation strategies. Finally, we show how to avoid stall conditions by implementing a further linearized constraint. As will be seen in the simulation results, the time period during which the demanded power is tracked, by maximizing kinetic energy, can be up to ten times longer with respect to other down-regulation strategies.

3.2.2. CONTROL ARCHITECTURE

WIND TURBINE MODEL

The non-linear wind turbine dynamics can be modelled using the rotor torque balance equation. By considering a rigid shaft and neglecting losses, this leads to the following model.

$$\dot{\omega}_g(t) = \frac{1}{J} \left[\frac{1}{G_B} T_r(t) - T_g(t) \right], \quad (3.10)$$

where J is the equivalent moment of inertia of the rotor-generator-drive-train assembly referred to the high speed shaft, $\dot{\omega}_g(t)$ the generator acceleration, $T_r(t)$ the aerodynamic torque, G_B the gearbox ratio and $T_g(t)$ the generator torque.

The non-linearity due to the aerodynamic torque relation can be expressed as

$$T_r(t) = \frac{0.5}{\omega_r(t)} \rho A_r v^3(t) C_p(\lambda(t), \theta(t)) \quad (3.11a)$$

$$= \Phi(v(t), \omega_r(t), \theta(t)) v^3(t) / \omega_r(t) \quad (3.11b)$$

$$= 0.5 \rho A_r R v^2(t) C_Q(\lambda(t), \theta(t)), \quad (3.11c)$$

where ρ the air density, A_r the rotor area, $\theta(t)$ the collective blade-pitch angle, and $\lambda(t) = R\omega_r(t)/v(t)$ is the tip-speed ratio, being R the rotor radius and $\omega_r(t) = \omega_g(t)/G_B$ the rotor speed. The representation in (3.11a) is as function of the power coefficient $C_p(\lambda(t), \theta(t))$. In (3.11b), instead the function $\Phi(v(t), \omega_r(t), \theta(t)) = 0.5 \rho A_r C_p(\lambda(t), \theta(t))$ is defined. Finally, the rotor torque in (3.11c) is a function of the torque coefficient $C_Q(\lambda(t), \theta(t))$, where it holds $C_Q(\lambda(t), \theta(t)) = C_p(\lambda(t), \theta(t)) / \lambda(t)$.

The collective blade pitch angle, generator speed and torque are limited by their upper and lower bounds as follows:

$$\theta_{\min} \leq \theta(t) \leq \theta_{\max}; \quad (3.12a)$$

$$\omega_{g,\min} \leq \omega_g(t) \leq \omega_{g,\max}; \quad (3.12b)$$

$$0 \leq T_g(t) \leq T_{g,\max}. \quad (3.12c)$$

The aerodynamic power extracted from the wind by the rotor is given as

$$P_r(t) = T_r(t) \omega_r(t) = 0.5 \rho A_r v^3(t) C_p(\lambda(t), \theta(t)), \quad (3.13)$$

while the electrical generator power is given by

$$P_g(t) = \eta_g T_g(t) \omega_g(t), \quad (3.14)$$

where η_g is the generator efficiency.

The electrical generator power is constrained by

$$0 \leq P_g(t) \leq P_{g,\text{rated}}, \quad (3.15)$$

where $P_{g,\text{rated}}$ is the rated generator power.

In terms of power flow and energy, the dynamics in (3.10) is rewritten as

$$\dot{K}(t) = P_r(t) - \frac{1}{\eta_g} P_g(t), \quad (3.16)$$

where $K(t)$ is the kinetic energy stored in the rotating components and relates to the generator speed as

$$K(t) = \frac{J \omega_g^2(t)}{2}. \quad (3.17)$$

In the proposed convex MPC formulation, P_r and P_g in (3.16) are chosen to be the decision variables. The set of constraints in (3.12) needs then to be rewritten as a function of P_r and

P_g and K as well, as the latter depends on the former via the system dynamics (3.16). Note that the transformed constraints should be also convex to lead to a convex problem [107]. Using (3.17) and (3.14), the rotor speed and generator torque constraints from (3.12b) and (3.12c) can be expressed respectively as

$$(J/2)\omega_{g,\min}^2 \leq K(t) \leq (J/2)\omega_{g,\max}^2 \quad (3.18)$$

$$0 \leq P_g(t) \leq \eta_g \sqrt{(2/J)K(t)} T_{g,\max}. \quad (3.19)$$

Since $\sqrt{(2/J)K(t)}$ is a concave function, (3.19) is a convex constraint on $P_g(t)$ and $K(t)$. Defining the available power as

$$P_{av}(v, K) = \max_{\theta_{\min} \leq \theta \leq \theta_{\max}} \Phi(v, (1/G_B) \sqrt{(2/J)K}, \theta) v^3,$$

the aerodynamic rotor power constraint is set as

$$P_r(t) \leq P_{av}(v(t), K(t)). \quad (3.20)$$

This includes the constraint (3.12a) in the formulation.

For a range of wind speeds and blade pitch angles and realistic Φ functions, the available power turns out to be a concave function of K . Therefore, by fitting k piecewise affine functions [108], the available power can be approximated as

$$\hat{P}_{av, v_i}(K(t)) = \min\{a_1 K(t) + b_1, \dots, a_k K(t) + b_k\} v_i^3,$$

where a linear interpolation is done between different wind speeds to obtain $\hat{P}_{av}(v(t), K(t))$.

$$\hat{P}_{av}(v(t), K(t)) = (1 - \Theta) \hat{P}_{av, v_1}(K(t)) + \Theta \hat{P}_{av, v_2}(K(t)), \quad (3.21)$$

with $\Theta = \frac{v(t) - v_1}{v_2 - v_1}$. The linear interpolation of concave functions results in a concave function.

The thrust force, which presents another non-linear behavior, is modelled as

$$F_T(t) = 0.5 \rho A_r v^2(t) C_T(\lambda(t), \theta(t)), \quad (3.22)$$

where C_T is the thrust coefficient.

In order to develop the down-regulation strategy that minimizes thrust force, we approximate the thrust force through a linearization with respect to the aerodynamic rotor power and kinetic energy by assuming the knowledge of the wind speed at each time-step as follows.

First, the power and thrust coefficients are expressed with a first-order Taylor series expression around the current kinetic energy K^* and blade pitch angle θ^* ,

$$\begin{aligned} C_P(K(t), \theta(t)) &\approx C_P(K^*, \theta^*) + \left. \frac{\partial C_P}{\partial K} \right|_{K^*, \theta^*} (K(t) - K^*) + \left. \frac{\partial C_P}{\partial \theta} \right|_{K^*, \theta^*} (\theta(t) - \theta^*) \\ &= q_P(t) \theta(t) + r_P(t) K(t) + s_P(t), \end{aligned} \quad (3.23)$$

$$\begin{aligned}
C_T(K(t), \theta(t)) &\approx C_T(K^*, \theta^*) + \left. \frac{\partial C_T}{\partial K} \right|_{K^*, \theta^*} (K(t) - K^*) + \left. \frac{\partial C_T}{\partial \theta} \right|_{K^*, \theta^*} (\theta(t) - \theta^*) \\
&= q_T(t)\theta(t) + r_T(t)K(t) + s_T(t),
\end{aligned} \tag{3.24}$$

where $q_P(t)$, $r_P(t)$, $s_P(t)$, $q_T(t)$, $r_T(t)$ and $s_T(t)$ are the corresponding time-varying parameters.

Then, combining (3.23) with (3.13) and (3.24) with (3.22), and eliminating the collective blade pitch angle, an affine relationship can be derived at each time step as

$$\hat{F}_T(t) = Q_{F_T}(t)P_T(t) + R_{F_T}(t)K(t) + S_{F_T}(t), \tag{3.25}$$

$$\begin{aligned}
\text{with } Q_{F_T}(t) &= \left(\frac{q_T(t)}{q_P(t)v(t)} \right), R_{F_T}(t) = 0.5\rho A_r v(t)^2 \left(r_T(t) - r_P(t) \frac{q_T(t)}{q_P(t)} \right), \text{ and} \\
S_{F_T}(t) &= 0.5\rho A_r v(t)^2 \left(s_T(t) - s_P(t) \frac{q_T(t)}{q_P(t)} \right).
\end{aligned}$$

DOWN-REGULATION

As discussed earlier, there are several practical benefits in being able to down-regulate turbines to track a specific demanded power from the grid. However, there are multiple control solutions to down-regulate wind turbines. In Table 3.3, the main strategies from the literature are summarized and qualitatively compared in terms of their capabilities to track a power reference, reduce structural loads and guarantee flow stability.

Table 3.3: Qualitative categorization of down-regulation strategies

Strategies	Power tracking	Structure Loads	Flow stability
Maximum ω_r	High	High	Low
Minimum C_T	Low	Low	Low
Constant λ	Medium	Medium	High
Constant ω_r	Depending on the ω_r value	Depending on the ω_r value	Low

3.2.3. THE DEGREE OF FREEDOM ON KINETIC ENERGY

The possibility of having multiple down-regulation strategies is a consequence of the following:

Proposition 2. *There exist a non-unique steady state operating condition when a power demand is below the maximum available power.*

Proof. Lets then assume a steady state condition with power demand and inflow wind as being $P_{\text{dem,ss}}$ and v_{ss} , respectively. Also, consider the down-regulation of a turbine to be asymptotic stable by feedback [109, 12], meaning that as $t \rightarrow \infty$ the demanded power flow tends to be reached by the generator, and the derivative of the kinetic energy from Eq. (3.16)

tends to zero in a steady state condition. Then, the following equation would hold near to an equilibrium.

$$0 \approx P_r(t) - \frac{1}{\eta_g} P_{\text{dem,ss}}(t), \quad (3.26)$$

From combining (3.26) with (3.13)

$$\frac{1}{\eta_g} P_{\text{dem,ss}} \approx 0.5 \rho A_r v_{\text{ss}}^3 C_P \left(\frac{\omega_r(t) R}{v_{\text{ss}}}, \theta(t) \right). \quad (3.27)$$

Therefore, as depicted by the C_P contours in Fig 3.7, a desired C_P value lower than the maximum C_P can be reached by different combinations of λ and θ . \square

Remark 4. *The fact that different combinations of λ are possible means that there is an extra degree of freedom on choosing a desired rotational speed and, thus, a kinetic energy. This will indeed be leveraged to reduce aerodynamic loads and the risk of stall conditions.*

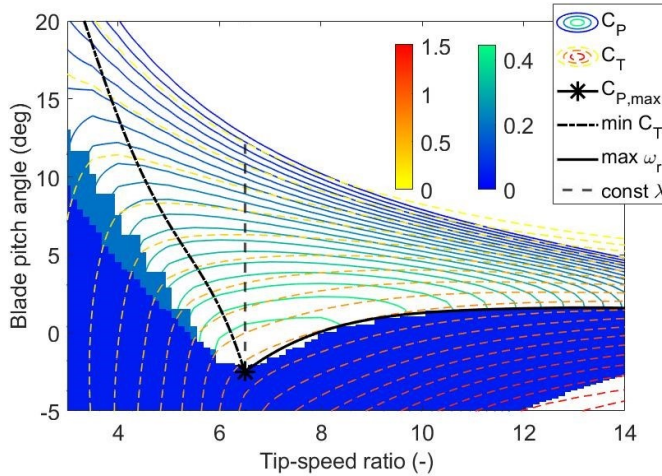


Figure 3.7: Operation curves of down-regulation methods and stall regions of an NREL 5MW turbine. The shades of bright and dim blue colors correspond to $\partial C_Q(\lambda, \theta) / \partial \theta > 0$ and $\partial C_Q(\lambda, \theta) / \partial \omega_r > 0$, respectively, characterizing the stall regions.

3.2.4. FLOW STABILITY

A current problem occurring when down-regulating turbines is due to the risk of loss of flow stability along the blades. This phenomenon, which can occur in low and high tip speed ratios, can lead to undesirable oscillations [110] and stall and is thus problematic for the design of turbine control.

Stall is characterized by the decrease of lift force on turbine blades as function of their angle of attack [9]. When the turbine is operating in a region where the derivatives of the aerodynamic torque with respect to rotor speed and pitch angle are positive, then it will eventually reach stall conditions [111, 74, 112]. These regions are shown by the blue

shades in Fig. 3.7 when the partial derivatives of the torque coefficient C_Q are positive, thus indicating the possible onset of stall.

In particular, each down-regulation method can be analyzed in terms of flow stability from their operation distance with respect to stall regions. First, the constant ω_r strategy can easily reach stall regions with low or high tip speed ratios depending on wind speed. From the same point of view, the maximum ω_r strategy operates on the boundary of the stall pitch region. The minimum C_T strategy is categorized as low flow stability as its operation is close to stall regions at low tip-speed ratios. Finally, the constant λ always remains far from stall regions, being the strategy that operates under the most stable flow conditions.

Remark 5. *The flow stability analysis herein is based on a steady state model. Dynamic flow effects and model-plant mismatches introduce a considerable uncertainty on the stall conditions. Conservative stall constraints should therefore be considered to avoid such regions.*

3.2.5. THE USE OF KINETIC ENERGY

On one hand, the high kinetic energy is beneficial for power tracking, for instance, in the case where the demanded power exceeds the current maximum available power in the wind. In that case, the stored kinetic energy on the rotor speed is released so power tracking can be maintained longer. On the other hand, high rotor speeds may lead to operation conditions close to stall regions and to higher aerodynamic loads as seen by the max ω_r curve and the C_T contours in Fig. 3.7. In this regard, the different down-regulation strategies are further explored in Section 3.2.7 in the convex MPC framework.

3.2.6. CONVEX MODEL PREDICTIVE CONTROL FORMULATION

Convex MPC is based on solving a convex optimization problem and is supported by a fairly complete body of research. Convex MPC can be solved numerically very efficiently, making it suitable to several applications.

The down-regulation in wind turbines is here formulated as an optimization problem based on the linear dynamics and convex constraints defined in Section 3.2.2. Different from previous works, such as [102], the turbine herein is set to track a demanded power instead of maximizing power extraction. As consequence of Proposition 2, a down-regulation operation is not uniquely defined, so an extra objective is added corresponding to the chosen down-regulation methodology.

First, we define the extra objectives - in Table 3.4- and corresponding additional constraints in terms of energy and power flows. Then, further the flow stability constrain is derived. In the end, the general optimization problem is defined for all down-regulation strategies.

The minimum C_T strategy is equivalent to minimize the thrust force $F_T(t)$, which is also equivalent to minimize the term $R_{F_T}K$ from Eq. (3.25) while the rotor power P_T would match its associated power reference. R_{F_T} is a time-varying parameter, which depends on the current operation point, so an extra variable $F_{T,extra}$ is instead minimized by including the following constraints:

$$(R_{F_T}K)'R_{F_T}K \leq F_{T,extra}, \quad (3.28)$$

$$F_{T,extra} \geq 0, \quad (3.29)$$

Table 3.4: Down-regulation strategies and equivalent objectives

Down-regulation Strategy	Equivalent Objective	Weights for (3.36) [$\alpha_5, \alpha_6, \alpha_7$]
Maximum ω_r	Maximizing $K(t)$	[$\alpha_5, 0, 0$]
Minimum C_T	Minimizing $F_T(t)$ from (3.25)	[$0, 0, \alpha_7$]
Constant λ^{opt}	Tracking $K^{\text{ref}}(t)$	[$0, \alpha_6, 0$]
Constant ω_r	Tracking constant K^{ref}	[$0, \alpha_6, 0$]

where the term $R_{F_T}K$ is therefore indirectly minimized based on the robust linear program [107]. This is done because the term $R_{F_T}K$ is composed by a time-varying parameter, instead of a constant, and a decision variable.

To obtain the constant λ^{opt} strategy, the kinetic energy is set to track the following reference:

$$K^{\text{ref}}(t) = \frac{J(\omega_g^{\text{ref}}(t))^2}{2}, \quad (3.30)$$

where

$$\omega_g^{\text{ref}}(t) = \frac{\lambda^{\text{opt}} \nu(t)}{R} G_B. \quad (3.31)$$

Now, a time-varying inequality that includes a positive tuning parameter δ is introduced to constrain the turbine operation out of the stall region as

$$\frac{\partial T_r(t)}{\partial \theta(t)} \leq -\delta, \quad (3.32)$$

where, using (3.11c),

$$\frac{\partial T_r(t)}{\partial \theta(t)} = 0.5\rho A_r R \nu^2(t) \frac{\partial C_Q(\lambda(t), \theta(t))}{\partial \theta(t)}. \quad (3.33)$$

The value of $\partial T_r(t)/\partial \theta(t)$ expresses how safe the current WT operation is from stall conditions and it should be always negative as previously discussed in Subsection 3.2.4. The parameter $\delta > 0$ is recommended to be added to increase robustness as result of Remark 5, therefore conservatively preventing stall to happen.

Similar with the derivation of (3.25), the affine time-varying constraint that avoids stall regions can be obtained by the linearization of the power coefficient $C_P(K(t), \theta(t))$ and the derivative of the aerodynamic torque coefficient with respect to the blade pitch $\partial C_Q(K(t), \theta(t))/\partial \theta(t)$. Such that the following constraint is obtained:

$$\frac{\partial T_r(t)}{\partial \theta(t)} \approx Q_{T_r'}(t) P_r(t) + R_{T_r'}(t) K(t) + S_{T_r'}(t) \leq -\delta, \quad (3.34)$$

where $Q_{T_r'}(t)$, $R_{T_r'}(t)$ and $S_{T_r'}$ are the corresponding time-varying parameters. An affine function is always convex, so also is this constraint.

Finally, the cost function is defined as the integral of the objective function F over the time horizon T while considering the linear dynamic model from (3.16) and the defined

convex constraints from (3.18), (3.19), (3.20) and (3.34) over the receding horizon. Then, we have

$$\begin{aligned} \max_{U(t)} \int_t^{T+t} F(x(\tau), u(\tau)) d\tau, \forall t \geq 0, \\ \text{s.t. (3.16), (3.18), (3.19), (3.20), (3.34),} \end{aligned} \quad (3.35)$$

where the objective function F is defined as

$$\begin{aligned} F(x(t), u(t)) = & -\alpha_1 \left[P_g(t) - P^{\text{ref}}(t) \right]^2 - \alpha_2 \dot{P}_g^2(t) - \alpha_3 \dot{P}_r^2(t) \\ & - \alpha_4 \left[\max\{K(t) - \frac{J}{2} \omega_{g,\text{rated}}^2, 0\} \right] + \alpha_5 K(t) - \alpha_6 \left[K(t) - K^{\text{ref}}(t) \right]^2 - \alpha_7 F_{T,\text{extra}}(t). \end{aligned} \quad (3.36)$$

In the previous equations, it holds $x(t) = [K(t)]$, $u(t) = [P_r(t), P_g(t)]^\top$, and $U(t) = [u^\top(t), \dots, u^\top(t+T)]^\top$. For each down-regulation strategy, the corresponding weights for F are listed in Table 3.4, where $\alpha_5, \alpha_6, \alpha_7 \in \mathbb{R}_{>0}$. The additional constraints (3.28) and (3.29) for the minimum C_T strategy are set only when this strategy is chosen.

In the proposed formulation, the optimization problem can be solved globally using efficient algorithms [107]. At a defined sampling time T_s , the optimal solution for $U(t)$ as a vector sequence along the time horizon T is obtained whereby the first input of the sequence is used to compute the current turbine command. Then, the prediction horizon moves ahead to the next step time, from which the optimization is repeated.

In particular, given the values of P_r, P_g obtained from the MPC solution, we can obtain the blade pitch command from Eq. (3.13) as

$$\theta(P_r(t), K(t)) = \theta_{\text{table}} \left(\frac{P_r(t)}{0.5\rho A_r v^3(t)}, \frac{R\sqrt{(2/J)K(t)}}{v(t)} \right), \quad (3.37)$$

and the generator torque command from Eq. (3.14) as

$$T_g(P_g(t), K(t)) = \frac{P_g(t)}{\eta_g \sqrt{(2/J)K(t)}}. \quad (3.38)$$

3.2.7. SIMULATION

In this section, the performances of the controller with different down-regulation strategies described in the previous section are compared for the case where a time-varying demanded power exceeds the current maximum available power in the wind. The control parameters used in the OpenFAST simulations are in Table 3.5. The normalized standard test signal from [89] is used for the reference power as in [12], where the time-varying reference power signal is herein set to exceed the maximum available power. The maximum available power is derived from the simulated constant and uniform wind speed of 8 m/s, that is a representative average annual value in a wind plant site.

For each down-regulation strategies, the mean values of kinetic energy and aerodynamic loads are computed before the power reference increases at 300 s. The amount of time that turbines can track the required power after it becomes saturated is presented in Table 3.6. The turbine's power and reference are depicted in Fig. 3.8. The reference power in green

Table 3.5: Control parameters

Parameter	Value
Weights, α_i	[10 0.1 0.1 0.1 0.1 0.1 0.01]
Time horizon, T	20 s
Sampling time, T_s	0.2 s
Stall constraint parameter, δ	0

Table 3.6: Comparison of Controller Power Output Tracking and Previous Aerodynamic Loading

Down-regulation Strategy	Kinetic Energy (J) [before 300 s]	Mean Load (kN) [before 300 s]	Time of Power Tracking after Saturation (s)
Maximizing $K(t)$	4.8675e+07	306	40
Minimizing $\hat{F}_T(t)$	0.7689e+06	259	4
Tracking $K^{\text{ref}}(t)$	1.3750e+07	264	5
Tracking const. K^{ref}	1.5086e+07	266	9

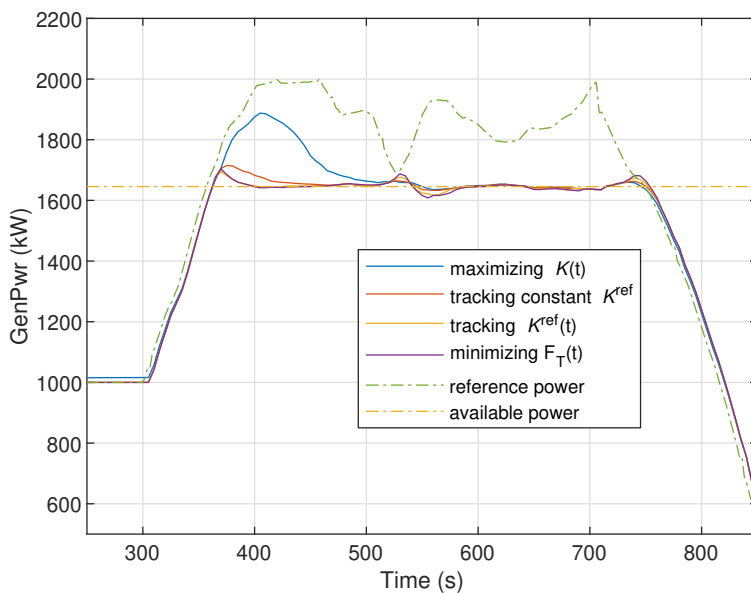


Figure 3.8: Active power signals (NREL 5MW).

is set to exceed the available power in orange. The generated powers from each down-regulation strategy present overshoots with respect to the available power when saturation

occurs due to the stored kinetic energy. The strategy that maximizes kinetic energy follows longer the reference power, although the turbine operates under higher aerodynamic loads.

3.2.8. CONCLUSIONS AND DISCUSSION

In this chapter, we proposed a linear convex MPC framework for implementing wind turbine down-regulation. Down-regulating a turbine leads to an additional degree of freedom on the value of the kinetic energy. We leveraged this and shown how different choices of the target kinetic energy can lead to existing down-regulation strategies. We further introduced a novel strategy aimed at reducing aerodynamic loads and reducing the risk of stall conditions. We have demonstrated the results of different down-regulation methodologies in terms of structural loading, flow stability and power tracking capability. Simulation on realistic models reveal the ability to maintain power tracking in saturation conditions, by means of the stored kinetic energy of the rotor.

The shifting paradigm from maximizing to tracking power and the use of kinetic energy as a storage presents a significant economic potential and encourages the research on active power control of wind turbines [109, 34]. As future work, the extension of the proposed MPC approach for the problem of power dispatch in wind farm control, and the effects of wakes, is of particular interest.

4

DISTRIBUTED WIND FARM CONTROL

Distribute to scale!

*It's important to have a sound idea,
but the really important thing is the implementation.*

Wilbur Ross

Chapter 2 presented controllers at the wind farm level. However, barriers emerge when implementing these controllers with a growing number of turbines and an expanding wind park size. These barriers include communication and computation issues. To address this concern, a distributed control approach is proposed and presented in this chapter. This approach achieves performance comparable to central controllers while utilizing constrained communication, relying on time-scale separation and consensus theory principles.

This chapter was submitted for publication and is under review.

4.1. INTRODUCTION

With the increasing share of renewable energy, concerns regarding ensuring power system stability are ever more relevant [16]. This demands further research in developing control algorithms that enable wind farm (WF) owners to effectively meet the requirements posed by future regulations. These regulations are evolving to support the seamless integration of WFs into power grids, moving from turbine power maximization to tracking [33, 113, 114]. Power tracking controllers [36, 63, 26] provide WF operators with tracking capabilities that are closer to those of conventional energy sources, enabling them to offer ancillary services to the grid [115, 34], including frequency regulation through frequency droop control schemes [116, 117]. The integration of wind energy into the grid is stipulated by specific grid codes in each country [37, 55]. In this work, we focus on active power control, which enables the provision of these services.

Additionally, power tracking controllers can be designed to simultaneously achieve secondary WF objectives, such as balancing structural loading [39, 72], thus permitting operators to better manage the WF's resources. We have proposed a WF controller that enhances power tracking capability and distributes the aerodynamic loading [54]. However, several challenges in WF control stem from the large number of involved WTs. Transmitting and receiving information from hundreds of WTs in a single node at a required rate is unfavorable. In addition, the computation effort required by controllers of large-scale WFs can be significantly high, as observed in centralized optimal controllers [14, 44, 118]. Therefore, facing applicability to large-scale WFs, we move from a centralized to a distributed control approach. Benefiting from the current turbine hardware, our proposed distributed control approach is implemented in individual WTs and resolves WF objectives by communicating only with neighbor WTs. Particularly, our distributed control approach distinguishes itself from others by consolidating all WF information at each WT before taking action.

4.1.1. A CENTRALIZED APPROACH AND ITS RELIANCE ON WAKE MODELING

As a wind turbine (WT) extracts energy from the wind, it reduces the downstream wind velocity and adds turbulence to the flow. The altered flow is called the wake of a WT. Under the wake, downstream WTs suffer from insufficient energy availability and additional loads [18]. When WTs are not capable of producing the required amount of power, i.e. the maximum power that can be produced is below the reference level set, we have the so-called turbine *saturation*.

Several design methods for WF controllers have been proposed in the literature, including those in [13, 109, 119], with strategies focusing on power maximization being tested in the field [28, 30]. Wake steering through yawing has been developed and utilized to maximize wind farm power output. However, in the context of on-demand energy, yaw misalignment could also be used to track a power demand, though it increases structural loads at the yawed turbine. Research in this area is still in its early stages [120, 121], along with emerging strategies, such as wake mixing [27]. Here, we manage the WF through the power distribution across the turbines, generally referred to as *axial induction control*, and account for wake effects while keeping the turbines aligned with the wind.

To design wind farm controllers, engineers and researchers have modeled the wind farm with analytical steady-state models [61]. However, these models can demonstrate

low accuracy through the validation by measurement data, as reported in [30]. The accurate modeling of wake effects is a nontrivial task to achieve because of the dynamic time-varying nature and uncertainty of the flow, for instance, induced by changes in atmospheric stability. The reliance on a wake model is therefore compromised. However, it is crucial to account for the wind flow interactions between WTs [12]. Instead of relying on WF models in open loop, we adopt a real-time feedback WF control framework to ensure that the WF meets its objectives according to its current conditions.

4.1.2. THE SHIFT FROM CENTRALIZED TO DISTRIBUTED CONTROLLERS

The implementation of centralized controllers in large-scale systems poses challenges, such as communication overhead, network topology constraints, and computation effort [122]. Additionally, central approaches are susceptible to a single point of failure and often lack flexibility to include new agents or remove failed ones without redesigning the controller, making them unsuitable for plug-and-play solutions. On the other hand, distributed control approaches, where networked local controllers are in charge of regulating parts of the entire farm, achieve *modularity* and *sparsity*. From an economic standpoint, distributed control systems are advantageous for large-scale WFs mainly attributed to the fact that each WT is not required to communicate to all other WTs, i.e. all-to-all communication, or a central computational unit that might be far apart. Therefore, equipping WTs with controllers capable of achieving global wind farm objectives can reduce significantly the costs associated with the required communication.

The future outlook for WF control envisions a shift toward decentralization, resembling the applications seen in micro-grids [123, 124] and power systems [125, 126, 127]. In [118] and [128], the authors propose algorithms to integrate the contribution of building energy systems and charging stations to the grid in a distributed manner. In [126] and [129], the authors proposed controllers for power systems going from a fully decentralized to a distributed control that results in an improvement in the damping of dominant oscillations. Moreover, robustness against failures in the control system can be achieved with distributed methods [130], in which local failures can be detected [131] and compensated for.

Among the first works towards distributed control in WFs are the works from Marden et al. [132] and Gebraad et al. [133]. In their works, the WT actions take into consideration their neighbor WTs. Avoiding a centralized controller, [134] and [135] maximize power production of the wind power plant using data-driven and learning approaches. In [136], the authors estimate the wind speed direction using an average consensus algorithm. Finally, coalitional control, a strategy where controllers are temporarily clustered into alliances, so-called *coalitions*, jointly achieve a control objective [122], applied to WFs in [44]. Also, clusters of turbines are identified in [137], which hinges on the correlation observed in the measured power signals, for yaw control.

Wind farm control is implemented with large sampling times because WTs should respond gradually to wind conditions. This approach helps prevent high-frequency signals from impacting the WTs, ensuring stable WT controllers. Additionally, the energy market generally does not demand immediate adjustments. However, this poses challenges for distributed WF controllers, as their convergence can be sluggish due to the distributed network topology and the extended sampling rates. As a result, responses to issues such as turbine saturation or failures may be delayed and inefficient.

4.1.3. OUR CONTRIBUTIONS

In this chapter, we design a distributed WF controller to achieve the following objectives:

- O1 Regulate the WF's active power generation to track a time-varying set point;
- O2 Distribute the WT power reference through the WF;
- O3 Achieve aerodynamic load balancing as a surrogate for structural loading.

To reduce the communication range while maintaining a lower WF control sampling rate and still attaining performance levels akin to centralized controllers [54], the WTs are suggested to engage in high-rate communication based on a multi-rate scheme [138, 139]. Our approach takes advantage of the low WF sampling rate and employs average consensus [140, 141] to estimate the entire WF information before taking action. This contrasts with typical distributed methods, such as the distributed averaging proportional and integral control [127] and the distributed model predictive control [42], that consider only the information of the neighbour turbines, i.e. partial information, to compute and implement local actions. Hence, we refer to our novel framework as multi-rate consensus-based distributed control (MCDC). The MCDC aims to achieve the objectives O1-O3 thereby counteracting power losses mainly attributed to wake effects and reaching balance in thrust forces across the WF. With the entire WF information being estimated through the communication network, this proposed method enables a distributed framework to achieve performance comparable to that of centralized approaches while using a lower WF control sampling rate.

To attain these WF objectives, the following steps are taken:

- S1 Objective O1 is achieved by cooperatively compensating for power losses stemming from low wind availability caused by, e.g., wake effects. The rationale for the power compensation is to account for this disturbance by altering the set-point of those WTs with excess available power, thus achieving WF-level reference tracking. The average of the WT power tracking errors is estimated by a high-frequency average consensus algorithm, and compensated at a lower sampling rate. By doing this, the total power tracking error is estimated at each turbine and compensated throughout the entire WF.
- S2 To achieve O2, we implement a leader-follower consensus algorithm to distribute the global power reference across the WF, solving the alignment problem. This power reference distribution eliminates the necessity of a central connection point for the power distribution.
- S3 Finally, O3 is attained by computing the average aerodynamic loads through a consensus algorithm, and then regulating the local aerodynamic loads to the obtained average. Treating aerodynamic loads as a surrogate of WT structural loading, the balance of aerodynamic loads leads to uniform degradation of WTs. Moreover, implementing thrust force balancing can avoid WT saturation, which may in turn increase the WF's total available power, compared to uniform power distribution.

The main contributions of this work include the development of the MCDC framework, a distributed approach that achieves the objectives outlined in O1-O3, the provision of stability conditions for designing the proposed MCDC scheme, and a comparison of MCDC with the centralized approach in a high-fidelity environment.

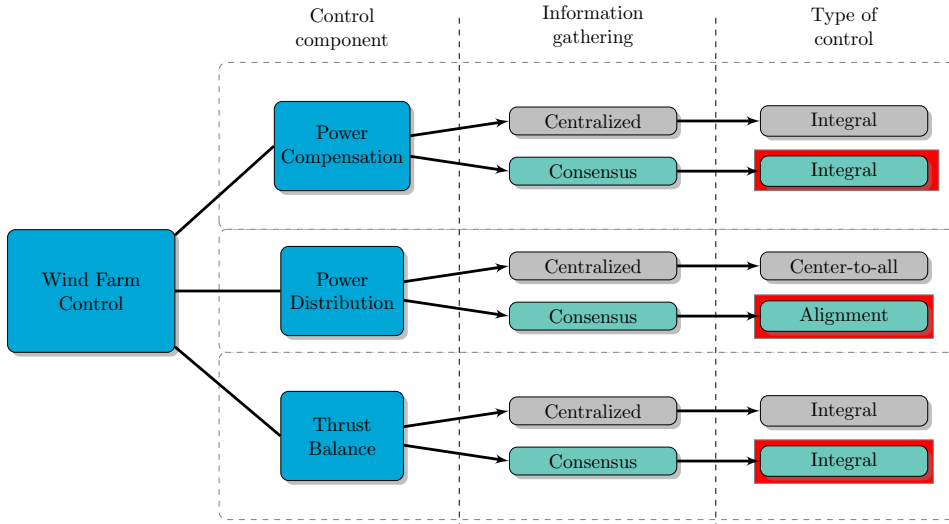





Figure 4.1: Summary of the approaches utilized in this chapter; which includes past works  and our contributions herein . The MCDC is composed of the set of three controllers highlighted as .

The novel wind farm controller proposed in this chapter is summarized in Figure 4.1.

4.1.4. OUTLINE OF THE REMAINDER OF THE CHAPTER

The structure of this chapter is as follows: first, the WF control problem will be formulated in Section 4.2. Second, the proposed distributed control, namely MCDC, for power compensation, power distribution, and thrust balance is presented in Section 4.3. In Section 4.4, simulation results will be presented using a high-fidelity simulator to evaluate the proposed controller. Lastly, conclusions and future works will be discussed in Section 4.5.

4.2. PROBLEM FORMULATION

In this section, before introducing the proposed MCDC, we present the simplified WF model, followed by the considered WF control problem. Finally, the existing centralized control design.

4.2.1. WIND FARM MODEL

We model the WF as a linear time-invariant dynamic system, composed of n WTs. Despite the non-linear open-loop dynamics of WT systems, each turbine is equipped with a dedicated feedback controller designed to track a reference power setpoint. This local controller leads the WTs to exhibit predominantly linear and stable behavior. The WT controller employs both blade pitching and generator torque to regulate the power generation, as presented in [54]. Then, we take this set of controlled WT as linear systems to be regulated by the WF controller. A similar procedure has been utilized in chemical processes [142], where a linear behavior is induced in the closed-loop system, allowing for

higher-level control via linear methods. Linear controllers are widely used in the industry. While the system may encounter disturbances and can exhibit nonlinear behaviors, linear control methods provide robust performance and yield satisfactory results. Poor adherence of the controller WT model to reality is compensated for by the WF controller.

We applied system identification to obtain the linear dynamic model of the controlled wind turbines based on numerical simulation data (see Figure 4.2). Step responses of generator power and thrust force to the reference power setpoint were used in the grey-box model identification process. The models are defined as single-input and multi-output (SIMO) systems, described by

$$\begin{bmatrix} P_{g,i}(k+1) \\ F_{T,i}(k+1) \end{bmatrix} = \begin{bmatrix} a_P & a_{P,T} \\ a_{T,P} & a_T \end{bmatrix} \begin{bmatrix} P_{g,i}(k) \\ F_{T,i}(k) \end{bmatrix} + \begin{bmatrix} b_P \\ b_T \end{bmatrix} P_{g,i}^{\text{ref}}(k) + \begin{bmatrix} q_{P,i}(k) \\ q_{T,i}(k) \end{bmatrix}, \quad (4.1)$$

where k is the WF discrete-time index; $F_{T,i}$, $P_{g,i}$ and $P_{g,i}^{\text{ref}}$ are the thrust force, generator power output and power reference of turbine i , respectively. The six parameters a_P , b_P , a_T , b_T , $a_{P,T}$ and $a_{T,P} \in \mathbb{R}^+$ are identified from simulation data. $q_{P,i}$ and $q_{T,i}$ represent the power and thrust force discrepancies, respectively, caused by model mismatch and possible turbine *saturation* of turbine i .

The first-order representation is adopted for both power and thrust force dynamics, simplifying the turbine responses. This choice is driven by our focus on the dominant transient characteristics to design the WF controller. The identification procedure utilized simulation data of the WT responses, including inflow turbulence and wake effects. The responses of the identified model (Id. sys.) are displayed in Figure 4.2, alongside the WT responses, which exhibit significant variations. Anticipating this, we propose WF controllers that in-

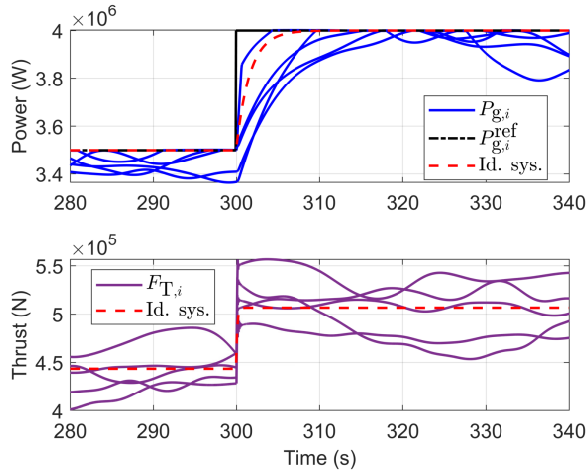


Figure 4.2: Multiple realizations of the power and thrust force response when a step is applied to the power reference with a turbulent inflow. The responses of the identified model are depicted.

corporate an integral term to provide robustness against fluctuations in system parameters and model mismatches, as demonstrated in [143, 144]. Although using higher-order models with only minor extensions in notation – by replacing the scalar model parameters with matrices – could improve fitting with one of the responses, it may not provide a generalized representation because of the significant variability due to turbulence and wake effects.

At the WF level, there exists a time-scale separation between the dynamics of WTs with the power tracking controller, designed at sampling time ranging from 0.00125-0.1 s and a response time of 5-10 s, and the dynamics of wake interactions, of 100-300 s, depending on the turbine spacing and wind speed. In our study case, with the average wind inflow of 10 ms^{-1} , the rise time of the power tracking controller is about 8 s and the wake propagation takes between 120 and 225 s, approximately. Due to this time-scale separation between the WT dynamics and the wake flow dynamics, we make the following assumption:

Assumption 3 (decoupled WF model). *Model (4.1) for WT i is decoupled from all other WTs.* \triangleleft

Note that, as a consequence of the definition of model (4.1) and Assumption 3, the disturbance signals $q_{P,i}$ and $q_{T,i}$ represent unmodeled behaviors. These include the effects from the turbulence in the flow, as well as the effects of the slow time-scale wake interaction, e.g, induced wake turbulence and turbine *saturation* caused by the wind deficit [12, 79].

4.2.2. WIND FARM CONTROL

As noted earlier, the WF controller must be designed to achieve objectives O1-O3. In this subsection, we present a solution to achieve these objectives using feedback and feedforward strategies. From our previous discussion on the WT modeling, the generator power reference $P_{g,i}^{\text{ref}}$ acts as the sole input to the i -th WT, and it is set as

$$P_{g,i}^{\text{ref}}(k) = \hat{P}_{g,i}^{\text{ref}}(k) + u_i(k), \quad (4.2)$$

where $\hat{P}_{g,i}^{\text{ref}}$ is the *feedforward term*, being the desired power reference for each WT and $u_i(k)$ is the *feedback term* defined to compensate for power tracking errors and to balance thrust forces across the WTs. Note that, so long as their sum adds to the global WF reference, there is some freedom in the definition of the feedforward terms; here we suppose $\hat{P}_{g,i}^{\text{ref}}$ are provided by the distribution of the power reference from objective O2. Conversely, the feedback term $u_i(k)$ is defined to achieve both objectives O1 and O3. Specifically,

$$u_i(k) = u_{P,i}(k) + u_{T,i}(k), \quad (4.3)$$

where $u_{P,i}(k)$ is designed for power compensation and $u_{T,i}(k)$ for thrust balance. In Figure 4.3, we visualize the proposed architecture in the distributed case, where the power reference signal received by the WT i is composed of its desired power reference, and the control signals, as defined in (4.2) and (4.3).

Following the electro-mechanical constraint of typical turbines, the power reference signal (4.2), as the input of the WTs, is saturated as

$$P_{g,i}^{\text{ref}}(k) = \begin{cases} 0, & \text{if } P_{g,i}^{\text{ref}}(k) \leq 0 \\ P_{g,i}^{\text{ref}}(k), & \text{if } 0 < P_{g,i}^{\text{ref}}(k) < P_{g,i}^{\text{rated}} \\ P_{g,i}^{\text{rated}}, & \text{else;} \end{cases} \quad (4.4)$$

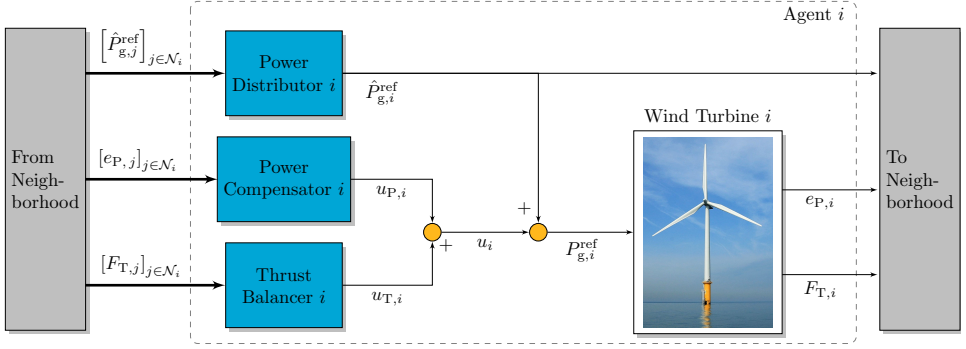


Figure 4.3: Block diagram of the distributed control scheme. At each agent i , there is a power distributor, a power compensator, and a thrust balancer that provides the power reference for WT i . Bold arrows represent vectors of signals from the neighborhood \mathcal{N}_i , distinguishing from the scalar ones.

4

where $P_{g,i}^{\text{rated}}$ is the rated power of turbine i .

CENTRALIZED CONTROLLER

As a benchmark solution to the design problem set in Section 4.2.2, we now summarize the centralized controller proposed in [54]. There, an integral controller is used for the power compensation, such that

$$u_{p,i}(k) = u_{p,i}(k-1) + K_P \mathbf{1}_{1 \times n} e_P(k), \quad (4.5)$$

where K_P is a scalar integrator gain, $\mathbf{1}_{1 \times n} = [1 \ 1 \ \dots \ 1]$ denotes a row vector of length n filled with ones, $e_P(k) = [e_{P,1}(k), e_{P,2}(k), \dots, e_{P,n}(k)]^\top$, with the superscript \top denoting transpose, is a vector containing the power tracking errors,

$$e_{P,i}(k) = \hat{P}_{g,i}^{\text{ref}}(k) - P_{g,i}(k), \quad (4.6)$$

of all WTs. The wind-farm-wide power tracking error is the aggregation of all WT errors, i.e. $e_P^{\text{total}}(k) = \mathbf{1}_{1 \times n} e_P(k) = \sum_{i=1}^n \left(\hat{P}_{g,i}^{\text{ref}}(k) - P_{g,i}(k) \right)$. The utilization of feedback control law (4.5) requires information from all WTs, and ensures that the effort for power compensation is distributed throughout the entire farm. This even distribution is advantageous as it results in a minor impact from the increased wake generated by the compensating WTs, as proposed in [18], and overlooked by Assumption 3.

Similarly, an integral control is utilized for aerodynamic load balancing,

$$u_{T,i}(k) = u_{T,i}(k-1) + K_T e_{T,i}(k), \quad (4.7)$$

where K_T is a scalar integrator gain for the thrust force balance control and

$$e_{T,i}(k) = F_T^{\text{avg}}(k) - F_{T,i}(k) \quad (4.8)$$

is the thrust force error between the average of thrust forces across the WF F_T^{avg} and the thrust force $F_{T,i}$ acting on WT i . To compute F_T^{avg} the information of all thrust forces

is required, as in the case of the power errors in the power compensation. We define the average matrix $W_{\text{avg}} = \frac{1}{n} \mathbf{1}_{n \times 1} \mathbf{1}_{1 \times n}$ and rewrite (4.5) and (4.7) in vector form, such that

$$u_{\text{P}}(k) = u_{\text{P}}(k-1) + \tilde{K}_{\text{P}} n W_{\text{avg}} e_{\text{P}}(k), \quad (4.9)$$

where $u_{\text{P}}(k) = [u_{\text{P},1}(k), u_{\text{P},2}(k), \dots, u_{\text{P},n}(k)]^{\top}$ and $\tilde{K}_{\text{P}} = \text{diag}(K_{\text{P}})$; and

$$u_{\text{T}}(k) = u_{\text{T}}(k-1) + \tilde{K}_{\text{T}} (W_{\text{avg}} - I_n) F_{\text{T}}(k), \quad (4.10)$$

where $u_{\text{T}}(k) = [u_{\text{T},1}(k), u_{\text{T},2}(k), \dots, u_{\text{T},n}(k)]^{\top}$, $F_{\text{T}}(k) = [F_{\text{T},1}(k), F_{\text{T},2}(k), \dots, F_{\text{T},n}(k)]^{\top}$, $\tilde{K}_{\text{T}} = \text{diag}(K_{\text{T}})$, and I_n is the identity matrix of order n .

Instead of employing a centralized approach, we propose that the average power tracking error vector $e_{\text{P}}^{\text{avg}} = W_{\text{avg}} e_{\text{P}}$ and the average thrust force vector $F_{\text{T}}^{\text{avg}} = W_{\text{avg}} F_{\text{T}}$ are obtained from a consensus algorithm. Moreover, a consensus algorithm is also proposed to distribute the power references $\hat{P}_{g,i}^{\text{ref}}$, by aligning them to a leader turbine that has the information of the WF power demand.

4.3. MULTI-RATE CONSENSUS-BASED DISTRIBUTED CONTROL

We propose the so-called Multi-rate Consensus-based Distributed Control (MCDC). To meet the objectives O1-O3, the scheme consists of three control components: a power compensator, a power distributor, and a thrust balancer. The overall proposed distributed WF control is depicted in Figure 4.3. The core idea is to reach a consensus estimate of the relevant WF states for each of the control components. This is accomplished by utilizing only neighborhood information, requiring a substantially less complex and resource-intensive WF communication network. Although local communication is engaged at a high frequency, its rate would remain constant and independent of the number of wind turbines in the farm. In contrast, the number of communications at the central node increases with the number of turbines, eventually surpassing the communication per second at a node in our approach. The consensus estimates are then utilized to compute the power reference for each turbine.

Firstly, we introduce graph notation and the WF communication network in Section 4.3.1, followed by the average consensus conducted within the WF control sampling time in Section 4.3.2. Next, Section 4.3.3 delves into the distributed power compensation. Subsequently, Section 4.3.4 presents the power distribution as a fully distributed approach, and Section 4.3.5 covers the distributed thrust force balance. Finally, stability conditions for the entire control framework are derived and discussed in Section 4.3.6.

4.3.1. GRAPH NOTATION AND WIND FARM COMMUNICATION NETWORK

As mentioned previously, the centralized controller from Section 4.2.2 requires information on the entire WF to compute the feedback terms, consisting of (4.9) and (4.10). Moving towards distributed architectures, WTs no longer require communication from hundreds of WTs to one controller. Instead, they would only communicate with their neighbor WTs. Additionally, it would avoid problems if that one controller fails. In this section, we introduce some preliminaries on graph theory, used in our design, as well as a critical assumption on the communication network linking WTs in the WF.

A graph \mathcal{G} is defined as $\mathcal{G} = (\mathcal{V}, \mathcal{E})$, where $\mathcal{V} = v_1, \dots, v_n$ is its vertex set, with $|\mathcal{V}| = n$ the number of agents, and $\mathcal{E} \subseteq \mathcal{V} \times \mathcal{V}$ its edge set. \mathcal{L} is the Laplacian matrix, defined by $\mathcal{L} = \mathcal{D} - \mathcal{A}$, where $\mathcal{D} = \text{diag}(d_1, \dots, d_n)$ is the in-degree matrix and \mathcal{A} is the adjacency matrix. The diagonal elements $l_{i,j}$ of \mathcal{L} are therefore equal to the in-degree of vertex v_i , and the off-diagonal elements $l_{i,j}$ are -1 if there is an edge from vertex v_i and v_j , or 0 otherwise. The open neighborhood of v_i is defined by the set of neighbors \mathcal{N}_i containing all the adjacent vertices to v_i excluding itself. A graph \mathcal{G} is said to be undirected if $e_{ij} \in \mathcal{E}$ implies $e_{ji} \in \mathcal{E}$.

A communication network in a wind farm induces a graph \mathcal{G} which shares the same topology, i.e., for two vertices $v_i, v_j \in \mathcal{V}$ there exists an edge between them if the two can exchange information. We assume the following.

Assumption 4 (connected network). *The communication network is such that the induced graph \mathcal{G} is undirected and connected.* \triangleleft

By Assumption 4, any two distinct vertices of the graph \mathcal{G} are connected through a path, meaning that there is always a directed spanning tree from a vertex to all other vertices in the graph. This assumption ensures that every agent can reach average consensus [140] and that the leader-follower consensus converges [141].

Consensus algorithms inherently provide robustness against packet loss, as demonstrated in [145]. Additionally, incorporating communication redundancies is crucial in the network design to enhance robustness and guarantee connectivity in the event of a communication failure from a WT. This is achieved by ensuring that each WT exchanges information with at least two others, meaning each vertex v_i has at least two connecting edges. In this case, when a link fails, consensus would still be achieved in all the remaining WTs with a functioning communication system. Furthermore, switching network schemes [141] can be implemented to address these failures and optimize operations through reconfiguration. However, we assume that the turbines have no issue in sharing information.

4.3.2. AVERAGE CONSENSUS BETWEEN WF CONTROL SAMPLINGS

Our proposed multi-rate controller assumes that the data exchange between WTs can occur at a higher rate than the WF control. The WF control typically operates at a low time scale, between 20 s and 10min [34], being suitable for conducting consensus algorithms [141, 140] to estimate the relevant WF information before the WF control action's execution. This inherently leads to a unitary delay in the action, which will be further discussed and assessed. This design consideration is in line with the control of power systems, where different time scales are accounted for [127]. In this subsection, we present a general formulation of the consensus algorithm, used to obtain the estimates for the power compensator and thrust balancer.

The average consensus of a state $x \in \mathbb{R}^n$, is to be achieved at each WT within $h \in \mathbb{N}$ iterations, the consensus horizon. For clarity, the average consensus algorithm is divided into three stages: *(re-)initialization*; *inner iteration*; and *final assignment*.

In the *(re-)initialization*, the state variable of the average consensus, x_i^{avg} is initialized as

$$x_i^{\text{avg}}(0) = x_i(k). \quad (4.11)$$

Then, the *inner iteration* is recursively conducted over the consensus horizon, as follows:

$$x_i^{\text{avg}}(c+1) = w_{i,i}x_i^{\text{avg}}(c) + \sum_{j \in \mathcal{N}_i} w_{i,j}x_j^{\text{avg}}(c), \quad (4.12)$$

for $c \in \{0, 1, \dots, h-1\}$, where $w_{i,i}$ is the weight on x_i^{avg} at vertex i , and $w_{i,j}$ are the weights on x_j^{avg} at vertex i . As the last stage, the *final assignment* is

$$x_i^{\text{avg, final}}(k|k+1) = x_i^{\text{avg}}(h), \quad (4.13)$$

where $x_i^{\text{avg, final}}$ is the final average value obtained after h steps and utilized for defining the WF control action. The notation $(k|k+1)$ is utilized to highlight that the estimate of the average of $x(k)$ can only be obtained at $k+1$.

By setting $w_{i,j} = 0$ for $j \notin \mathcal{N}_i$, we can then rewrite (4.11)-(4.13) in a vector form

$$x^{\text{avg}}(0) = x(k), \quad (4.14a)$$

$$x^{\text{avg}}(c+1) = Wx^{\text{avg}}(c), \forall c \in \{0, 1, \dots, h-1\}, \quad (4.14b)$$

$$x^{\text{avg, final}}(k|k+1) = x^{\text{avg}}(h), \quad (4.14c)$$

where $W = [w_{i,j}]$ is the average consensus weight matrix. The matrix W is structured to respect the communication topology and has to satisfy the following conditions:

$$\lambda_1(W) = 1 \text{ and } |\lambda_i(W)| \leq 1 \text{ for all } i = 2, \dots, n, \quad (4.15a)$$

$$W\mathbf{1}_{n \times 1} = \mathbf{1}_{n \times 1}, \quad (4.15b)$$

$$\mathbf{1}_{1 \times n}W = \mathbf{1}_{1 \times n}. \quad (4.15c)$$

While average consensus is only reached in the limit, as $h \rightarrow \infty$, a suitable average can be achieved in finite iterations, by choosing a sufficiently large h . Moreover, the optimal design of W to achieve the fastest convergence rate and enhance accuracy is obtained by solving the following optimization problem, the so-called Fastest Discrete-Time Consensus (FDTC) problem [146]:

$$\underset{w_{ij}}{\text{minimize}} \quad \rho(W - W_{\text{avg}}) \quad (4.16a)$$

subject to

$$W\mathbf{1}_{n \times 1} = \mathbf{1}_{n \times 1}, \quad (4.16b)$$

$$W = W^\top, \quad (4.16c)$$

$$w_{i,j} = 0, \text{ if } (i, j) \notin \mathcal{E} \text{ and } i \neq j, \quad (4.16d)$$

where $\rho(S)$ is the spectral radius of S , and the convergence speed decreases with $\rho(S)$; and, reiterating, $W_{\text{avg}} = \frac{1}{n}\mathbf{1}_{n \times 1}\mathbf{1}_{1 \times n}$ is the average matrix. Since we impose W to be symmetric as a design choice, the spectral radius of a symmetric matrix is also its spectral norm, then (4.16a) can be cast as the minimization of $\|W - W_{\text{avg}}\|$, where the operator $\|\cdot\|$ is the induced matrix 2-norm. This problem is convex and can be solved globally and efficiently.

Notice that for plug-and-play capabilities, the optimization problem should be reconsidered taking into account the new addition or removal to keep overall optimality. Otherwise, at least, the elements of W associated with their neighbors should be changed accordingly to maintain the conditions in (4.15).

4.3.3. DISTRIBUTED POWER COMPENSATION

Let us now address the solution to objective **O1** in a distributed manner. The main idea is to utilize WTs with enough wind resources to cooperatively compensate for power-tracking errors. This ensures that overall power tracking at the WF level can still be attained in the case of turbine *saturation*. Figure 4.4 illustrates our proposed distributed strategy for power compensation. Each WT i initiates its consensus protocol based on its own power error. Then, the average power error across the entire farm is estimated through the average consensus process that communicates the power errors in a neighborhood at a high rate. Subsequently, the control computes the feedback control signal $u_{p,i}$ at a low rate using the estimates of the WF power error. This strategy is detailed as follows, divided into Estimation and Control.

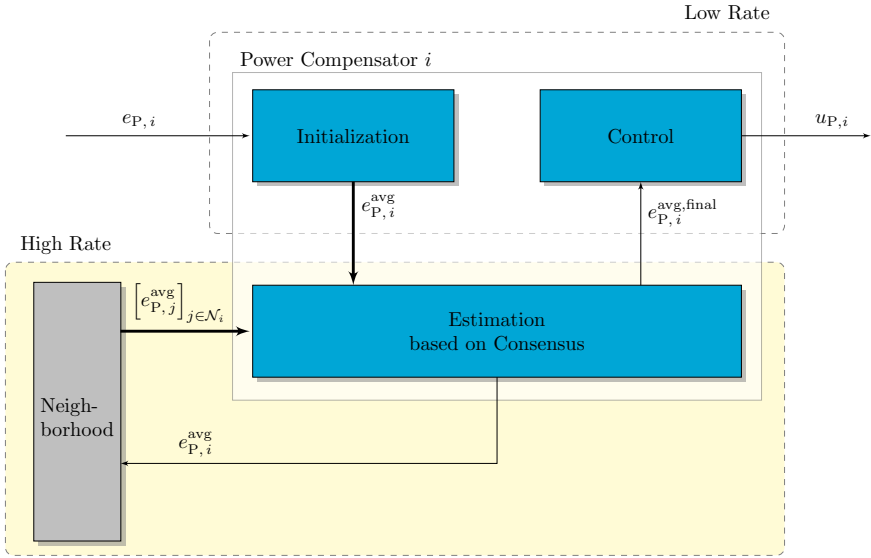


Figure 4.4: Block diagram of the power compensator based on the consensus of the power errors.

Estimation: The first step in our distributed power compensation strategy is to estimate the WF power error. This is accomplished by computing the average power error at each WT using the average consensus algorithm, as presented in Section 4.3.2. The algorithm leverages the current power error information at each WT and disseminates it by engaging in high-frequency communication with neighboring WTs. If Assumption 4 holds, and provided that h is sufficiently large, the average consensus value is obtained in the subsequent low-rate time step. Theoretically [140, 146], we have

$$\begin{aligned} \lim_{h \rightarrow \infty} W^h e_p(k) &= W_{\text{avg}} e_p(k) \\ &= e_p^{\text{avg, final}}(k|k+1), \end{aligned} \quad (4.17)$$

where e_p is the vector containing all power tracking errors of each WT, W is the average consensus weight matrix, which is structured to respect the communication topology,

and W_{avg} is the average matrix. The notation $(k|k+1)$ signifies that the average of power losses $e_{\text{p}}^{\text{avg, final}}$ from k is only obtained at $k+1$. This notation emphasizes the delay attained by utilizing our proposed approach. Thus, the WF power error is estimated to be $ne_{\text{p}}^{\text{avg, final}}(k|k+1)$.

During the design stage, a finite value for h is determined, constrained by the speed of the communication system in transmitting information and the time required by the local controller to execute the algorithm. Since communication speed and computation time are “hard” constraints, the designer must account for some tolerance in the attained average consensus. The choice of h affects the distribution of the power compensation, moving from uniform, widespread compensation across the farm with h sufficiently large, to a more localized compensation with a low value of h . This localized compensation is acknowledged without significant prejudice, as (4.15b) guarantees that the sum of the vector of node values is preserved and h is factored into the stability conditions derived further in this work.

A high convergence rate, dictated by the network’s topology and the chosen average consensus weights, allows more flexibility in selecting h , where choosing a low value of h is essential to guarantee that the practical constraints are satisfied, therefore obtaining a satisfactory average consensus within the wind farm control sampling time.

Control: We propose a compensation strategy following the integral method derived for centralized controller in [54] and presented in Section 4.2.2. The integral method is demonstrated to achieve stability even with the presence of the additional step-time delay for the execution of the consensus algorithm. The control law at each WT uses the final estimated average power error $e_{\text{p}}^{\text{avg, final}}(k-1|k)$ from the previous time step $k-1$ obtained at k , and it is defined as:

$$u_{\text{p},i}(k) = u_{\text{p},i}(k-1) + K_{\text{p}} ne_{\text{p},i}^{\text{avg, final}}(k-1|k), \quad (4.18)$$

where K_{p} is the integrator gain for the power compensator. In vector form, we can rewrite (4.18) as

$$u_{\text{p}}(k) = u_{\text{p}}(k-1) + \bar{K}_{\text{p}} W_{\text{p}} e_{\text{p}}(k-1), \quad (4.19)$$

where \bar{K}_{p} is the gain matrix defined as $\bar{K}_{\text{p}} := \text{diag}(K_{\text{p}})$, and $W_{\text{p}} = nW^h$ a weight matrix. Notice that differing from a central control law (4.9), the average depends on the value of h , if $h \rightarrow \infty$ then $W_{\text{p}} = nW_{\text{avg}}$. Importantly, the computation of the average consensus adds a sampling time delay to the power error signal in (4.19), compared to the centralized controller in (4.9).

Remark 6. *With the control law (4.18) utilizing the average consensus with a sufficiently large h , the compensation equally spreads the additional power demand, as in the centralized approach. This equal compensation across all turbines is simple and effective. Furthermore, the compensation can be expanded to take the intensity of the turbine interactions into account in (4.18), e.g., using a WF model-based optimization [119], or estimations of available power [14]. A weighted approach across the turbines considering the intensity of the interactions is a direct extension. Our proposed controller combines power compensation with aerodynamic load balancing, implicitly accounting for their interactions and promoting a power distribution that leads to uniform degradation and prevents turbine saturation.* \triangleleft

4.3.4. POWER DISTRIBUTION

In a fully distributed WF system, the desired power references $\hat{P}_{g,i}^{\text{ref}}(k)$, as a solution of objective O2, should also be obtained in a distributed manner. The information regarding the desired power reference for each turbine can be disseminated throughout the communication network by solving the *alignment problem* [141], also known as leader-follower consensus.

The alignment problem is accomplished by converging all the desired power references to leader turbines. The leader turbines leave their values unchanged, while all others asymptotically agree with them according to the consensus protocol, achieving alignment. The leader-follower consensus is conducted between the WF control sampling time, so it also follows the notations from Section 4.3.2.

A widely employed benchmark approach is to divide the WF power reference uniformly among all WTs [14]. As a *feedforward* term, the desired power reference provides an initial reference to the WTs, with the primary goal of sharing implicit information on the total farm power demand, while the *feedback* terms are also incorporated into the power reference signals. For simplicity, we assume a single leader identified as the WT $i = m$. The leader's power reference is determined by dividing the total WF power reference $P_{\text{WF}}^{\text{ref}}$ by the number of WTs in the WF; such that the (*re*)*initialization* of the leader turbines is defined as follows

$$P_{g,m}^{\text{ref, align}}(0) = P_{\text{WF}}^{\text{ref}}(k)/n, \quad (4.20)$$

while the (*re*)*initialization* of the other turbines is

$$P_{g,i}^{\text{ref, align}}(0) = \hat{P}_{g,i}^{\text{ref}}(k-1), \forall i \neq m, \quad (4.21)$$

and for $k \geq 1$, where $P_{g,i}^{\text{ref, align}}$ is the internal state variable.

Then, in the *inner iteration* stage, the leader's power reference remains constant, being

$$P_{g,m}^{\text{ref, align}}(c+1) = P_{g,m}^{\text{ref, align}}(c), \forall c = 0, 1, \dots, h-1, \quad (4.22)$$

where c is an internal discrete-time index. On the other hand, the followers $i \neq m$ converge to the leader as:

$$\begin{aligned} \hat{P}_{g,i}^{\text{ref, align}}(c+1) &= a_{i,i} \hat{P}_{g,i}^{\text{ref, align}}(c) + \sum_{j \in \mathcal{N}_i \setminus m} a_{i,j} \hat{P}_{g,j}^{\text{ref, align}}(c) \\ &\quad + b_i P_{g,m}^{\text{ref, align}}(c), \end{aligned} \quad (4.23)$$

$\forall c = 0, 1, \dots, h-1$, where $a_{i,j} \in \mathbb{R}$, and b_i is either $\beta_i \in \mathbb{R}$ if agent i is connected to the leader, or 0 otherwise.

At the *final assignment* stage,

$$\hat{P}_{g,i}^{\text{ref}}(k|k+1) = P_{g,i}^{\text{ref, align}}(h), \forall i. \quad (4.24)$$

For a single leader, without loss of generality, we can assume that this agent is the one labeled with $m = n$. Then, the multi-agent system is said to achieve alignment between the WF control sampling time when

$$\lim_{h \rightarrow \infty} \|\hat{P}_{g,i}^{\text{ref}}(k|k+1) - \hat{P}_{g,n}^{\text{ref}}(k|k+1)\| = 0, \quad (4.25)$$

$\forall i \in \{1, 2, \dots, n-1\}$. The *inner iteration* defined by (4.22) and (4.23) can be written in state form as

$$\begin{bmatrix} P_{i=1:n-1}^{\text{ref, align}}(c+1) \\ P_n^{\text{ref, align}}(c+1) \end{bmatrix} = \underbrace{\begin{bmatrix} A_{\text{lf}} & B_{\text{lf}} \\ \mathbf{0}_{1 \times n-1} & \mathbf{1}_{1 \times 1} \end{bmatrix}}_{L_{\text{lf}}} \begin{bmatrix} P_{i=1:n-1}^{\text{ref, align}}(c) \\ P_n^{\text{ref, align}}(c) \end{bmatrix}, \quad (4.26)$$

$\forall c = 0, 1, \dots, h-1$, where $A_{\text{lf}} = [a_{i,j}]_{n-1 \times n-1}$, with $a_{i,j} = 0$ for $j \notin \mathcal{N}_i$, and $B_{\text{lf}} = [b_1, b_2, \dots, b_{n-1}]^\top$. The design of the parameters $a_{i,j}$ and $b_i \in \mathbb{R}$ is conducted by an equivalency with the alignment problem derived in [141]. It then follows

$$A_{\text{lf}} = (I_{n-1} + \mathcal{D}_{n-1 \times n-1} + B')^{-1} (I_{n-1} + \mathcal{A}_{n-1 \times n-1}), \quad (4.27)$$

$$B_{\text{lf}} = (I_{n-1} + \mathcal{D}_{n-1 \times n-1} + B')^{-1} B', \quad (4.28)$$

where B' is a $n-1 \times n-1$ diagonal matrix whose i th diagonal element is 1, if i is the neighbor of the leader, and 0 otherwise; $\mathcal{D}_{n-1 \times n-1}$ and $\mathcal{A}_{n-1 \times n-1}$ are the degree and adjacency matrices removing the last column and row, respectively. In this way, L_{lf} in (4.26) is a stochastic matrix, i.e. $L_{\text{lf}} \mathbf{1}_{n \times 1} = \mathbf{1}_{n \times 1}$ and L_{lf} is square with all entries non-negative.

Utilizing this approach, the distribution of WF power reference is not made by a central workstation to each turbine, as typically observed in the general centralized scenario. Instead, the communication is distributed in exchange for a time-step delay. This time-step delay, on the other hand, can be designed to be as small as necessary, constrained by the execution of the consensus algorithm.

4.3.5. THRUST FORCE BALANCE CONTROL

Following objective O3, we aim to evenly distribute the thrust forces throughout the entire farm in a distributed manner. Our solution in this section also takes advantage of the average consensus and the time-scale separation from the WF and WT controllers to compute the average thrust forces.

For computing the feedback control signal $u_{T,i}(k)$, we use the average thrust force across the entire farm obtained from average consensus. Then, we estimate the thrust force errors from the average thrust force to the current values.

Estimation: The thrust force errors from the average thrust force to current values are estimated from our distributed thrust force balance strategy. This is achieved by computing the average thrust force across the WF at each WT employing the average consensus algorithm from Section 4.3.2. The thrust force tracking errors $e_{T,i}$ is defined as

$$e_{T,i}(k) = F_{T,i}^{\text{avg}}(k) - F_{T,i}(k), \quad (4.29)$$

where $F_{T,i}^{\text{avg}}$ is the average of thrust forces known at i -th WT and $F_{T,i}$ is the current thrust force.

Different from the centralized controller, $F_{T,i}^{\text{avg}}$ is computed across the WF by the average consensus algorithm from Section 4.3.2, such that the estimations of the thrust force errors are defined as

$$\begin{aligned} e_{T,i}(k-1|k) &= (W^h - I_n) F_T(k-1) \\ &= -W_T F_T(k-1), \end{aligned} \quad (4.30)$$

where $W_T = -(W^h - I_n)$. When $h \rightarrow \infty$,

$$e_T(k-1|k) = (W_{\text{avg}} - I_n) F_T(k-1). \quad (4.31)$$

This indicates that the strategy introduces a sampling time delay besides the consensus algorithm being conducted with a finite h in practice. Similarly to the power compensation, the choice of h dictates the level of smoothness in the averaging of the thrust forces across the WF.

Control: The control protocol that balances the thrust force is proposed to be composed of pure integrators. The sampling time delay originating from the computation of the average consensus is embedded into the proposed control law (4.32) by considering the definition of the error signals from (4.30), contrasting with the central control law in (4.7).

$$u_{T,i}(k) = u_{T,i}(k-1) + K_T e_{T,i}(k-1|k), \quad (4.32)$$

which can be rewritten in a vector form as:

$$\begin{aligned} u_T(k) &= u_T(k-1) + \bar{K}_T e_T(k-1|k) \\ &= u_T(k-1) - \bar{K}_T W_T F_T(k-1), \end{aligned} \quad (4.33)$$

where $\bar{K}_T = \text{diag}(K_T)$.

Remark 7. Note that the weight matrix W_T is a double-stochastic matrix by definition, therefore it guarantees that $\sum_i u_{T,i}(k) = 0 \forall k$. Indeed, from (4.33):

$$\begin{aligned} \sum_i u_{T,i}(k) &= \mathbf{1}_{1 \times n} u_T(k) \\ &= \mathbf{1}_{1 \times n} u_T(0) - \sum_{\tau=1}^k \mathbf{1}_{1 \times n} \bar{K}_T W_T F_T(\tau-1). \end{aligned} \quad (4.34)$$

Thus, provided that $u_{T,i}(0) = 0 \forall i$ is established as the initial condition for the integrators, $\mathbf{1}_{1 \times n} \bar{K}_T W_T F_T(k-1) = 0 \forall k$ is a sufficient condition for $\sum_i u_{T,i}(k) = 0 \forall k$. Thus, by the definition of W_T ,

$$\mathbf{1}_{1 \times n} \bar{K}_T W_T F_T(k-1) = 0 \quad (4.35)$$

holds, where $\mathbf{1}_{1 \times n} W_T = 0_n$ follows from the definition of $W_T = -(W^h - I_n)$, as W^h is a double-stochastic matrix. \triangleleft

Remark 8. When turbine saturation¹ occurs in one of the WTs, the balancing of thrust forces would reduce the total WF power generation. The saturated turbine can not increase power generation and it typically has a lower thrust force compared to the remaining turbines. Consequently, the saturated turbine affects the power generation of the other turbines by diminishing their power output and failing to compensate for their reduced generation with its own increased power generation. Hence, we exclude saturated turbines from the balancing of thrust forces, departing from the previous practice in the central approach

¹Turbine saturation refers to a condition where a turbine operates at maximum capacity and cannot produce any more power when demanded. This condition is imposed by unavailable wind and high power demand.

in [72, 54]. This prioritizes object *OI* and is justified by the fact that the thrust forces of saturated turbines are lower than the remaining ones. To accomplish this, we define the consensus algorithm, such that W^h reaches the definition of the average matrix in (4.36) when $h \rightarrow \infty$.

$$W_{\text{avg, sat}} = [w_{i,j}] = \begin{cases} 1, & \text{if } i = j \text{ is saturated,} \\ 0, & \text{if } i \neq j \text{ and } i \text{ or } j \text{ is saturated,} \\ \frac{1}{n-n_s}, & \text{otherwise,} \end{cases} \quad (4.36)$$

where n_s is the number of saturated turbines. The saturation information is also obtained through average consensus, thereby maintaining distributed communication. Since this follows directly from Section 4.3.2, it is omitted for brevity. The double-stochasticity property in (4.36) persists and the result thrust force error of the saturated turbines is zero, granting an anti-windup property for the integrators. An example of the weighted matrix of a 3-turbine farm with saturation in the second turbine is

$$W_{\text{avg, sat}} = \begin{bmatrix} \frac{1}{2} & 0 & \frac{1}{2} \\ 0 & 1 & 0 \\ \frac{1}{2} & 0 & \frac{1}{2} \end{bmatrix}.$$

◀

Remark 9. In the event of a scheduled shutdown for maintenance at specific WTs, the power compensation and power distribution, as discussed in Section 4.3.3 and Section 4.3.4, could remain unchanged. In this way, the power error at the shutdown turbine will be compensated by the other from the feedback loop. The information of the turbine to be shut down can be transmitted through the communication network by the alignment consensus algorithm. The turbine undergoing shutdown must be removed from the thrust force balancing and this can be handled in the same manner as when turbine saturation occurs, following (4.36). ◀

4.3.6. STABILITY OF THE PROPOSED CONTROL SCHEME

To start the discussions in this section, we consider the concept of Bounded Input Bounded Output (BIBO) stability and how it relates to turbine saturation in the farm. Here, exogenous inputs, i.e. the references \hat{P}_g^{ref} , and the disturbances q_P and q_T , are acknowledged as bounded, as substantiated by the following assessments:

1. The contribution of the inflow turbulence or other unmodelled effects is bounded, such that $|q_{P,i}| < K_1$ and $|q_{T,i}| < K_2$ for all i , where K_1 and $K_2 \in \mathbb{R}$, governed by the convergence of the dedicated feedback controller at each WT;
2. Owing to potential saturation $q_{P,i} < 0$, and $q_{P,i} \geq -P_{g,i}^{\text{rated}}$, as a result of the constraints imposed by the turbines and the reference signal, $P_{g,i} \geq 0$, $P_{g,i}^{\text{ref}} \geq 0$, and $P_{g,i}^{\text{ref}} \leq P_{g,i}^{\text{rated}}$, and, similarly, $q_{T,i} < 0$, and $q_{T,i} \geq -F_{T,i}^{\text{max}}$, where $F_{T,i}^{\text{max}}$ is the maximum thrust force admitted by an individual WT.

For the closed-loop system to be BIBO stable - meaning that the norms of the power and thrust force errors remain bounded for bounded inputs - a necessary condition is that

the poles of the closed-loop system must be in a stable region. From (4.1), the dynamics of the power generation and thrust force are rewritten in vector form as

$$P_g(k+1) = A_P P_g(k) + A_{T,P} F_T(k) + B_P P_g^{\text{ref}}(k) + q_P(k), \quad (4.37)$$

$$F_T(k+1) = A_T F_T(k) + A_{P,T} P_g(k) + B_T P_g^{\text{ref}}(k) + q_T(k), \quad (4.38)$$

where, given Assumption 3, $A_P = \text{diag}(a_P)$, $A_{T,P} = \text{diag}(a_{T,P})$, and $B_P = \text{diag}(b_P)$; and $A_T = \text{diag}(a_T)$, $A_{P,T} = \text{diag}(a_{P,T})$, and $B_T = \text{diag}(b_T)$. Thus, we convert (4.37) and (4.38) from their discrete-time description to the z -domain [147], and reorganize them using matrix algebra:

$$P_g = (I_n z - A_P)^{-1} (A_{T,P} F_T + B_P P_g^{\text{ref}} + q_P) \quad (4.39)$$

$$= G_{T,P} F_T + G_P P_g^{\text{ref}} + G_{P,q} q_P,$$

$$F_T = (I_n z - A_T)^{-1} (A_{P,T} P_g + B_T P_g^{\text{ref}} + q_T) \quad (4.40)$$

$$= G_{P,T} P_g + G_T P_g^{\text{ref}} + G_{T,q} q_T,$$

where P_g , F_T , \hat{P}_g^{ref} , q_P , and q_T represent the Z -transform of the respective vectors from this point, calculated as $Z[x(k+a)] = z^a x(z)$ with $a \in \mathbb{Z}$; and $G_{T,P} = (I_n z - A_P)^{-1} A_{T,P}$, $G_P = (I_n z - A_P)^{-1} B_P$, $G_{P,q} = (I_n z - A_P)^{-1}$, $G_{P,T} = (I_n z - A_T)^{-1} A_{P,T}$, $G_T = (I_n z - A_T)^{-1} B_T$, $G_{T,q} = (I_n z - A_T)^{-1}$ are defined transfer functions that represents the open-loop system (see the block diagram representation in Figure 4.5). For simplicity, we denote $\bar{q}_P = G_{P,q} q_P$ and $\bar{q}_T = G_{T,q} q_T$. Replacing (4.39) and (4.40) into each other and rearranging the terms, we have the following representation of the WF dynamics:

$$P_g = (I_n - G_{T,P} G_{P,T})^{-1} [(G_P + G_{T,P} G_T) P_g^{\text{ref}} + G_{T,P} \bar{q}_T + \bar{q}_P], \quad (4.41)$$

$$F_T = (I_n - G_{P,T} G_{T,P})^{-1} [(G_T + G_{P,T} G_P) P_g^{\text{ref}} + G_{P,T} \bar{q}_P + \bar{q}_T]. \quad (4.42)$$

Furthermore, we also convert the power reference input signal to the Z -domain, which incorporates the control laws previously defined in (4.19) and (4.33), such that

$$P_g^{\text{ref}} = \hat{P}_g^{\text{ref}} + u_P + u_T, \quad (4.43)$$

$$u_P = (I_n z - I_n)^{-1} \bar{K}_P W_P e_P \quad (4.44)$$

$$= C_P W_P (\hat{P}_g - P_g),$$

$$u_T = (I_n z - I_n)^{-1} \bar{K}_T e_T \quad (4.45)$$

$$= C_T W_T F_T,$$

where u_P , u_T , e_P , and e_T represent the Z -transform of the respective vectors from this point forward, and $C_P = (I_n z - I_n)^{-1} \bar{K}_P$, $C_T = (I_n z - I_n)^{-1} \bar{K}_T$ are the defined control transfer functions. To emphasize, these control transfer functions represent a backward numerical integration due to the delay inherent in our approach, contrasting with the forward integration used in centralized control.

The feedback system is illustrated in the block diagram in Fig. 4.5. In this representation, the input disturbance d_i includes the feedforward term, which is the reference power

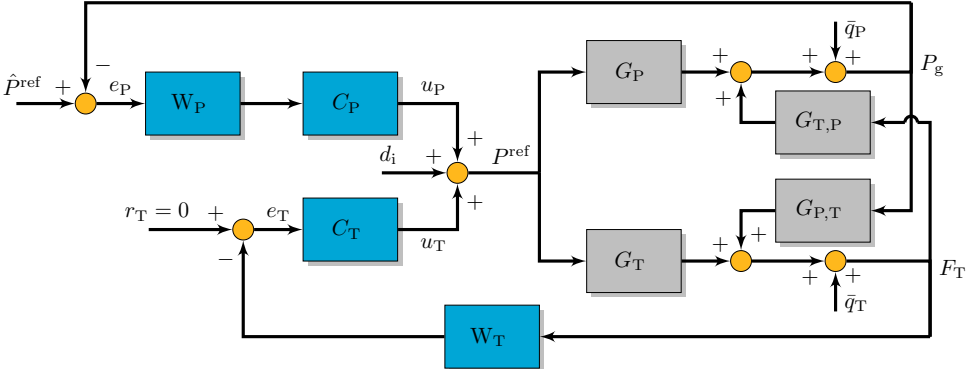


Figure 4.5: Block diagram of the closed-loop system with both feedback loops. The communication is represented by W_P and W_T .

\hat{P}_g^{ref} , an exogenous signal. To assess stability, we close both feedback loops using the system equations (4.41) and (4.42), along with the control signal (4.43). Consequently, we can formulate the following theorem:

Theorem 1. *The closed-loop stability, utilizing both feedback control laws (4.44) and (4.45) simultaneously, is ensured when the following matrix inequalities are satisfied:*

$$A_0 - A_3 < 0, \quad (4.46a)$$

$$A_0 + A_1 + A_2 + A_3 > 0, \quad (4.46b)$$

$$A_0 - A_1 + A_2 - A_3 < 0, \quad (4.46c)$$

and

$$A_2^2 - A_0^2 + A_0 A_2 - A_1 A_3 > 0, \quad (4.47)$$

where $A_3 = I_n$, $A_2 = -(I_n + A_P + A_T)$, $A_1 = A_P A_T + A_P + A_T + A_{T,P} A_{P,T} + B_P \bar{K}_P W_P + W_T B_T \bar{K}_T$, $A_0 = -A_P A_T + A_{T,P} A_{P,T} - A_T B_P \bar{K}_P W_P + A_{T,P} B_T \bar{K}_P W_P - A_P W_T B_T \bar{K}_T + A_{P,T} W_T B_P \bar{K}_T$, and $|\cdot|$ is the determinant operation.

Proof of Theorem 1. Taking (4.43), and replacing with the control laws (4.44) and (4.45), and subsequently replacing with (4.41) and (4.42), we have

$$P_g^{\text{ref}} = \hat{P}_g^{\text{ref}} + u_P + u_T \quad (4.48a)$$

$$= \hat{P}_g^{\text{ref}} + C_P W_P (\hat{P}_g^{\text{ref}} - P_g) - C_T W_T F_T \quad (4.48b)$$

$$= (I_n + C_P W_P) \hat{P}_g^{\text{ref}} - C_P W_P (I_n - G_{T,P} G_{P,T})^{-1} [(G_P + G_{T,P} G_T) P_g^{\text{ref}} + G_{T,P} \bar{q}_T + \bar{q}_P] - C_T W_T (I_n - G_{P,T} G_{T,P})^{-1} [(G_T + G_{P,T} G_P) F_T^{\text{ref}} + G_{P,T} \bar{q}_P + \bar{q}_T] \quad (4.48c)$$

$$= [I_n + C_P W_P (I_n - G_{T,P} G_{P,T})^{-1} (G_P + G_{T,P} G_T) + C_T W_T (I_n - G_{P,T} G_{T,P})^{-1} (G_T + G_{P,T} G_P)]^{-1} \{ (I_n + C_P W_P) \hat{P}_g^{\text{ref}} - C_P W_P \bar{q}_P - C_T W_T \bar{q}_T \} \quad (4.48d)$$

From (4.48c) to (4.48d), we rearranged (4.48c) by isolating the power reference P_g^{ref} and we denote $\tilde{q}_P = (I_n - G_{T,P}G_{P,T})^{-1} (G_{T,P}\tilde{q}_T + \tilde{q}_P)$ and $\tilde{q}_T = (I_n - G_{P,T}G_{T,P})^{-1} (G_{P,T}\tilde{q}_P + \tilde{q}_T)$, having stable relationships with \tilde{q}_P and \tilde{q}_T by the definitions of $G_{P,T}$ and $G_{T,P}$. Substituting the transfer functions accordingly and utilizing algebraic manipulations, the inverse term that includes the closed-loop characteristic equation becomes

$$\begin{aligned} & [I_n + C_P W_P (I_n - G_{T,P} G_{P,T})^{-1} (G_P + G_{T,P} G_T) + C_T W_T (I_n - G_{P,T} G_{T,P})^{-1} (G_T + G_{P,T} G_P)]^{-1} = \\ & [(I_n z - A_P)(I_n z - A_T)(I_n z - I_n) - (I_n z - I_n) A_{T,P} A_{P,T} + (I_n z - A_T) \tilde{K}_P W_P B_P + A_{T,P} \tilde{K}_P W_P B_T \\ & + (I_n z - A_P) \tilde{K}_T W_T B_T + A_{P,T} \tilde{K}_T W_T B_P]^{-1} [(I_n z - A_P)(I_n z - A_T) - A_{T,P} A_{P,T}] (I_n z - I_n). \end{aligned}$$

To ensure stability, we must guarantee that the solutions to the characteristic matrix polynomial

$$\begin{aligned} \det((I_n z - A_P)(I_n z - A_T)(I_n z - I_n) - (I_n z - I_n) A_{T,P} A_{P,T} + (I_n z - A_T) \tilde{K}_P W_P B_P \\ + A_{T,P} \tilde{K}_P W_P B_T + (I_n z - A_P) \tilde{K}_T W_T B_T + A_{P,T} \tilde{K}_T W_T B_P) = 0 \end{aligned} \quad (4.49)$$

lie within the unit circle. To demonstrate this, we rely on the multivariate extension of the Jury stability criterion [148], as presented in [149]. Specifically, let us start by defining $Q(z) = (I_n z - A_P)(I_n z - A_T)(I_n z - I_n) - (I_n z - I_n) A_{T,P} A_{P,T} + (I_n z - A_T) \tilde{K}_P W_P B_P + A_{T,P} \tilde{K}_P W_P B_T + (I_n z - A_P) \tilde{K}_T W_T B_T + A_{P,T} \tilde{K}_T W_T B_P$. Then, $\det(Q(z)) = 0$ has a solution only if $\exists x \neq 0$ such that $x^\top Q(z)x = 0^2$. Thus, solving (4.49) and verifying its solutions is equivalent to evaluating

$$\begin{aligned} x^\top Q(z)x &= x^\top [(I_n z - A_P)(I_n z - A_T)(I_n z - I_n) - (I_n z - I_n) A_{T,P} A_{P,T} + (I_n z - A_T) \tilde{K}_P W_P B_P \\ & + A_{T,P} \tilde{K}_P W_P B_T + (I_n z - A_P) \tilde{K}_T W_T B_T + A_{P,T} \tilde{K}_T W_T B_P] x \\ &= x^\top [I_n z^3 - (I_n + A_P + A_T) z^2 + (A_P A_T + A_P + A_T + A_{T,P} A_{P,T} \tilde{K}_P W_P B_P \\ & + \tilde{K}_T W_T B_T) z - A_P A_T + A_{T,P} A_{P,T} - A_T \tilde{K}_P W_P B_P + A_{T,P} B_T \tilde{K}_P W_P - A_P \tilde{K}_T W_T B_T \\ & + A_{P,T} W_T B_P \tilde{K}_T] x \\ &= x^\top A_3 x z^3 + x^\top A_2 x z^2 + x^\top A_1 x z + x^\top A_0 x = 0, \end{aligned} \quad (4.50)$$

where $A_3 = I_n$, $A_2 = -(I_n + A_P + A_T)$, $A_1 = A_P A_T + A_P + A_T + A_{T,P} A_{P,T} + B_P \tilde{K}_P W_P + W_T B_T \tilde{K}_T$, $A_0 = -A_P A_T + A_{T,P} A_{P,T} - A_T B_P \tilde{K}_P W_P + A_{T,P} B_T \tilde{K}_P W_P - A_P W_T B_T \tilde{K}_T + A_{P,T} W_T B_P \tilde{K}_T$. Then, it is possible to exploit the Jury stability criterion [148]. Having solutions of $\det(Q(z)) = 0$ restricted to the complex unit disc is equivalent to satisfying the stability constraints of the third-order polynomial (4.50), such that:

$$\begin{cases} x^\top (A_3 + A_2 + A_1 + A_0) x > 0, & (4.51a) \\ x^\top (A_3 - A_2 + A_1 - A_0) x > 0, & (4.51b) \\ x^\top (A_3 - A_0) x > 0, \text{ and} & (4.51c) \end{cases}$$

²For any matrix $A \in \mathbb{R}^{n \times n}$, $\det(A) = 0$ is equivalent to $\text{rank}(A) < n$ and therefore $\text{nullity}(A) = \dim(\ker(A)) \geq 1$. This latter fact implies that $\exists x \neq 0 \in \mathbb{R}^n$ s. t. $x \in \ker(A) \implies Ax = 0 \implies v^\top Ax = 0, \forall v \in \mathbb{R}^n$. Taking $v = x$, $x^\top Ax = 0$.

$$\begin{vmatrix} x^\top A_0 x & x^\top A_1 x \\ x^\top A_3 x & x^\top A_2 x \end{vmatrix} - \begin{vmatrix} x^\top A_0 x & x^\top A_3 x \\ x^\top A_3 x & x^\top A_0 x \end{vmatrix} > 0, \quad (4.52)$$

In turn, given that A_3, A_2, A_1, A_0 are symmetric by construction, the conditions in (4.51) are equivalent to the linear matrix inequalities in (4.46); and (4.52) equivalent to (4.47). \square

The stability conditions from Theorem 1 imply internal stability for our proposed MCDC framework in our study case, which we evaluate through the closed-loop system in a standard MIMO feedback configuration [150], as illustrated in the block diagram in Figure 4.6.

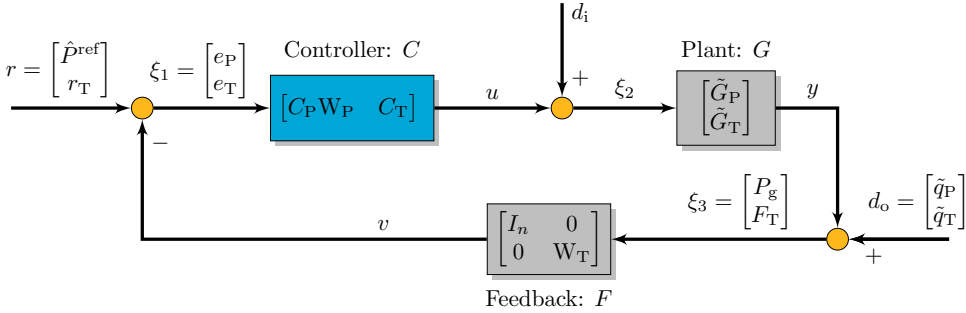


Figure 4.6: Block diagram of the closed-loop system in a basic feedback loop representation.

We define the vector signals r , d_i , and d_o , being the exogenous signals; ξ_1 , ξ_2 , ξ_3 , u , y , v , being the internal signals; and the system transfer functions, $\tilde{G}_P = (I_n - G_{T,P} G_{P,T})^{-1} (G_P + G_{T,P} G_T)$ and $\tilde{G}_T = (I_n - G_{P,T} G_{T,P})^{-1} (G_T + G_{P,T} G_P)$. Following the approach in [150], the internal transfer functions are obtained by

$$\begin{bmatrix} \xi_1 \\ \xi_2 \\ \xi_3 \end{bmatrix} = \begin{bmatrix} I_{2n} & 0_{2n \times n} & F \\ -C & I_n & 0_{n \times 2n} \\ 0_{2n} & -G & I_{2n} \end{bmatrix}^{-1} \begin{bmatrix} r \\ d_i \\ d_o \end{bmatrix}, \quad (4.53)$$

where $G = [\tilde{G}_P; \tilde{G}_T]$, $C = [C_P W_P \ C_T]$, $F = [I_n \ 0_n; 0_n \ W_T]$. Twenty-five internal closed-loop transfer functions from \hat{P}_g^{ref} , r , d_i , \tilde{q}_P , and \tilde{q}_T to e_P , e_T , P_g^{ref} , P_g and F_T can be derived from (4.53). For conciseness, these functions are not explicitly presented. All transfer functions retain the characteristic matrix polynomial shown in (4.49). Moreover, they are well-defined and proper, and have possible pole and zero cancellations inside the unit circle when satisfying the stability matrix conditions in (4.46) and (4.47). Consequently, Theorem 1 also ensures the internal stability of the closed-loop system based on these properties.

We can demonstrate this argument by applying the block matrix inversion in the inverse term in Eq. (4.53), such that

$$\begin{bmatrix} I_{2n} & 0_{2n \times n} & F \\ -C & I_n & 0_{n \times 2n} \\ 0_{2n} & -G & I_{2n} \end{bmatrix}^{-1} =$$

$$\left[\begin{array}{c|c|c} \frac{I_{2n} - F(I_{2n} + GCF)^{-1}GC}{(I_n - \bar{C}\bar{F}(I_{2n} + \bar{G}\bar{C}\bar{F})^{-1}\bar{G})\bar{C}} & \frac{-F(I_{2n} + GCF)^{-1}G}{(I_{2n} + \bar{G}\bar{C}\bar{F})^{-1}\bar{G}} & \frac{-F(I_{2n} + GCF)^{-1}}{(I_{2n} + GCF)^{-1}} \\ \hline \frac{(I_n - \bar{C}\bar{F}(I_{2n} + \bar{G}\bar{C}\bar{F})^{-1}\bar{G})\bar{C}}{(I_{2n} + GCF)^{-1}\bar{G}} & \frac{-F(I_{2n} + GCF)^{-1}G}{(I_{2n} + \bar{G}\bar{C}\bar{F})^{-1}\bar{G}} & \frac{-F(I_{2n} + GCF)^{-1}}{(I_{2n} + GCF)^{-1}} \\ \hline \frac{(I_n - \bar{C}\bar{F}(I_{2n} + \bar{G}\bar{C}\bar{F})^{-1}\bar{G})\bar{C}}{(I_{2n} + GCF)^{-1}\bar{G}} & \frac{-F(I_{2n} + GCF)^{-1}G}{(I_{2n} + \bar{G}\bar{C}\bar{F})^{-1}\bar{G}} & \frac{-F(I_{2n} + GCF)^{-1}}{(I_{2n} + GCF)^{-1}} \end{array} \right]. \quad (4.54)$$

Having derived (4.54), we can analyze the stability of each block. We note that each block can be seen as the series and parallel interconnection of a number of different MIMO systems, namely: G , C , F , and $(I_{2n} + GCF)^{-1}$. Thus it is sufficient to analyze the stability of each of these to guarantee internal stability. Additionally, we note immediately that $(I_{2n} + GCF)^{-1}$ is the output sensitivity transfer function from d_o to ξ_3 , which we define as S , and shows up directly in (4.54).

Firstly, the systems described by the transfer matrices G , C are stable by either assumption (G) or design (C), while F is a static gain. Thus, to show internal stability it is sufficient to show stability of $S = (I_{2n} + GCF)^{-1}$. Thus, applying Woodbury's formula, also known as the matrix inversion lemma, and replacing the definitions for G , C , and F , we obtain

$$S = (I_{2n} + GCF)^{-1} = I_{2n} - G(I_n + CFG)^{-1}CF = \left[\begin{array}{cc} I_n - \tilde{G}_P(I_n + C_P W_P \tilde{G}_P + C_T W_T \tilde{G}_T)^{-1} C_P W_P & -\tilde{G}_P(I_n + C_P W_P \tilde{G}_P + C_T W_T \tilde{G}_T)^{-1} C_T W_T \\ -\tilde{G}_T(I_n + C_P W_P \tilde{G}_P + C_T W_T \tilde{G}_T)^{-1} C_P W_P & I_n - \tilde{G}_T(I_n + C_P W_P \tilde{G}_P + C_T W_T \tilde{G}_T)^{-1} C_T W_T \end{array} \right]. \quad (4.55)$$

Thus, defining

$$S = \begin{bmatrix} S_{11} & S_{12} \\ S_{21} & S_{22} \end{bmatrix},$$

replacing \tilde{G}_P , \tilde{G}_T , C_P , and C_T by their definitions, and performing some algebraic manipulations (which include some stable zero-pole cancellations, given stability of G and C) we obtain:

$$S_{11} = I_n - \tilde{G}_P(I_n + C_P W_P \tilde{G}_P + C_T W_T \tilde{G}_T)^{-1} C_P W_P = I_n - (I_n - G_{T,P} G_{P,T})^{-1} (G_P + G_{T,P} G_T) [I_n + C_P W_P (I_n - G_{T,P} G_{P,T})^{-1} (G_P + G_{T,P} G_T) + C_T W_T (I_n - G_{P,T} G_{T,P})^{-1} (G_T + G_{P,T} G_P)]^{-1} C_P W_P = \quad (4.56a)$$

$$[(I_n z - A_P)(I_n z - A_T)(I_n z - I_n) - (I_n z - I_n) A_{T,P} A_{P,T} + (I_n z - A_T) \bar{K}_P W_P B_P + A_{T,P} \bar{K}_P W_P B_T + (I_n z - A_P) \bar{K}_T W_T B_T + A_{P,T} \bar{K}_T W_T B_P]^{-1} [(I_n z - A_P)(I_n z - A_T)(I_n z - I_n) - (I_n z - I_n) A_{T,P} A_{P,T} + (I_n z - A_T) \bar{K}_P W_P B_P + A_{P,T} \bar{K}_T W_T B_P]. \quad (4.56b)$$

$$S_{12} = -\tilde{G}_P(I_n + C_P W_P \tilde{G}_P + C_T W_T \tilde{G}_T)^{-1} C_T W_T = -(I_n - G_{T,P} G_{P,T})^{-1} (G_P + G_{T,P} G_T) [I_n + C_P W_P (I_n - G_{T,P} G_{P,T})^{-1} (G_P + G_{T,P} G_T) + C_T W_T (I_n - G_{P,T} G_{T,P})^{-1} (G_T + G_{P,T} G_P)]^{-1} C_T W_T = \quad (4.57a)$$

$$-[(I_n z - A_P)(I_n z - A_T)(I_n z - I_n) - (I_n z - I_n) A_{T,P} A_{P,T} + (I_n z - A_T) \bar{K}_P W_P B_P + A_{T,P} \bar{K}_P W_P B_T + (I_n z - A_P) \bar{K}_T W_T B_T + A_{P,T} \bar{K}_T W_T B_P]^{-1} [(I_n z - A_T) \bar{K}_T W_T B_P + A_{T,P} \bar{K}_T W_T B_T]. \quad (4.57b)$$

$$\begin{aligned}
S_{21} = & -\tilde{G}_T(I_n + C_P W_P \tilde{G}_P + C_T W_T \tilde{G}_T)^{-1} C_P W_P = \\
& -(I_n - G_{P,T} G_{T,P})^{-1} (G_T + G_{P,T} G_P) [I_n + C_P W_P (I_n - G_{T,P} G_{P,T})^{-1} (G_P + \\
& G_{T,P} G_T) + C_T W_T (I_n - G_{P,T} G_{T,P})^{-1} (G_T + G_{P,T} G_P)]^{-1} C_P W_P = \quad (4.58a) \\
& -[(I_n z - A_P)(I_n z - A_T)(I_n z - I_n) - (I_n z - I_n) A_{T,P} A_{P,T} + (I_n z - A_T) \tilde{K}_P W_P B_P + \\
& A_{T,P} \tilde{K}_P W_P B_T + (I_n z - A_P) \tilde{K}_T W_T B_T + A_{P,T} \tilde{K}_T W_T B_P]^{-1} \\
& [(I_n z - A_P) \tilde{K}_P W_P B_T + A_{P,T} \tilde{K}_P W_P B_P]. \quad (4.58b)
\end{aligned}$$

$$\begin{aligned}
S_{22} = & I_n - \tilde{G}_T(I_n + C_P W_P \tilde{G}_P + C_T W_T \tilde{G}_T)^{-1} C_T W_T = \\
& I_n - (I_n - G_{P,T} G_{T,P})^{-1} (G_T + G_{P,T} G_P) [I_n + C_P W_P (I_n - G_{T,P} G_{P,T})^{-1} (G_P + \\
& G_{T,P} G_T) + C_T W_T (I_n - G_{P,T} G_{T,P})^{-1} (G_T + G_{P,T} G_P)]^{-1} C_T W_T = \quad (4.59a) \\
& [(I_n z - A_P)(I_n z - A_T)(I_n z - I_n) - (I_n z - I_n) A_{T,P} A_{P,T} + (I_n z - A_T) \tilde{K}_P W_P B_P + \\
& A_{T,P} \tilde{K}_P W_P B_T + (I_n z - A_P) \tilde{K}_T W_T B_T + A_{P,T} \tilde{K}_T W_T B_P]^{-1} \\
& [(I_n z - A_P)(I_n z - A_T)(I_n z - I_n) - (I_n z - I_n) A_{T,P} A_{P,T} + \\
& (I_n z - A_T) \tilde{K}_P W_P B_P + A_{T,P} \tilde{K}_P W_P B_T]. \quad (4.59b)
\end{aligned}$$

In (4.56b), (4.57b), (4.58b), and (4.59b) we have rewritten S_{ij} in its left Polynomial Matrix Fractional Description (l-PMFD), as defined in [151, Ch. 7], i.e.:

$$S_{ij}(z) = D_{ij}(z)^{-1} N_{ij}(z), \quad (4.60)$$

where D_{ij} and N_{ij} are $n \times n$ polynomial matrices. We conclude by noting not only that $D_{ij}(z)$ is the same for all $i, j \in \{1, 2\}$, but also, and most importantly, that it is the matrix characteristic polynomial derived in Theorem 1. Thus, given that the poles of S_{ij} are equivalent to the roots of $\det(D_{ij})$, i.e., the solutions to the matrix characteristic equation, we see that S is stable by satisfaction of the conditions in Theorem 1.

The robustness against output disturbances, which represents unmodeled effects and deviations from our identified simplified WF model, is characterized by the output sensitivity transfer function S from d_o to ξ_3 . Norms are often employed for robustness analysis [150], but this approach can be computationally expensive and susceptible to numerical issues as our MIMO system scales with the number of turbines. As an alternative, we visually inspect the locations of the zeros and poles of S_{ij} . The matrix polynomial equations $N_{ij}(z)$ and $D_{ij}(z)$ are formulated as generalized eigenvalue problems [152] to find the zeros and poles, respectively. This approach is scalable for large numbers of turbines and, possibly, higher-order system models.

In Figure 4.7, we compare the zero and pole mappings of the four transfer functions derived from S using the MCDC formulation to those of the Central-WFC for our study case of thirty-two WTs. Considering the same control gains, we can see slight changes in the locations of the zeros and poles due to the different approaches. All poles are situated within the unit circle, characterizing stability, along with all zeros and possible cancellations. The

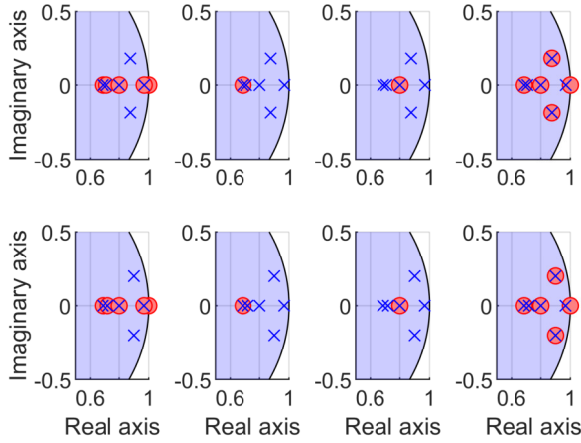


Figure 4.7: Zero and pole mappings of the sensitivity function for centralized control (upper subplots) and our proposed MCDC (down subplots) in our study case. Slight dislocations are observed due to the delay in the MCDC formulation.

greater the distance between the poles and zeros and the unit circle, the more robust the approach is. The poles of the MCDC shifted slightly to the right-hand side, indicating a minor reduction in robustness. Additional details of our study case are presented in the subsequent section.

4.4. RESULTS AND DISCUSSION

The proposed MCDC presented in Section 4.3 is evaluated in the high-fidelity large-eddy simulator SOWFA [84]. The WF layout is based on the TotalControl reference wind power plant [87] and the adopted set of neighbors \mathcal{N}_i is set based on the communication range of each WT as depicted in Figure 4.8. A low wake interaction scenario (Scenario 1) and a medium wake interaction scenario (Scenario 2) are considered, which differ in the prevailing wind direction, as illustrated in Figure 4.9 and 4.10, respectively. The wind farm power reference is taken from a portion of the 40-minute ‘RegD’ test signal [89], normalized to have an amplitude of 32 MW with an additional persistent value of 112 MW. The simulations were set with a 10Hz sampling rate, which was utilized in each wind turbine power tracking controller, while a sampling rate of 2Hz was implemented for the WF control. To reach average consensus, we conservatively set the number of steps at $h = 400$, acknowledging that the WF control’s sampling time does not necessitate

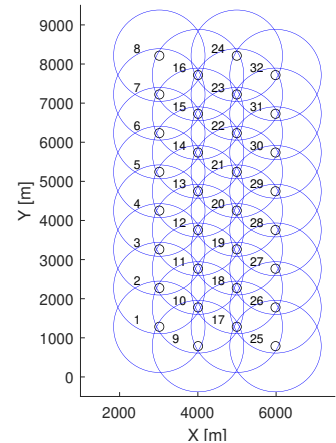


Figure 4.8: Illustration of the communication range spanning $5\sqrt{2}$ of the turbine diameter.

the same level of swiftness as the WT control. This results in a high-frequency communication rate of 800 Hz across the neighbor turbines, which is acceptable for typical low-range wireless communication devices.

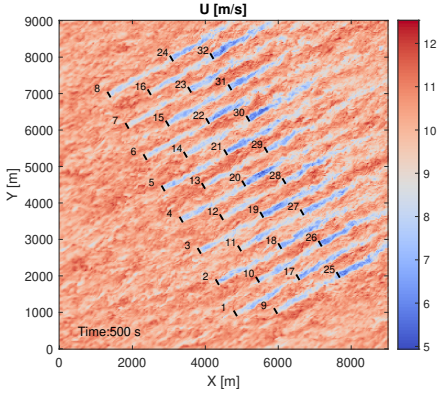


Figure 4.9: Scenario 1 - wind speed direction perpendicular to the TotalControl Reference Wind Power Plant [87].

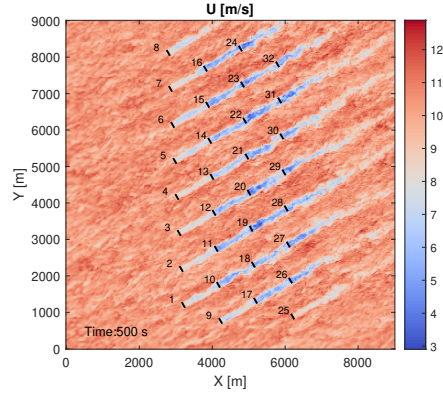


Figure 4.10: Scenario 2 - wind speed direction of 26.565 degrees to the TotalControl Reference Wind Power Plant [87].

The controller gains were selected as $K_P = \frac{1}{4} \frac{1}{n}$ and $K_T = 0.25$ based on insights from previous works [54, 18], and in accordance with the stability conditions outlined in Theorem 1. The same values were applied in both the Central-WFC and the MCDC to assess the impacts of the introduced delays and the finite number of interactions to consensus from the MCDC approach.

We start by presenting the comparisons of the WF's active power generation, depicted in Figure 4.11 for Scenario 1 and Figure 4.12 for Scenario 2. The figures illustrate the power production of the WF over time which is regulated to a power demand from the operator. Both the central and the proposed distributed control approaches maintain the track of the WF power reference without an offset, in contrast to the offset observed in the absence of a wind farm controller (No-WFC). This offset results from the combination of power losses, where turbines generate less power than expected, caused by turbulence effects. While compensation strategies in open loop can help reduce this offset, turbine saturation further exacerbates the offset in Scenario 2, significantly impacting total power generation. A quantitative assessment of the WF's power tracking has been conducted and conveniently summarized in Table 4.1. This evaluation is based on the root mean square error (RMSE) between the desired power reference and the actual power generation, as well as its peak error (PE). The performance results of the MCDC prove to be satisfactory and nearly equivalent to the centralized approach. The key performance indicators are calculated from the 300-second mark onward.

Despite the added delay from the average consensus computation, the MCDC showcases comparable performance when compared to the Central-WFC. Particularly, in Scenario 2, the MCDC achieves a 96.25% reduction in the RMSE of power compared with the No-WFC, which is comparable to the 97.65% reduction by the Central-WFC compared with the No-WFC.

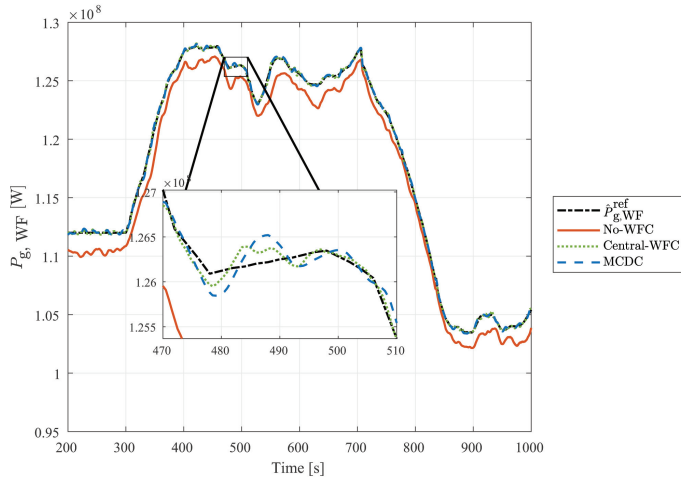


Figure 4.11: Wind farm active power generation in Scenario 1.

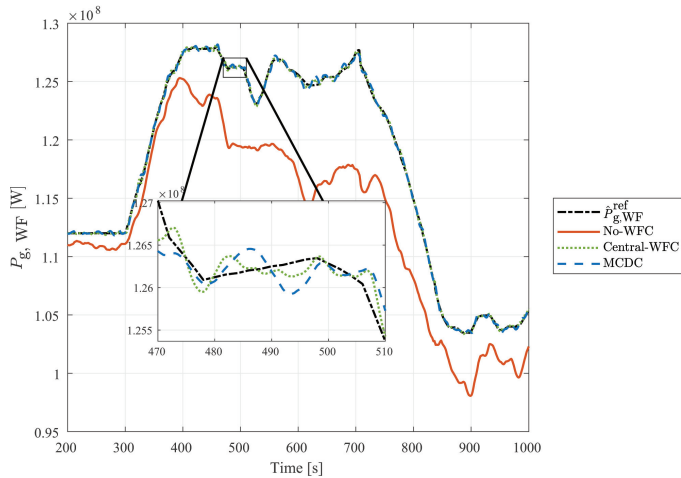


Figure 4.12: Wind farm active power generation in Scenario 2.

Shifting our focus to the structural loads, the mean and standard deviation of the aerodynamic loads across the turbines are depicted in Figure 4.13. A reduction in the standard deviation, illustrated by the shaded regions, is evident with the implementation of both the central and the proposed distributed control approaches. Again, it demonstrates equivalence between the approaches in balancing structural loads, in which the shaded region is reduced compared to the results from the No-WFC.

The quantitative evaluation of the thrust balancers is additionally provided in Table 4.1 in terms of the mean and peak of the computed thrust force variance across the turbines. In Scenario 2, the MCDC achieves a 91.97% reduction in the mean of the thrust force

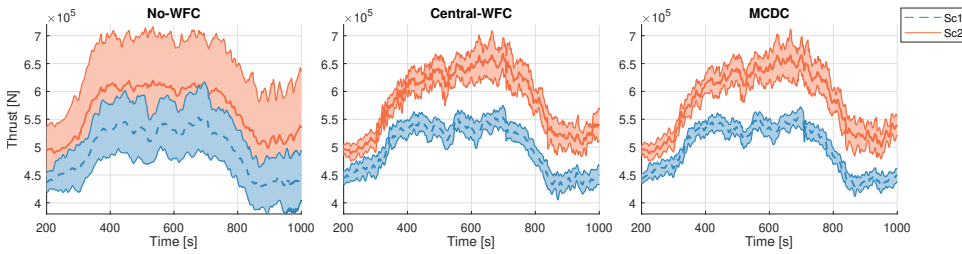


Figure 4.13: Mean and standard deviation of thrust forces of all turbines in both scenarios 1 and 2.

variance, compared to the 92.29% reduction observed with the Central-WFC. Interestingly, in Scenario 1, with a reduction of 91.92% compared to 88.31% the MCDC overperforms the Central-WFC in the mean of the thrust force variance. This may seem counter-intuitive and it is ascribed to the inherent additional delay introduced by the MCDC, where we adopted the same gains in the controller from the Central-WFC. While the delay negatively impacts power compensation, it reflects positively on the thrust balancing, as the two loops exert opposing effects on each other. However, the control gains can be adjusted accordingly to balance these effects.

These findings emphasize the potential of an effective distributed control approach. Leveraging established theories, our approach holds potential for innovative applications in managing future large-scale wind parks and other multi-agent systems, with promising and satisfactory results demonstrated in high-fidelity simulations.

Our high-fidelity simulations examine the wind farm's ability to meet power demand using the proposed wind farm control strategy at an average wind speed of 10ms^{-1} and a turbulence intensity of 5-6% in the inflow. Nevertheless, it is important to acknowledge the limitations of our strategy in the following remarks:

Table 4.1: Performance of WF controllers.

Scenario	Approach	RMSE of power [MW]	PE of power [MW]	Mean of thrust variance [GN^2]	Peak of thrust variance [GN^2]
1	No-WFC	1.2950	2.6982	2.3297	4.1050
	MCDC	0.1258	0.5536	0.1883	0.3881
	Central-WFC	0.1142	0.4612	0.2723	0.6272
2	No-WFC	6.0417	10.7650	8.0316	10.9100
	MCDC	0.2268	0.9006	0.6447	2.2425
	Central-WFC	0.1422	0.5021	0.6195	2.0546

*The colors in the cells go from light green as the lowest value to yellow as the highest value across each performance indicator, i.e. across each column. NA stands for non-applicable. [-] refers to simulations that were not conducted.

Remark 10. *Rapid wind condition changes in real settings can affect the proposed design's performance, with consensus diverging from current conditions. Reducing the wind farm sampling time can mitigate this, but it demands faster, yet feasible, communication.*

Remark 11. *Low or no wind conditions can compromise WF power generation despite the controller's efforts. Managing this volatility requires complementary strategies, such as energy storage and integrating wind with other energy sources.*

4.5. CONCLUSION

As wind parks transition towards large-scale systems, the prominent future trajectory for WF control is toward decentralization. However, this transformation introduces numerous challenges in effectively controlling the WTs cooperatively. This work presents the MCDC, a fully distributed control approach for power compensation, power distribution, and aerodynamic load balance. At a high rate, consensus is obtained for the variables of interest, and, at a low rate, the control takes place. This novel, practical approach integrates the wind farm objectives using well-established control methods, achieving effective results. The main advantages of the proposed MCDC framework include:

1. MCDC does not rely on explicitly modeling WT interaction;
2. MCDC is both distributed and computationally tractable, facilitating straightforward implementation;
3. MCDC achieves performance comparable to the centralized controller.

Remarkably, the MCDC does not require a communication central point. This facilitates the implementation of WF control, which can be embedded locally in each WT. This paves the way for the production of WTs with WF control capabilities. Moreover, it requires only the current WT hardware and a short-distancing communication system, minimizing associated costs. While the MCDC relies on more frequent communication with neighboring WTs in comparison to the alternative approaches in the literature of distributed control, it is important to note that communication is limited to the neighboring WTs, and its performance matches the centralized controller.

As future venues of research, the proposed MCDC could be broadened to encompass additional applications in operation and management, such as distributing critical local structural information. Furthermore, the framework may prove advantageous for detecting cyber-attacks and corrupted signals within the communication channels. The high rate layer utilized to reach consensus provides space to integrate detection algorithms, thus enhancing security and robustness against such malicious threats before actions are taken in the lower rate layer. Additionally, extensions of this work include exploring strategies to accommodate link and node failures, as well as communication rate limitations. In these scenarios, consensus might not sufficiently converge within the sampling time of the WF control. The use of strategies that enhance convergence are of great value, such as robust network design and restarting mechanisms. Moreover, sufficient conditions for stability in the presence of extra delays are direct extensions of this work.

5

WIND TUNNEL TESTING OF WIND FARM CONTROLLERS

The true method of knowledge is experiment.

William Blake

*It doesn't matter how beautiful your theory is,
it doesn't matter how smart you are.
If it doesn't agree with experiment, it's wrong.*

Richard P. Feynman

The outcomes presented in the preceding chapters were derived from simulations. While simulations rely on advanced engineering models, they may overlook physical phenomena that remain incompletely understood in practical scenarios. In this chapter, we put the power-tracking control concepts and wind farm control algorithms into action by conducting experiments in a controlled setup.

The work of this chapter has been published in Silva et al. [153].

5.1. INTRODUCTION

Current wind turbines usually operate to maximize their own power generation. When placing them together, the deployment cost and the amount of area needed for usage are reduced. However, a notable challenge arises from the interactions between turbines induced by their wakes [12] - the turbulent downstream wind structures created by the energy extraction from the rotor blades. The conventional operation of wind turbines, neglecting each turbine's impact on other turbines through its wake, is considered a greedy approach. Strategies such as axial induction and wake steering control have been proposed in the literature to address the wake interactions [15]. Recently, wake-mixing techniques have been suggested that apply a sinusoidal thrust excitation to enhance wake recovery [31]. The emphasis on maximizing power generation is predominantly employed because wind energy constitutes a small share of the total power generation, with other energy sources typically taking over the grid regulation.

As the share of wind energy grows, the maximization paradigm is expected to shift to a demand-response source. To supply sufficient stability throughout the electrical grid, wind farms would instead regulate their power generation to the demand [55, 34, 1]. Such a transformation is beneficial for the future of wind energy. Yet, insufficient wind may still render the grid susceptible to system splits, blackouts, and instabilities. Therefore, discussions to address power system stability challenges due to the variability of wind sources are gathering momentum [2, 154]. To overcome these challenges, for instance, storage units have been proposed as presented by Morales et al. [155], including batteries and hydrogen plants. Also, the integration with other energy sources that present flexible power regulation capabilities, such as hydro power, solar power, and nuclear energy have been recommended [156, 157, 158]. While energy integration efforts are crucial for the future, in this work, we focus on wind farm control techniques to provide more flexible and reliable wind energy solutions from the wind power plants themselves. Through wind tunnel testing, we explored the on-demand power tracking capability of single turbines and their collaboration within a farm.

To enhance wind energy flexibility, requirements have been placed to equip wind turbines with derating capabilities [33]. This aims to improve the integration of wind energy into the grid. With the increasing penetration of wind energy, it is important for wind farms to actively contribute to frequency regulation, i.e. providing active power control (APC) services to the grid. In the existing literature, different derating control strategies have been proposed [36, 20, 26]. Aho et al. [36] presented two derating approaches: APC torque control and APC pitch control. The APC torque control maintains a high rotor speed, which is favorable for power regulation since energy is stored as kinetic energy by the rotating components. This kinetic energy enables greater responsiveness to rapid changes in power demand. On the other hand, lowering rotor speed, with the APC pitch control, leads to lower structural loads, as demonstrated by van der Hoek et al. [20]. It is important to note that there is an infinite number of operating conditions that can achieve a desired down-regulation, a point underscored by Lio et al. [26]. The wind flow and the interaction between the turbines vary based on the adopted derating control strategy. In the works of Ma et al. [19] and Kim et al. [63], lower rotor speed methods are suggested in a wind farm context because they result in lower thrust forces, reducing the wind deficit and consequently benefiting downstream turbines. Ideally, derating while considering a minimum

thrust force would maximize wind farm power availability. However, this approach relies heavily on accurate wind speed estimates, which are challenging to obtain in highly waked scenarios. This reliance often leads to degraded performance [159] and can result in shut-downs at lower rotor speeds. Here, we derive and investigate a low rotor speed approach similar to APC pitch control that does not directly use the wind speed information in the controller, overcoming the challenges of the minimum thrust force method.

Wind farm control considering aerodynamic loads is in the early stages. The concept was presented and assessed by simulations in Vali et al. [39] and Silva et al [54], where the contributions of individual turbines to the total power output are modified online through feedback based on the turbines' structural loading. Taking into account thrust forces not only can reduce the wind deficit but also avoid the overloading of specific turbines due to prevailing wind conditions, thereby reducing sporadic failures and consequently maintenance costs. These are promising outcomes, especially within the offshore wind sector. In offshore sites, the access for maintenance operations is limited and the turbines are placed in a highly corrosive environment that accelerates degradation and amplifies fatigue, thereby increasing failure rates [68].

Regarding wind farm power regulation, a fundamental approach involves employing a balanced and equitable power generation across turbines [14]. This strategy entails derating all turbines equally to meet an overall demand lower than the wind farm's capacity. Each turbine receives an equal share of the total power demand, aiming to prevent overloading of any particular turbine, irrespective of wake interactions. However, uniform power generation may result in uneven power availability due to the wake effects, potentially leading to turbine *saturation*, where turbines fail to meet demands that surpass their maximum available power capacity. In such scenarios, as a remedy, turbines with available power can increase power generation and compensate for others with insufficient power availability. A real-time closed-loop solution, introduced by van Wingerden et al. [18] using a simple but effective PI controller, shows through simulations to enhance wind farm power output by alleviating power fluctuations. In Silva et al. [72, 54], the authors extended this approach to assess power losses due to turbine *saturation* and implemented it concurrently with the thrust force balancing in simulations. The real-time feedback approach contrasts with typical axial induction control approaches, which rely on steady-state models and lookup tables to maximize power and have demonstrated limited benefits in realistic conditions [119, 28].

This chapter contributes by deriving derating control strategies and elucidating their impact from a wind farm perspective through wind tunnel testing. Additionally, it validates wind farm control strategies, particularly real-time feedback controllers for thrust force balancing and power compensation in the presence of turbine *saturation*, transitioning from numerical simulations to experimental setups. Previous experimental works, such as those by Campagnolo et al. [160], focused on power maximization. Furthermore, Petrovic et al. [161] performed experiments with a closed-loop wind farm controller for APC, but did not evaluate turbine saturation scenarios nor account for loads.

Our findings highlight the advantages of balancing aerodynamic loads across the farm, preventing turbine saturation, and enhancing power availability by 3-5% compared to a uniform power dispatch. Furthermore, the inclusion of power compensation results in a heightened upper limit in wind farm power tracking, indicating a 22% boost in wind farm power availability. This research underscores the potential benefits of innovative turbine

regulation strategies for optimizing wind farm performance and enhancing overall energy flexibility.

The remainder of this chapter is structured as follows: The experiments are conducted with scaled wind turbines in the wind tunnel, described in Section 5.2. The considered derating control strategies are presented in Section 5.3.1. The wind farm controller, which compensates for power and balances loads in the farm, is described in Section 5.3.2. The results are reported in Section 5.4, where we first demonstrate the effects of different derating control strategies on a single turbine and in a wind farm setting in Section 5.4.1. Next, we evaluate the effectiveness of thrust force balancing to showcase the reduction of fatigue loads and the enhancement of wind farm power availability in Section 5.4.2 and Section 5.4.3, respectively; Then, we assess the effectiveness of power compensation in the presence of turbine saturation in Section 5.4.3. Finally, the conclusions are presented in Section 5.5.

5.2. EXPERIMENTAL SETUP

The experiments were performed in a novel modular wind tunnel at the Delft University of Technology. The wind tunnel was tailored to replicate diverse wind conditions, prioritizing practicality through modular compartments. The wind tunnel consists of a WindShape

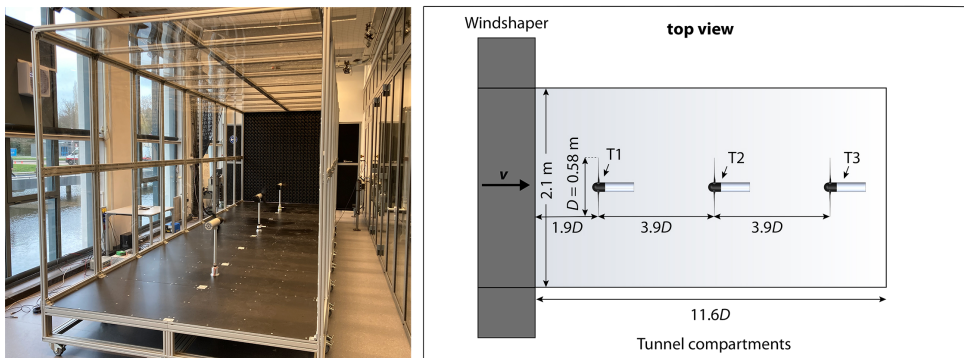


Figure 5.1: Illustrations of the experimental setup: the photo of the wind tunnel and the three scaled turbines in operation on the right; and the layout details on the left.

unit [162] with a square outlet of 2.1 by 2.1 m, typically utilized for drone testing. The WindShape is composed of 9 by 9 modules, each containing 9 pairs of counter-rotating computer fans, which allow personalizing the desired wind profile, with a maximum wind speed of 15 m/s. Additionally, the wind tunnel includes modular compartments that contain the flow for a desired length. The scaled wind turbines are placed in specific modular compartments, defining their distancing. An overview of the experimental setup is provided in Figure 5.1.

For the experiments, we utilized three MoWiTo-0.6 wind turbines developed by the University of Oldenburg [163]. This three-bladed, horizontal-axis wind turbine has a rotor diameter of $D = 0.58$ m and is equipped with a generator that allows torque control and a stepper motor for collectively pitching blades. The base of the turbine tower is equipped

with a set of strain gauges in a full Wheatstone bridge to measure the tower bending moment.

The wall interference from the tunnel compartments can be considered negligible [164], where the blockage effect, defined as the ratio of the rotor-swept area divided by the wind tunnel cross-sectional area, is 6%. The hub center of the turbines was $0.672D$ above the tunnel floor. Hence, interference effects from the ground are about as expected at full scale. The three wind turbines are spaced $3.9D$ apart to operate in full wake conditions. Only the full wake condition is considered because it represents the worst-case scenario regarding power availability. The tests were conducted at constant inflow velocities at 7 and 8 m/s with an inherent turbulence intensity of $TI \approx 4\%$, and no vertical wind profile.

The control system is established as illustrated in Fig. 5.2. Communication between the wind turbines and the computer is arranged with a dSPACE *MicroLabBox*. The dSPACE *MicroLabBox* offers a real-time interface with MATLAB's Simulink[®] through dSPACE *ControlDesk* software. The controllers for the wind turbines and the wind farm, as well as the estimators for wind speed and thrust, are developed in MATLAB's Simulink[®] and compiled to run within dSPACE *ControlDesk* at a frequency of 2 kHz. The recorded signals from the turbines encompass rotor speed, pitch angles, generator torque, and strain at the tower base. These signals are utilized in the controllers and estimators. The actuator signals include the generator torque and blade-pitch angles; yaw control is not considered in the scope of this work. Aiming to investigate control algorithms in an experimental setup, this setup has also been used to explore wake mixing strategies [165].

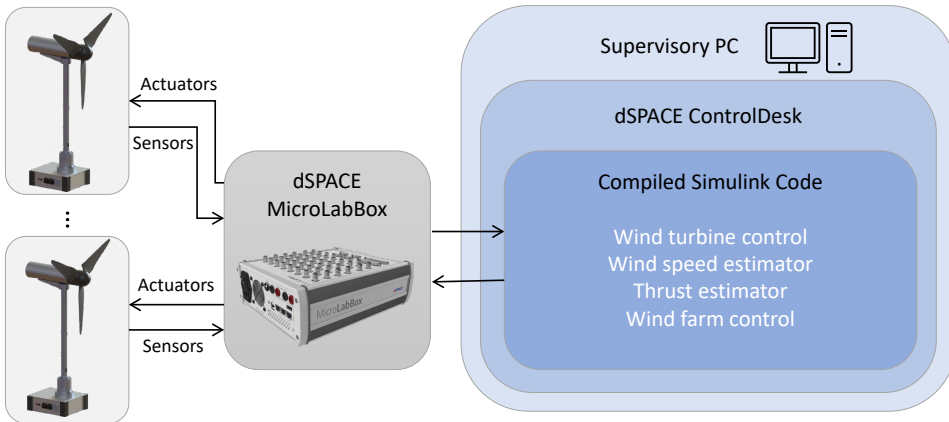


Figure 5.2: Control structure utilizing real-time interface with dSPACE and Simulink.

5.3. ADOPTED STRATEGIES

5.3.1. DERATING CONTROL STRATEGIES

Control strategies utilizing blade pitching for derating purposes have been demonstrated as beneficial for wind farms, not only in terms of reducing structural loading but also in enhancing wind farm power availability [19, 63]. The advantage in terms of wind farm power generation lies in the significant reduction of wind deficit achieved through blade pitching,

as opposed to relying solely on pure generator torque control for derating. This reduction of wind deficit behind the derated turbine is particularly beneficial for downstream turbines, enhancing overall wind farm power availability. Consequently, our focus is on derating strategies that utilize blade pitching.

The definition of a derating strategy involves establishing a framework for determining the blade pitching strategy, consequently affecting the generator torque through the changes in the rotor speed. First, we formulate the closed-loop controller that regulates the rotor speed based on blade pitching in Section 5.3.1. Different definitions of the reference rotor speeds lead to different operating conditions, i.e. combinations of blade pitching and generator torque, that result in distinct turbine performances and wake characteristics. As a result, we propose and evaluate two strategies: derating control by blade pitching based on the greedy generator torque control, presented in Section 5.3.1; and derating control by blade pitching with constant tip speed ratio, in Section 5.3.1.

BLADE-PITCH CONTROLLER FOR DERATING STRATEGIES

The main goal of the blade-pitch controller is to regulate the rotor speed to a desired set point by pitching the blades. To obtain the blade-pitch controller for the derating control strategies, we follow the derivation of the baseline blade-pitch control utilized in the above-rated wind speed conditions from Hansen et al. [25] and Jonkman et al. [77]. The blade-pitch controller is designed using the drive-train model defined as

$$T_{\text{aero}} - G_b T_{\text{gen}} = J_{\text{LSS}} \Delta \dot{\omega}_r, \quad (5.1)$$

where T_{aero} is the low-speed shaft aerodynamic torque, T_{gen} is the high-speed shaft generator torque, G_b is the high-speed to low-speed gearbox ratio, J_{LSS} is the rotational components' equivalent inertia, corresponding to the low-speed shaft, $\Delta \dot{\omega}_r$ is the low-speed shaft rotational acceleration. The generator torque T_{gen} can be configured in two ways. First, it can be adjusted to match the specified reference power P^{ref} . In that case, it exhibits an inverse relationship with the generator speed and is referred to as a *tracking* mode. Alternatively, the generator torque can be set to maximize power extraction, operating in a mode known as *greedy*. This mode is reached when the turbine cannot meet the power demand, so it maximizes the power extraction instead. Therefore, the torque is set as

$$T_{\text{gen}} = \begin{cases} T_{\text{gen,tracking}}(P^{\text{ref}}, \omega_r) = \frac{P^{\text{ref}}}{G_b \omega_r}, & \text{if in tracking mode;} \\ T_{\text{gen,greedy}}(\omega_r) = K_{\text{gen}} \omega_r^2, & \text{else if in greedy mode.} \end{cases} \quad (5.2)$$

where K_{gen} is the greedy generator torque gain based on the steady-state aerodynamics, and ω_r is the low-speed shaft rotational velocity. Conversely, the aerodynamic torque is dependent not only upon the rotor speed but also on the blade-pitch angles and wind speed, as expressed in the following:

$$T_{\text{aero}}(\theta, \omega_r, v) = \frac{P(\theta, \omega_r, v)}{\omega_r}, \quad (5.3)$$

where P is the mechanical power, θ is the collective blade-pitch angle, and v is the inflow wind speed.

Taking the first-order Taylor series expansion of the above expressions, we have:

$$T_{\text{gen,tracking}}(P^{\text{ref}}, \omega_r) \approx \frac{P_0^{\text{ref}}}{G_b \omega_{r,0}} - \frac{P_0^{\text{ref}}}{G_b \omega_{r,0}^2} \Delta \omega_r + \frac{1}{G_b \omega_{r,0}} \Delta P^{\text{ref}}, \quad (5.4)$$

$$T_{\text{gen,greedy}}(\omega_r) \approx K_{\text{gen}} \omega_{r,0}^2 + 2K_{\text{gen}} \omega_{r,0} \Delta \omega_r, \quad (5.5)$$

and

$$T_{\text{aero}}(\theta, \omega_r, v) \approx \frac{P_0}{\omega_{r,0}} + \frac{1}{\omega_{r,0}} \left. \frac{\partial P}{\partial \theta} \right|_0 \Delta \theta + \frac{1}{\omega_{r,0}} \left. \frac{\partial P}{\partial \omega_r} \right|_0 \Delta \omega_r - \frac{P_0}{\omega_{r,0}^2} \Delta \omega_r + \frac{1}{\omega_{r,0}} \left. \frac{\partial P}{\partial v} \right|_0 \Delta v, \quad (5.6)$$

where $\Delta \omega_r$, ΔP^{ref} , $\Delta \theta$ and Δv are small perturbations from the operation point 0 of the low-speed shaft rotational speed, the reference power, the collective blade-pitch angle, and the inflow wind speed, respectively. $\left. \frac{\partial P}{\partial \theta} \right|_0$, $\left. \frac{\partial P}{\partial \omega_r} \right|_0$ and $\left. \frac{\partial P}{\partial v} \right|_0$ are the sensitivity of aerodynamic power to collective blade-pitch angle, to the rotor speed and to the inflow wind speed, respectively. The terms of the aerodynamic torque associated with the perturbations of the low-speed shaft rotation speed and the inflow wind speed are expected to be approximately three orders of magnitude lower than the term associated with the perturbation of collective blade-pitch angle. This assessment is based on the observed rates of change—approximately 5 rad/s² for the low-speed shaft rotation speed, 1°/s for the collective blade-pitch angle, and 0.02 m/s² for the inflow wind speed—and the operational conditions, which include a low-speed shaft rotation speed of 130 rad/s, a power output of 13 W, a collective blade-pitch angle of 6°, and an inflow wind speed of 8 m/s. Therefore, as a design decision, we focus on the aerodynamic torque changes with respect to the collective blade-pitch angle solely, so the aerodynamic torque is simplified, in accordance with [25, 77], as

$$T_{\text{aero}}(\theta) \approx \frac{P_0}{\omega_{r,0}} + \frac{1}{\omega_{r,0}} \left. \frac{\partial P}{\partial \theta} \right|_0 \Delta \theta. \quad (5.7)$$

We apply a proportional-integral-derivative (PID) control law to dynamically adjust the collective blade-pitch angle based on the rotor-speed perturbation, acting as the reference error. This strategy ensures precise rotor speed regulation while tracking the desired power set-point. The variation in the collective blade-pitch angle is defined as

$$\Delta \theta = K_P G_b \Delta \omega_r + K_I \int_0^t G_b \Delta \omega_r dt + K_D G_b \Delta \dot{\omega}_r, \quad (5.8)$$

where K_P , K_I , and K_D are the blade-pitch controller proportional, integral, and derivative gains, respectively. If the applied generator torque corresponds to the tracking generator torque outlined in Eq. (5.4), combining with Eq. (5.1), Eq. (5.7), and Eq. (5.8), the equation of motion for the rotor-speed error can be derived as

$$\underbrace{\left[J_{\text{LSS}} + \frac{1}{\omega_{r,0}} \left(- \left. \frac{\partial P}{\partial \theta} \right|_0 \right) K_D G_b \right]}_M \Delta \ddot{\omega}_r + \underbrace{\left[\frac{1}{\omega_{r,0}} \left(- \left. \frac{\partial P}{\partial \theta} \right|_0 \right) K_P G_b - \frac{P_0^{\text{ref}}}{\omega_{r,0}^2} \right]}_C \Delta \dot{\omega}_r + \underbrace{\frac{1}{\omega_{r,0}} \left(- \left. \frac{\partial P}{\partial \theta} \right|_0 \right) K_I G_b}_{K} \Delta \omega_r = - \frac{1}{\omega_{r,0}} \Delta P^{\text{ref}}. \quad (5.9)$$

On the other hand, if the applied generator torque matches the greedy generator torque from Eq. (5.5), analogously, it follows

$$\underbrace{\left[J_{LSS} + \frac{1}{\omega_{r,0}} \left(-\frac{\partial P}{\partial \theta} \Big|_0 \right) K_D G_b \right]}_M \Delta \dot{\omega}_r + \underbrace{\left[\frac{1}{\omega_{r,0}} \left(-\frac{\partial P}{\partial \theta} \Big|_0 \right) K_P G_b + 2G_b K_{gen} \omega_{r,0} \right]}_C \Delta \dot{\omega}_r + \underbrace{\frac{1}{\omega_{r,0}} \left(-\frac{\partial P}{\partial \theta} \Big|_0 \right) K_I G_b}_{K} \Delta \omega_r = 0. \quad (5.10)$$

To obtain the response of the rotor-speed error resembling that of an idealized second-order system, the PID control with gain-scheduling corresponding to the operation condition needs to be employed. A second-order system is characterized by the natural frequency, ω_n , and damping ratio, ξ . The recommended values for these parameters in controlling the scaled turbines are equal to

$$\omega_n = \sqrt{\frac{K}{M}} = 0.3 \text{ rad/s} \quad \text{and} \quad \xi = \frac{C}{2M\omega_n} = \frac{C\omega_n}{2K} = 0.7. \quad (5.11)$$

Therefore, the desired second-order system would respond to a step time with a rise time, t_r , and settling time, t_s , equal to

$$t_r = \frac{1}{\omega_n \sqrt{1-\xi^2}} \left[\pi - \arctan \left(\frac{\sqrt{1-\xi^2}}{\xi} \right) \right] = 10.95 \text{ s} \quad \text{and} \quad t_s = \frac{4}{\xi \omega_n} = 19.05 \text{ s}. \quad (5.12)$$

To achieve these desired performance criteria, we employ the following gain scheduling:

$$K_P(\omega_r, \theta, v) = \frac{-2J_{LSS}\omega_r\xi\omega_n}{G_b \frac{\partial P(\omega_r, \theta, v)}{\partial \theta} \Big|_0}, \quad K_I(\omega_r, \theta, v) = \frac{-J_{LSS}\omega_r\omega_n^2}{G_b \frac{\partial P(\omega_r, \theta, v)}{\partial \theta} \Big|_0}, \quad \text{and} \quad K_D = 0. \quad (5.13)$$

The gains are scheduled with the measurements of the rotor speed and with the computed sensitivity of aerodynamic power to the collective blade-pitch angle. The measurements of the rotor speed, the current blade-pitch angle, and the wind speed information are utilized to compute the sensitivity of aerodynamic power to the collective blade-pitch angle. The derivative gain is neglected as past work indicates that it does not effectively impact the rotor speed tracking performance [77]. Notice that the negative damping from the tracking generator torque, $P_0^{\text{ref}}/\omega_{r,0}^2$, and the positive damping from the greedy generator torque, $2G_b K_{gen} \omega_{r,0}$ that are consolidated into the lumped damping parameter C are neglected in the gain scheduling in (5.13). They are neglected because transitioning between generator torque modes would result in an undesirable and non-smooth switch in K_P .

The sensitivity of aerodynamic power to the collective blade-pitch angle is computed based on the measurements of the rotor speed, blade-pitch angles, and wind speed, utilizing the information of the C_P mapping through the following relationship:

$$\frac{\partial P}{\partial \theta}(\omega_r, \theta, v) = \frac{1}{2} \rho \pi R^2 v^3 \frac{\partial C_P(\lambda, \theta)}{\partial \theta}, \quad (5.14)$$

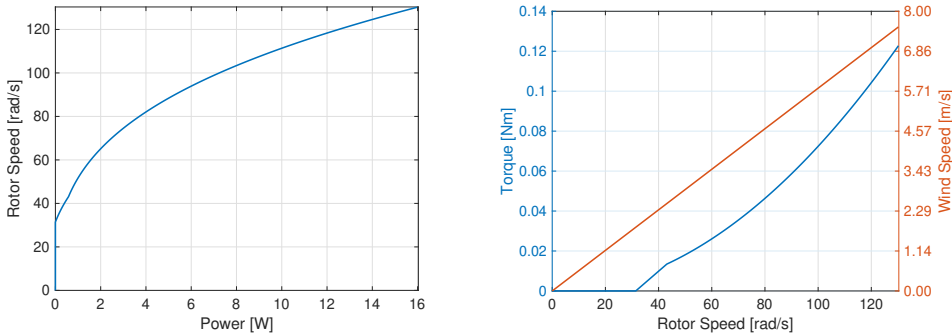
where ρ is the air density, R is the rotor radius, and C_p is the power coefficient, which relates the efficiency of the power extraction with the tip speed ratio $\lambda = R\omega_r/v$ and the collective blade-pitch angle θ .

This design does not include any blade-pitch actuator dynamic effects. The blade-pitch actuator dynamics are neglected because the blade-pitch actuator response is much faster than the desired pitch response from Eq. (5.11), with a pitch rate of approximately 30 deg/s. Moreover, we saturate the integration of the error in the PI controller once the minimum or the maximum blade-pitch angles are reached, as a windup prevention. The minimum blade-pitch angle is set as the fine blade-pitch angle that refers to the blade-pitch angle that jointly with the optimal generator torque maximizes power extraction.

As previously discussed, in power setpoint tracking control, the choice of the reference rotor speed dictates the derating control strategy. This choice impacts the performance at both the wind turbine and wind farm levels. In this work, we assess two methodologies proposed in the following subsections.

DERATING CONTROL STRATEGY I: BLADE-PITCHING BASED ON THE GREEDY GENERATOR TORQUE CONTROL

Adopted by Fleming et al. [12] and Kim et al. [63], and further extended to align with loading constraints in Silva et al. [70], this methodology maps the reference power to a reference rotor speed. This relationship is established on the foundation of the greedy generator torque control law, as depicted in Figure 5.3b. To generate the map Γ , such that $\omega_r^{\text{ref}} = \Gamma(P^{\text{ref}})$, illustrated in Figure 5.3a, the associated greedy generator torque for a given rotor speed is multiplied by the rotor speed itself. In this way, the reference rotor speed correlates with the rotor speed attained when the wind speed is reduced utilizing the greedy generator torque control and fine blade-pitch angles. After determining the rotor speed through the map Γ , the blade-pitch controller derived in Section 5.3.1 is applied, utilizing the calculated reference rotor speed. Notice that wind speed information is not required to determine the reference rotor speed, given the map Γ .



(a) reference rotor speed map from power reference

(b) greedy generator torque control

Figure 5.3: Mapping from the reference power setpoint to a reference rotor speed (a) based on the greedy generator torque control (b).

To avoid shut-downs due to the use of the tracking generator torque law, the generator

torque is saturated as

$$T_{\text{gen}} = \min(T_{\text{gen,greedy}}, T_{\text{gen,tracking}}), \quad (5.15)$$

where $T_{\text{gen,greedy}}$ and $T_{\text{gen,tracking}}$ were previously defined in Eq. (5.2). This constraint will leave the power regulation to be led by the blade pitching control with a slower response when fast transients lead the tracking generator torque to high values. Furthermore, when P^{ref} is higher than the available power in the wind, i.e. the turbine reaches saturation, the blade pitch angle meets the fine blade pitch angle value and Eq. (2.2) ensures that the turbine operates at maximum energy extraction.

DERATING CONTROL STRATEGY II: BLADE-PITCHING WITH CONSTANT TIP SPEED RATIO

With this strategy, we keep the tip speed ratio constant by computing the reference rotor speed as

$$\omega_r^{\text{ref}} = \frac{\lambda^{\text{opt}} \nu}{R}, \quad (5.16)$$

and utilizing it in the blade-pitch controller from Section 5.3.1. λ^{opt} is the optimal tip speed ratio corresponding to the maximum power extraction. The reference rotor speed is therefore directly related to the wind inflow velocity ν that has to be estimated. The unscented Kalman filter [166] was utilized to estimate the wind speed, as implemented by Silva et al. [159]. Because wind speed estimators can provide uncertain information due to unmodeled effects, such as shear and induced turbulence from waked conditions, this approach can lead to deviations of the actual turbine behavior from the desired one [159]. Despite uncertainties in wind speed estimation, this derating control strategy maintains a rotor speed higher than the previous strategy, which is beneficial for power tracking as it stores more kinetic energy in the rotating components. Additionally, we saturate the reference rotor speed to the rated rotor speed $\omega_r^{\text{rated}} = 130$ rad/s. This saturation results in a decrease in the tip speed ratio when the rated rotor speed is attained during high wind speeds, such as at the above-rated condition in the baseline turbine control for power maximization. Likewise for derating control strategy I, the generator torque is set as in Eq. (5.15).

Figures 5.4 and 5.5 depict the gain-scheduling mapping with both derating control strategies across different derating levels and wind speeds. The derating levels are denoted by the power ratios (f) ranging from 0.5 to 0.9, representing derating from 50% to 90% of the maximum power for a given wind speed. The gains change based on the current measured blade-pitch angle and rotor speed (Figures 5.4a and 5.4b), as well as wind speed (Figures 5.5a and 5.5b), according to Eq. (5.13).

5.3.2. WIND FARM CONTROL STRATEGIES

Individual wind turbines can track a specified power demand by employing the derating control strategies presented in Section 5.3.1. However, in scenarios where wake effects are involved, such as in dense farms, notable variations in structural loading across turbines may occur, potentially resulting in an uneven lifespan for the components of the turbines. To tackle this, we suggest implementing a thrust force balance feedback to equalize aerodynamic loads throughout the farm. The aerodynamic loads serve as a proxy for structural loading in turbine components.

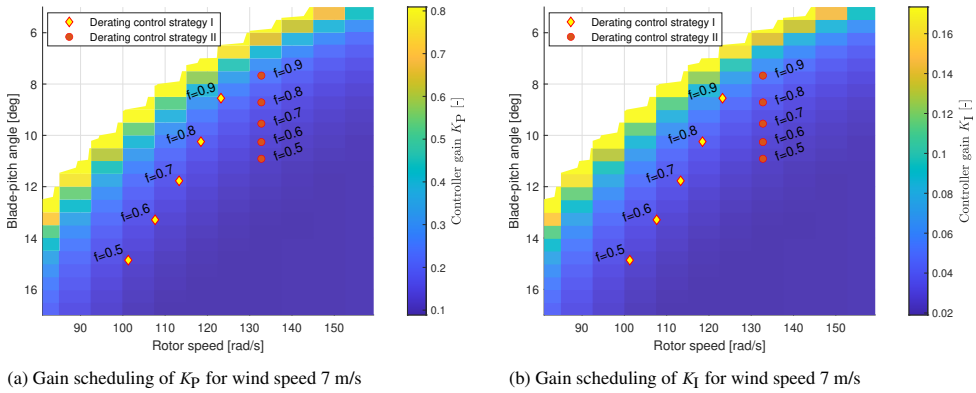


Figure 5.4: PI gain scheduling of the blade-pitch control for the two derating control strategies at wind speed of $v = 7$ m/s. The derating is indicated by the power ratios ranging from $f = 0.9$ to $f = 0.5$.

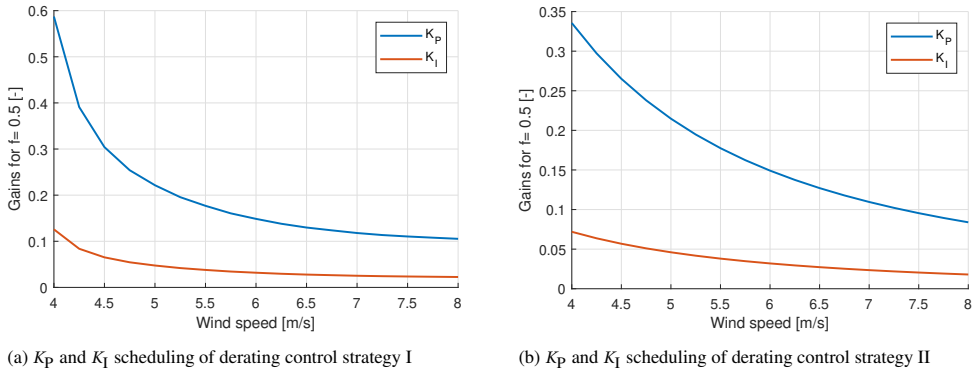


Figure 5.5: PI gain scheduling of the blade-pitch control for the two derating control strategies as a function of wind speed. The gain scheduling curves are given for a derating level of $f = 0.5$.

Additionally, as a concern related to wakes on a farm, downstream turbines may have trouble meeting their power demand due to the reduced wind availability caused by the wakes. Consequently, these downstream turbines become saturated by the available power in the wind flow as they try to keep up with demand but generate power-tracking errors. To address this issue, we propose a feedback scheme designed to compensate for these power errors. This feedback scheme is utilized for the compensation of turbine saturation resulting from wake effects.

Hence, we employ the two closed-loop wind farm controllers, previously presented in Silva et al. [54], and summarized in the upcoming sections: the thrust force balance and the power compensation.

THRUST FORCE BALANCE

Figure 5.6 illustrates the proposed thrust force balance feedback, which employs an integral control action to achieve a balance in thrust force. The thrust force errors $e_{TB,i}^k$ of the turbine i at the discrete time index k are calculated from the mean thrust force of the M

non-saturated turbines and the measured/estimated thrust force $\hat{F}_{T,i}^k$. These errors are then integrated, resulting in additional power signals $\Delta u_{TB,i}$ that are added to each power demand signal $P_{dem,i}^k$. The $N_T \times N_T$ matrix \mathbf{W} aggregates the thrust force measurements for the non-saturated turbines, where N_T is the total number of turbines, and is defined as

$$\mathbf{W}_{N_T \times N_T} = [w_{i,j}] = \begin{cases} 1, & \text{if } i = j \text{ is saturated,} \\ 0, & \text{if } i \neq j \text{ and } i \text{ or } j \text{ is saturated,} \\ 1/M, & \text{otherwise.} \end{cases} \quad (5.17)$$

The elements $w_{i,j}$ represent the individual weights of turbine $j \in 1, 2, \dots, N_T$ in the average computed for turbine $i \in 1, 2, \dots, N_T$. The vector multiplication of $\mathbf{W}_{N_T \times N_T}$ with $\hat{F}_{T,i}^k$ yields the averaged thrust forces, from which $\hat{F}_{T,i}^k$ is subtracted to determine $e_{TB,i}^k$. In this framework, saturated turbines - those unable to meet their power demand - are excluded from the thrust force balance and their thrust force errors are zero, as defined in (5.17). This exclusion is important because, in cases of turbine saturation, the thrust balance feedback loop may negatively impact power tracking. As these turbines cannot generate the demanded power, the thrust force balance feedback would cause the power demand of the non-saturated turbines to decrease, while not meeting the power demand on the saturated turbines. Since saturated turbines typically experience lower aerodynamic loads, their removal is practical.

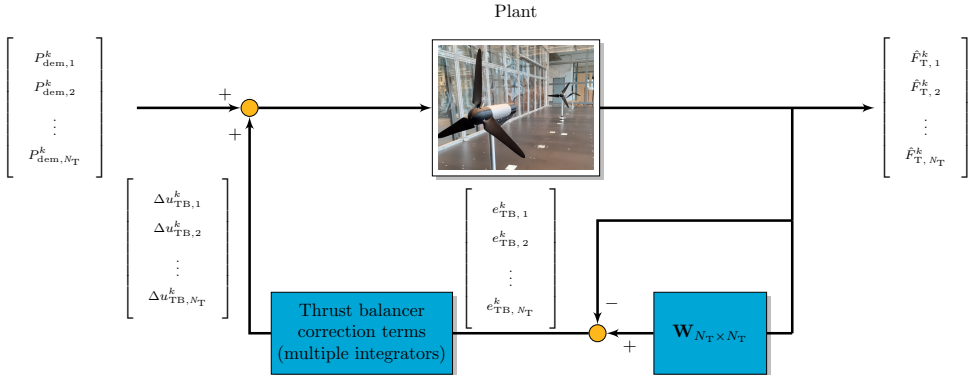


Figure 5.6: Block diagram of the thrust balancer.

POWER COMPENSATION

A feedback scheme, illustrated in Figure 5.7, is employed to offset power mismatch within the wind farm among turbines with available resources. The power compensation feedback is composed of an integral controller to track the wind farm power demand r^k with zero steady-state power error e^k by taking the total generated power \hat{P}^k . In a feedforward manner, r^k is distributed through the use of α_i weights, in which $\sum_{i=1}^{N_T} \alpha_i = 1$. Specifically, in this work, we define $\alpha_i = 1/N_T, \forall i$. The integral controller is fed with the wind farm power error e^k , and subsequently provides the vector signal Δu_{PC}^k as output, which is added on

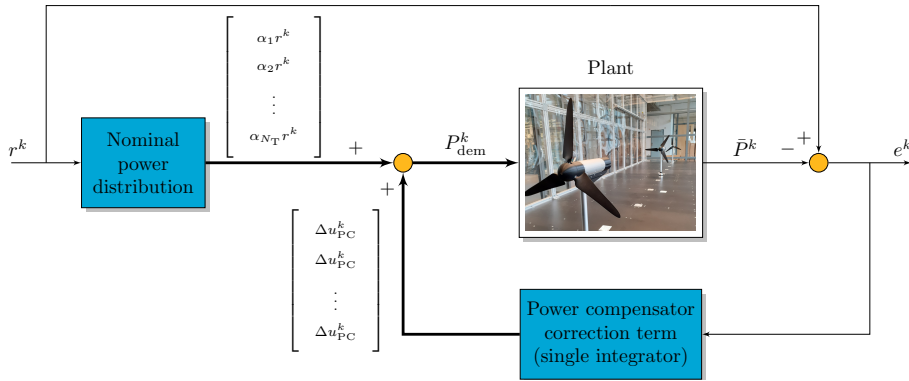


Figure 5.7: Block diagram of the power compensator.

top of the distributed power signals $\alpha_i r^k$ to define the power demand vector P_{dem}^k . Thus, wind farm power tracking can be maintained until all turbines become saturated.

The accuracy of wind farm models can be challenging due to the complexity of atmospheric phenomena and scarce measurement information. Therefore, a pragmatic approach is considered by designing the scheme without needing a model of wind turbine interactions but the individual dynamic behavior.

The common signal Δu_{PC}^k , the output of the integrator, is added in all channels ensuring that the compensation efforts are equally spread throughout the entire farm. This approach achieves simplicity and satisfying performance due to the time-scale separation between the turbine and wake dynamics [18].

5.4. EXPERIMENTAL RESULTS

In this section, we present the results obtained from the conducted experimental campaigns involving the proposed controllers. The evaluation covers the wind turbine control, spanning both individual turbine and farm scales, as well as the wind farm controllers.

5.4.1. DERATING CONTROL PERFORMANCE

Before delving into an analysis of the wind farm controllers, we assess the performance of the wind turbine controllers. The derating control strategy implemented at the wind turbine level defines the dynamics of power tracking and significantly influences the behavior of the wind flow within the farm. Therefore, we examine the application of the two distinct derating control strategies presented in Section 5.3.1 and Section 5.3.1 in different settings.

SINGLE-TURBINE SETTING

To this aim, a single wind turbine was first utilized, and its responses to changes in the power reference signal were recorded and presented in Figure 5.8. The experiment involved a series of stepwise changes in the reference power, ranging from 50% to 90% of the capacity of power extraction, where the maximum power extraction at an inflow wind speed of 7 m/s would yield approximately 15 W. The depicted reference rotor speeds, utilized in the

blade-pitch controller, were distinctly obtained according to the derating control strategies previously presented in Section 5.3.1 and Section 5.3.1.

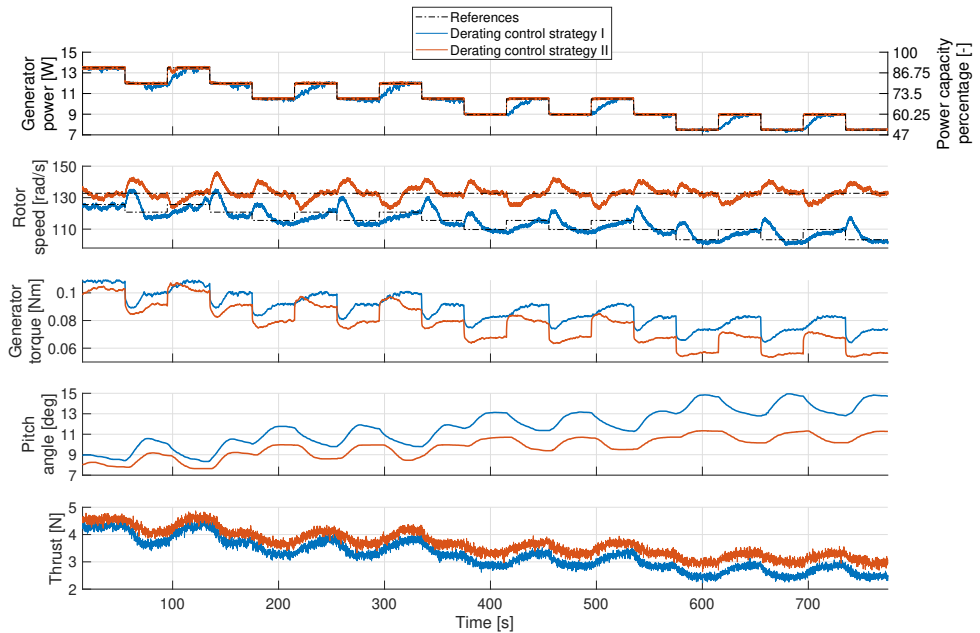


Figure 5.8: Wind turbine measurements for constant inflow velocity ($v = 7$ m/s) and stepwise changes in the power reference of a single turbine.

Several interesting observations can be drawn from the results depicted in Figure 5.8:

- Derating control strategy I, where blade-pitching is based on the greedy generator torque control law, demonstrates comparable performance with the derating control strategy II in terms of power tracking when the requested power is reduced. This is driven by the dominance of the tracking generator torque over the greedy generator torque. However, when the requested power increases, the generator torque in the derating control strategy I is constrained by the greedy generator torque. This constrained torque defaults to a more cautious, lower-value torque to prevent shutdowns caused by the low rotational speed and high generator torque values.
- Utilizing the derating control strategy II, the wind turbine demonstrated nearly flawless power tracking behavior compared to derating control strategy I. This is attributed to the higher rotor speed, which decreases the tracking generator torque below the greedy generator torque, therefore taking precedence by following the generator torque law defined in Eq. (5.15). However, the higher rotor speed leads to higher thrust forces compared to derating strategy I. This results in higher loads on components affected by thrust forces, such as the stresses on the base of towers.
- The tracking generator torque introduces an undesirable transient behavior in the relationship between power reference and rotor speed. This is identified analytically

from Eq. (5.9), rewritten in the frequency domain, such that we have the transfer function

$$\frac{\Delta\omega_r}{\Delta P^{\text{ref}}} = \frac{-(1/\omega_{r,0})s}{Ms^2 + Cs + K}. \quad (5.18)$$

The presence of a zero and a negative steady-state gain in the transfer function of Eq. (5.18) explain the behavior of the rotor speed in Figure 5.8. This peculiarity becomes particularly noticeable during significant shifts in the power reference, as exemplified in the conducted experiment. When the power reference is lowered, the rotor speed initially increases before stabilizing. Nevertheless, in practical scenarios, the active power demand is expected to exhibit a slow-time-varying pattern, making this behavior minor. In addition, rate-limiters in the power reference signal should be considered to mitigate this effect.

- Examining the time constants, it becomes apparent that the time response of the rotor speed is longer than what was originally defined during the design (refer to Eq. (5.11)), approximately $\sim 40 - 50\%$. This outcome was anticipated and stems from the considered simplifying assumptions, mainly from neglecting the damping from the greedy generator-torque controller and from the variation of the aerodynamic torque with the rotor speed on the blade-pitch control design.

TWO-TURBINE SETTING

To assess the increase of power availability at downstream turbines due to the distinct derating control strategies, we set two scaled turbines in a full wake configuration at a free stream inflow velocity of $v = 7$ m/s. The upstream turbine is gradually derated from its greedy operation through a step-wise reduction of the power reference, while the downstream turbine always operates with greedy generator torque control and fine blade-pitch angles. The downstream turbine maximized power extraction to quantify the available power downstream. The mean and standard deviation were taken from the steady-state period after the steps in the power reference were applied in the upstream turbine. This procedure was repeated three times for each derating control strategy and the mean and standard deviation were combined.

When observing the power on the downstream turbine due to the derating of the upstream turbine, the advantages of employing the derating control strategy I are noticeable (see Figure 5.9). In the specific scenario when derating 50% in the power of the upstream turbine, employing the derating control strategy I leads to the mean power of 4.9 W compared to employing the derating control strategy II achieving 3.5 W. This means a 40% increase in the power obtained by the downstream turbine. This is justified by the 25.5% reduction in thrust force in the upstream turbine, moving from derating control strategy II to derating control strategy I, while generating in the upstream turbine the same amount of power. The reduction in thrust force upstream allows more energy in the flow to the downstream turbine.

However, compared to the operation with both turbines with greedy control, derating the upstream turbine by 50% in power generation results in a significant decrease in total power generation, approximately 20% with derating control strategy I (see Fig. 5.10). Although there is an increase in power generation of the downstream turbine, a reduction in total power generation is observed, consistent with findings in previous numerical studies [119].

Nevertheless, depicted in Figure 5.9, a substantial impact in structural loading is observed by derating 50% of the upstream turbine employing derating control strategy I compared to the greedy operation. This impact relates to roughly a 50% decrease in its thrust force in the upstream turbine.

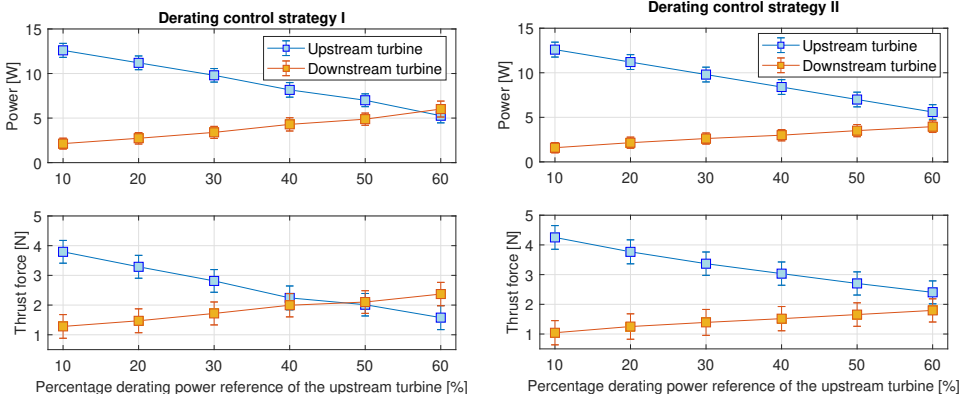


Figure 5.9: Turbine power resulting from gradually derating the upstream turbine with the two derating methods in a two-turbine setting.

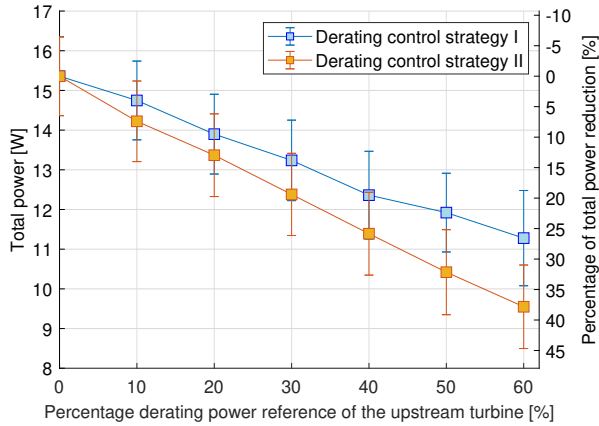


Figure 5.10: Total power resulting from gradually derating the upstream turbine with the two derating methods in a two-turbine setting.

THREE-TURBINE SETTING

To further analyze the effects of the derating control strategies on the power availability in the wind farm setting, we set the three scaled turbines under full-waked conditions. We increased the inflow velocity from 7 m/s to 8 m/s to make more energy available to the downstream turbines. During this experiment, we decreased the power request at the upstream turbine (T1) from its greedy value of around 15 W to 6 W, and set a demand of 6 W

at the second turbine in the flow stream (T2). Meanwhile, the turbine furthest downstream (T3) was controlled to maximize power extraction using greedy generator torque control and fine blade-pitch angles. The power maximization of T3 is used to measure the available energy in the flow stream while applying the different derating strategies in T1 and T2.

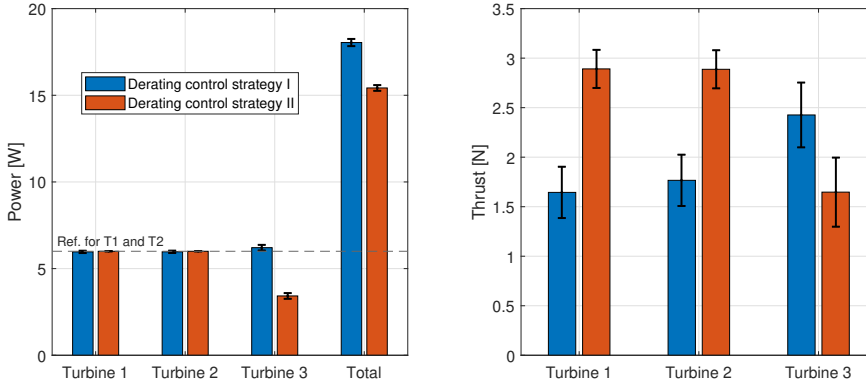


Figure 5.11: Wind turbine power and thrust force results of a three-turbine setting in constant inflow velocity ($v = 8$ m/s). The power references of the two upstream turbines are set constant at $P_{\text{dem}1,2} = 6$ W.

The results illustrated in Figure 5.11 show that, by reaching the power demand at both upstream turbines, the wind farm power output is 23% higher with derating control strategy I compared to derating control strategy II. The turbine T3 experiences an approximately 81% increase in its power generation. Additionally, the thrust forces are 19% and 12% lower for turbines T1 and T2, respectively. This clearly indicates the benefits of derating by blade-pitching based on the greedy generator torque control compared to derating by blade-pitching with constant tip speed ratio in a wind farm setting. Throughout the remainder of this chapter, our attention is directed toward derating by blade-pitching based on the greedy generator torque control, i.e. derating control strategy I. This focus is driven by the findings indicating its superiority regarding power capacity and structural loading.

5.4.2. THRUST FORCE BALANCE

In this Section, we present an analysis of the fatigue loading, drawing insights from one instance of the previous open-loop wind farm results. We consider the two-turbine setting from Section 5.4.1 in two specific conditions: with greedy control in both turbines; and derating the upstream turbine up to reaching thrust force balance. In the latter, the upstream turbine is derated by 50% reducing its thrust force and allowing wind flow to the downstream turbine to achieve thrust force balance. From strain gauges placed on the bottom of each tower, the measured bending moments are utilized to estimate the fatigue loading. The procedure for estimating fatigue loading is conducted as follows:

- Repeating and fluctuating stresses with non-zero mean components are counted by a rain flow counting algorithm [167].
- The stresses are translated to equivalent fully-reversed alternating stresses [168].

- The fatigue damage is computed utilizing short damage equivalent load and compared between the conditions.

Fatigue loading is influenced by both the mean and the alternating stress, in which, generally, the alternating stress has a greater impact. Parts of these stress-time waveforms are shown in Figure 5.12. As expected, wake effects downstream reduce mean stress while increasing alternating stress. The thrust force balance mitigates these effects downstream, while in the upstream turbine, it reduces the mean stress and might slightly increase the alternating stress. Roughly, we can see in Figure 5.12 that the mean thrust force of turbine T1 reduces significantly while the alternating behavior slightly increases, resulting in a small reduction of fatigue loading at T1. On the other hand, at turbine T2, the mean value increases but, as a positive outcome, the alternating stress at the tower structure is significantly reduced. Reducing the alternating stresses in turbine T2 leads to a significant fatigue loading reduction of the tower structure.

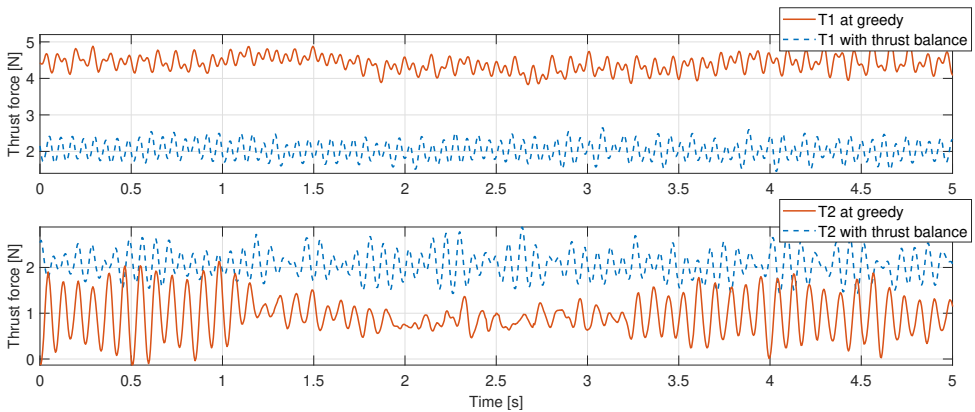


Figure 5.12: Structural loading of the two turbines in greedy control operation and thrust force balance operation.

We display the results in Table 5.1, which demonstrate a reduction in fatigue loading not only in the derating upstream turbine T1 but mainly in turbine T2 positioned downstream. The fatigue loading calculations were conducted after the turbines had reached a steady state, determined to be 25 seconds after establishing the power reference setpoints. Our estimation of fatigue loading utilized data collected over a 25-second time interval. Figure 5.12 displays measurements from only 5 seconds of this duration, focusing on visualizing the oscillation periods. Although the mean thrust force increases at T2, the result is justified by the reduction of oscillations, mainly associated with induced turbulent wake effects.

5.4.3. WIND FARM CONTROL PERFORMANCE

BALANCING OF AERODYNAMIC LOADING IN CLOSED LOOP

Extending the arrangement back to three machines as depicted in Figure 2.6 under full-waked conditions, we tested the proposed closed-loop controller presented in Section 5.3.2. For the remainder of the chapter, we employed an inflow velocity of 8 m/s. The experiments

Table 5.1: Fatigue loading results transitioning from greedy control to derating control strategy I reaching thrust force balance.

Derating T1 [%]	Total power [%]	Fatigue loading tower T1 [%]	Fatigue loading tower T2 [%]
50	-22.4	-4.18	-127.64

began with a low wind farm power set-point (18 W), followed by incremental increases. The goal is to identify the operational conditions that trigger turbine saturation and compare the wind farm power generation. Turbine saturation occurs when the pitch angle reaches the fine blade pitch angle and the generator torque operates in greedy mode. In this state, the turbine maximizes power extraction, while its power demand exceeds the power being extracted.

The first experiment was carried out in an open-loop configuration, employing a uniform power distribution as our baseline, where individual power references were identical for all turbines. Figure 5.13 shows the time evolution of the total wind farm power, the generated power of the three wind turbines, and their thrust forces from this experiment. The thrust variation across turbines is seen as expected, along with the occurrence of turbine saturation in downstream turbines. The turbine saturation is visually noticed in Figure 5.13 by the mismatch between the wind turbine power reference and its measured power output, also indicated by the vertical dashed lines. .

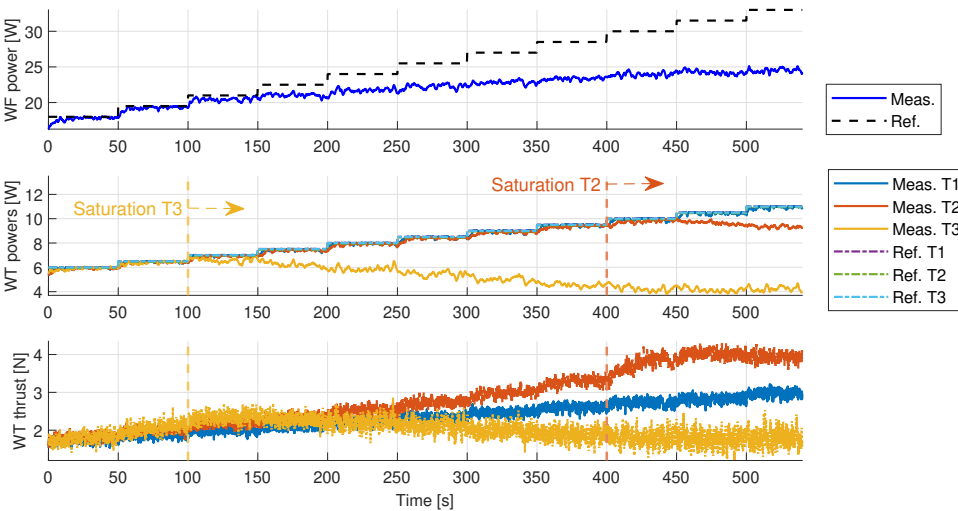


Figure 5.13: Results of uniform power distribution: WF power (on the top), WT power (center), and WT thrust (on the bottom). In the WT power plot, all references are identical.

In contrast to the data presented in Figure 5.13, the results depicted in Figure 5.14 illustrate the outcomes of employing the thrust balance feedback. This feedback configuration not only balances the thrust forces of non-saturated turbines but also prevents turbine satu-

ration and enhances overall power generation compared to the open-loop configuration with uniform power distribution. The thrust force balancing leads to an increase of the wind farm power of approximately 3–5% observed between 450 to 500 seconds. This is attributed to the increase of power availability in downstream turbines, a result which is in line with what was reported utilizing simulations by Silva et al. [72]. The prevention of turbine saturation is evident when comparing Figure 5.13 to Figure 5.14.

As discussed in Section 5.3.2, when a turbine saturates, it is excluded from the thrust force balance controller, resulting in a noticeable disparity in the thrust forces between saturated and unsaturated turbines. This measure was adopted to avoid conflicting behavior with power generation. Saturated turbines, unable to meet their power demand, typically have lower thrust forces. If the saturated turbine is not excluded, it would decrease the power demand on unsaturated turbines through the thrust force balance feedback. Consequently, this would create a gap in the total power generation since saturated turbines cannot generate their counterparts. However, by removing saturated turbines from thrust force balancing, total power generation remains unaffected by turbine saturation, while their thrust forces are generally lower than those still undergoing balancing.

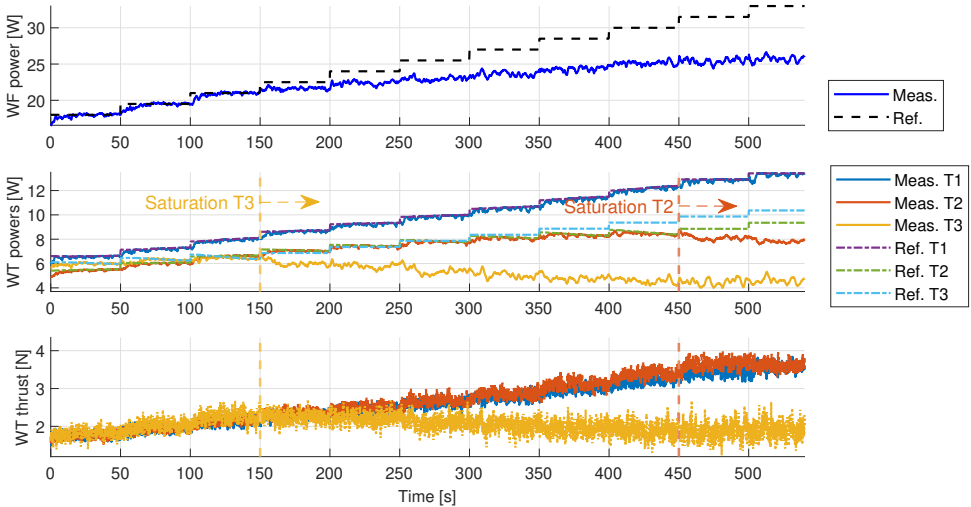


Figure 5.14: Results of thrust force balancing: WF power (on the top), WT power (center), and WT thrust (on the bottom).

COMPENSATION OF WAKE POWER LOSSES IN CLOSED LOOP

Increasing the reliability of energy production in wind farms is considered an important research challenge [27]. In the results, we show that energy production can be enhanced by wind farm control. With the proposed power compensator from Section 5.3.2, although the growth of the total power demand triggers turbine saturation, the energy losses can be redistributed and harvested by the turbines that are still capable of generating additional power.

The measurements shown in Figure 5.15 make it clear that the closed-loop approach for power compensation leverages the wind farm power tracking capability. The thrust balance

controller was not applied during these measurements. Focusing on the total wind farm power illustrated in the top subplots, we observe that the offset in the wind farm power in the two previous experiments is significantly reduced, such that the wind farm power output better agrees with its increasing reference. The power losses were compensated with the implementation of the power compensation feedback. Despite the occurrence of turbine saturation in T3 and T2, respectively, the wind farm power set-point could still be maintained for up to 350 seconds at 27 W, as opposed to 22 W in 150 seconds observed in Figure 5.14. Beyond 400 seconds, all turbines reached saturation, and the escalating power demand could not be met.

Sustaining the power tracking comes at the expense of heightened load variability across the turbines. We combine the two control strategies to mitigate this effect while the thrust force balancing does not influence the power compensation. The results are depicted in Figure 5.16 and demonstrate power compensation while balancing the thrust forces of the non-saturated turbines. However, the thrust force difference across turbines is still significant because the thrust balance is limited to the unsaturated turbines. Nevertheless, in the first steps of the experiment, it has a positive effect by spreading the structural loads and avoiding saturation without compromising the power tracking.

5.5. DISCUSSION AND CONCLUSION

The work in this chapter introduced a blade-pitch controller designed for derating control strategies. Subsequently, derating control strategies were proposed and assessed for their distinct impacts, taking into account not only individual turbine performance but also their influence on downstream turbines. After selecting the derating control strategy aimed at mitigating loading and enhancing the farm's available power, we conducted the experiments with the closed-loop control structures that effectively balanced thrust forces and

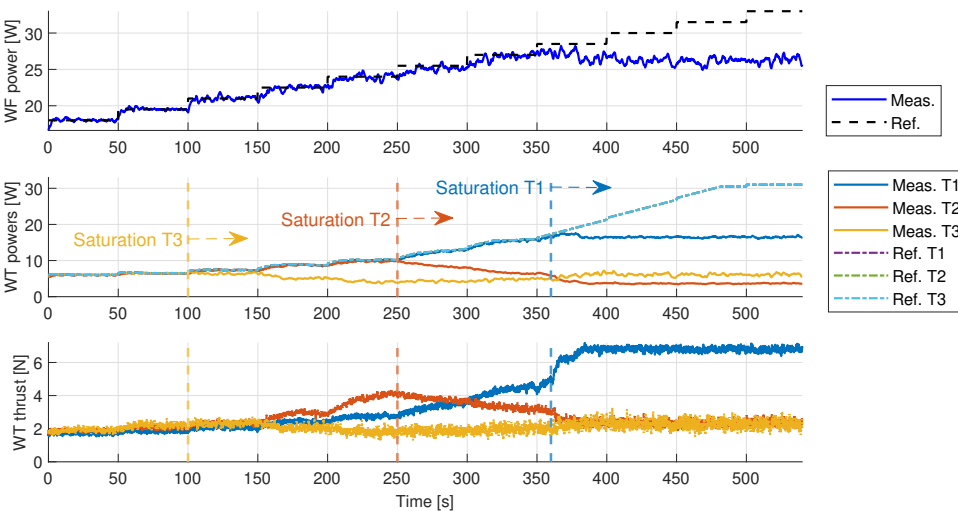


Figure 5.15: Results of power compensation: WF power (on the top), WT power (center), and WT thrust (on the bottom). In the WT power plot, all references are identical.

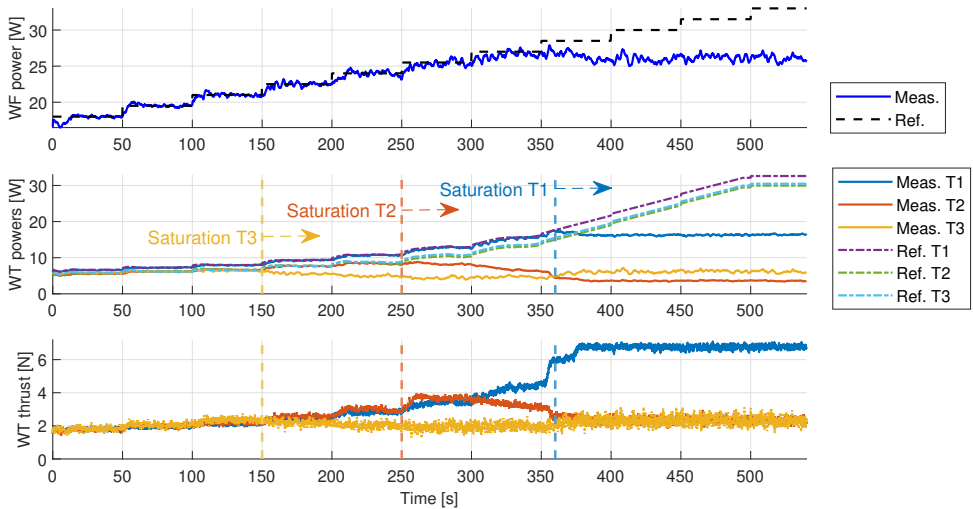


Figure 5.16: Results of power compensation and thrust force balancing: WF power (on the top), WT power (center), and WT thrust (on the bottom).

compensated for power losses due to wake effects.

The experimental findings reveal promising avenues for the implementation of active power controllers in wind farms. The closed-loop blade-pitch control derived for derating control strategies provides precise target power output and rotor speed, in contrast to open-loop approaches that make use of lookup tables. Notably, the performance of the wind farm is directly associated with the adopted derating control strategy. The derating control strategy based on the greedy generator torque control, although having a slower response in the power tracking, favors the wind farm's total power generation compared to the strategy with constant tip speed ratio. In the two-turbine case, the power capacity downstream showed an increase of approximately 40%, whereas in the three-turbine case, the power capacity increase at the third turbine reached about 81%. Furthermore, derating the upstream turbines exhibits significant reductions in thrust force and fatigue loading on the tower structure, albeit at the expense of a decrease in the total power generation when transitioning from greedy farm operation to a thrust force balancing condition in a full-waked scenario. Moving from maximizing power generation to on-demand power generation, thrust force balancing remains a potential strategy by anticipating requests for low power levels. Still, the thrust force balancing shall be implemented only in the non-saturated turbines not affecting the wind farm power generation.

In the evaluation of the proposed wind farm controllers, three different approaches were considered: an open-loop configuration with uniform power distribution; a closed-loop controller for balancing thrust forces; and a closed-loop controller for power compensation. Achieving thrust force balance in the non-saturated turbines, the closed-loop controller for balancing thrust forces avoids turbine saturation and enhances the total power capacity compared to the uniform power distribution in approximately 3–5%. Furthermore, the application of power compensation significantly enhances power tracking by eliminating

power errors caused by turbine saturation. This results in meeting the upper limit power demand of 27 W, compared to 22 W from the other two approaches, reflecting a 22% boost in power tracking capability.

The results of power gains and fatigue loading reduction in this chapter hold for the specific experimental setting. The reduction in fatigue loading is computed based on the specific structure geometry and material properties of the scaled turbines. To extrapolate these results to multi-megawatt wind turbines, a comprehensive analysis must be conducted accordingly, along with non-scaled experimental campaigns. Nonetheless, the same trends are expected in the context of large-scale turbines, with these findings positively contributing to enhancing wind farm control strategies and advancing research efforts further.

6

CONCLUSIONS AND RECOMMENDATIONS

In this chapter, the main conclusions of the application of wind farm control are summarized, our research limitations are elucidated, and the recommended directions for future research are discussed. Finally, we elaborate on the societal implications of implementing innovations in wind farm control.

6.1. CONCLUSIONS

Research on wind farm control has demonstrated notable enhancements for wind energy generation, increasing power capacity. These enhancements help to mitigate the challenges posed by the volatile nature of the wind. The emphasis on the reliability of wind energy generation should encompass both short-term power regulation capabilities and long-term structural degradation. This thesis derived wind farm control strategies and explored the challenges associated with their implementation, aligning with our main objective:

Thesis Objective

To design wind farm control strategies that can allow on-demand energy generation while taking into account structural loads.

The primary objective of our wind farm control is to provide power delivery to meet grid requirements. We saw that operating turbines cooperatively reinforce the quality of the overall farm power output. Moreover, reliability is associated with the turbines' life, which can be extended by considering structural loading. This consideration of structural loading applies not only to the local operation of individual turbines but also to their collective operation. We have derived and investigated control frameworks to address these topics. Our designed wind farm control strategies were assessed using high-fidelity simulations and experimental tests. In the remainder of this section, we discuss in detail the findings of this research.

Turbines equipped with power tracking controllers, also referred as down-regulation or derating control strategies, offer flexibility on energy generation, limited to the available energy in the wind inflow. In this thesis, we demonstrated different behaviors resulting from different power tracking controllers. Derating while keeping high rotor speeds leads to more kinetic energy in the rotating parts, facilitating fast responses to varying power demands. Conversely, derating with low rotor speeds reduces structural loads and wake effects. At one hand, simulations indicate that high rotor speed derating can sustain power tracking more than 10 times longer after saturation. At the other hand, experimental results in a wind farm setting indicate that low rotor speed derating significantly enhances power availability by 40% in downstream turbines and reduces fatigue loading by over 100% in high-wake scenarios.

As wind farms expand with more turbines, their energy capacity increases, along with the diversity encountered with a large range of wind conditions. However, space and cost limitations associated with installation and operation lead to higher densification. With wind farms becoming more densely packed, wake interactions intensify, resulting in significant variations in available power across the farm. Wind farm control strengthens power delivery within these constraints by operating turbines cooperatively, and should be considered as an important element in the design of new wind power plants. With wind penetration reaching noteworthy levels, advancements in power reliability that align with grid requirements hold significant value.

In this thesis, we evaluate a proposed wind farm controller that compensates for power losses attributed to wake effects. The proposed controller enhances power generation in conditions of low power availability through a feedback loop that utilizes real-time data.

This loop directs turbines with available power to compensate for the shortfall produced by others. The results of high-fidelity simulations show that the wind farm control significantly reduces the power-tracking error. In a mid-wake scenario, the RMSE is reduced from 1.295 MW without wind farm control to 0.114 MW, and in a high-wake scenario, it drops from 6.044 to 0.142 MW. In other words, this means reductions in the power-tracking error of 91 - 97%, depending on the wake scenario. Further, in the experimental testing, we see a 22% increase in the power-tracking capability by employing the wind farm controllers in a high-wake scenario. These results demonstrate that wind farm controllers can enhance resilience against turbine saturation in densely packed wind farms by closing the proposed power compensation feedback loop.

However, focusing solely on power considerations can result in significant disparities in the structural loads experienced by turbines. Wake effects exacerbate these differences, causing turbines to endure varying levels of structural stress and fatigue. Consequently, the lifetime of wind turbine components may be significantly depending on their location within the farm. To mitigate structural load discrepancies, we recommend using the wind farm controller to evenly distribute structural loading among the turbines through a feedback loop.

In the on-demand energy framework, achieving the thrust force balancing is feasible without conflicting with power objectives, as long as sufficient power is available within the farm. When the wind farm power demand is below capacity, there is flexibility in the power distribution that can be utilized to balance structural loads. However, if a turbine reaches saturation, operating at a maximum capacity lower than its demand, the thrust balance controller will lead to a conflict with power objectives. Hence, in our approach, we equalize structural loads on the turbines that are not saturated without compromising the power delivery.

In this thesis, we showcase the effectiveness of the proposed thrust force balancing controller by assessing various scenarios with different wind availabilities using high-fidelity simulations and wind tunnel experiments. When there is sufficient wind, the proposed feedback loop enables wind farms to achieve thrust force balance across the entire farm. In scenarios with low inflow wind speeds, thrust forces are partially balanced according to the design that prioritizes power delivery. Moreover, the findings from experiments illustrate that the thrust force balancing can benefit the power reference distribution, resulting in a 3-5% increase in power capacity compared to uniform power distribution. Additionally, it helps to prevent turbine saturation downstream in high-wake conditions.

Additional measures are still necessary to prevent turbine failures from mechanical issues beyond those related to wind-induced loading, such as degradation from corrosion and installation problems. Advanced wind turbine controllers using the current health information could enable appropriate operation during periods that maintenance has been assigned, thereby ensuring energy safety.

At a wind turbine level, we have developed load-limiting controllers to restrict structural loads based on real-time health status data. The necessity of ensuring safety in fault and degraded structures is becoming relevant since turbines in the field are reaching the maturity of their lifetime and are situated in challenging environments with low accessibility, such as offshore sites. Pushed by safety concerns, load-limiting wind turbine controllers would enable turbines to continue to generate energy outside nominal conditions.

From a control perspective, reducing structural loads can be pursued through two approaches. In the first approach, we can treat structural loads as a hard constraint that takes precedence over power production. In this regard, we have proposed a switching control framework that switches from power tracking to thrust tracking based on a given threshold for structural loads. A second approach is to incorporate structural loads into an optimization framework as part of a multi-objective strategy. Within the optimization framework, we further explored its formulation to address concerns stemming from flow stability and to benefit from the kinetic energy in the rotors for power tracking.

We showcased through simulations that load-limiting controllers can reduce structural loads to defined thresholds, ensuring safety in operation. Although this requires a compromise with short-term power delivery goals, it guarantees sustained production in the long term. Nevertheless, when constraints are necessary, other turbines with available power can compensate for this compromise, as illustrated by our findings on turbine saturation due to wakes.

Furthermore, we broaden the scope of wind farm controllers by introducing a distributed control strategy that takes advantage of multi-rate ideas to execute consensus algorithms, achieving performance comparable to centralized controllers. The proposed distributed controller inherits a delay and uses a finite number of communication interactions to reach consensus. These non-ideal factors are considered in its design. Being a fully distributed control approach, it addresses implementation challenges, making our proposed wind farm controllers more suitable for large-scale wind farms. The distributed control framework necessitates only the existing turbine hardware and a short-range communication system, thereby minimizing associated costs.

High-fidelity simulations demonstrate the effectiveness of the distributed wind farm controller, reaching a power tracking error of 0.2268 MW, compared to 0.1422 MW with the centralized controller. In the baseline case with no controller, the error is 6.0417 MW. This represents a reduction in power tracking error of 96.25% with the distributed controller, compared to 97.65% with the centralized controller. Additionally, the distributed wind farm controller achieved a 91.97% reduction in the mean of the thrust force variance, compared to a 92.29% reduction with the centralized controller. The achieved performance serves as evidence of the efficacy of the proposed distributed control while facilitating the implementation of the wind farm controllers for large-scale wind farms.

The combined contributions of this thesis stimulates the advancement of wind energy technology and pushes the implementation of next-generation wind farm controllers. These advancements enhance reliability and improve integration with the electricity grid, ultimately lowering the cost of wind energy.

6.2. LIMITATIONS

Although wind farm control enhances the reliability of energy generation by bolstering resilience to low wind availability and considering structural loads, it is limited by the overall availability of wind. If there is no wind, no energy can be generated, which means that wind energy is dependent on the wind availability and is inherently volatile. However, it can take benefits from the use of storage systems and integration with other sources, a technology known as power-to-X.

An ongoing challenge encountered in this research is precisely delineating the relation-

ship between health status and loads on particular components. This relationship hinges on material fatigue, a long-term cumulative phenomenon influenced not only by load experienced but also by external factors. One such factor is environmental conditions, which can lead to accelerated material corrosion - a critical process that has impact on fatigue. Comprehending this influence is peculiar to the application and involves numerous variables.

Continued research to mature power tracking controllers is imperative. Although promising, these novel approaches require thorough validation to be applicable in MW-scale turbines, which includes accounting for flow stability and resonance frequencies. Depending on the adopted strategy for power tracking, the airflow over the blades can induce undesirable non-linear effects, drastically reducing drag and potentially causing turbine shutdown. Additionally, there is a risk of reaching frequencies that correspond with the resonance frequencies of the turbine structure, resulting in substantial oscillations and associated loads. Therefore, detailed research tailored to each turbine design must be considered to address these challenges effectively.

This research, among recent works from other authors, marks the initial steps in showcasing the capabilities and benefits of the proposed wind farm controllers in an on-demand energy panorama, particularly transitioning from high-fidelity simulations to experimental setups. Further research and collaboration must be considered to leverage the ideas and concepts presented in this thesis into practical implementation.

6.3. RECOMMENDATIONS

Based on the findings presented in this thesis, we advocate for the implementation of wind farm controllers in wind power plants. Real-time cooperative operation of the wind turbines has demonstrated superior performance compared to uncontrolled scenarios.

Furthermore, incorporating structural load considerations into wind farm control proves both advantageous and feasible without conflicting with power goals within the framework of on-demand energy. Balancing structural loads extends the aggregated life of turbines, thereby prolonging the operational efficiency of the entire farm. Additionally, enabling wind turbines to generate energy safely by limiting their individual operation ensures continued power generation even under non-nominal conditions.

In cases where implementing wind farm control poses challenges due to the large number of turbines, we recommend distributed controllers that can facilitate this process with minimal resource requirements. Such controllers require only the existing turbine hardware and a low-range communication system.

In addition to the concepts and findings presented in this thesis, the following recommendations are proposed as extension of this work:

1. **Exploration of advanced wind farm control strategies:** Investigate advancements in wind farm control, such as wake steering and wake mixing strategies, which also hold promise in the on-demand energy panorama. Implementing these strategies could enhance the wind farm capacity and provide more power to meet the demand in scenarios with low available power.
2. **Integration of Electric Market:** Consider the integration of turbine structure degradation into frameworks that factor in electricity prices and the energy market to provide the wind farm power reference. This approach could enhance the sustainability

and cost-effectiveness of wind farm operations from an economic standpoint, considering the short- and long-term implications

3. **Incorporation of Storage Systems:** Explore the integration with storage systems, such as batteries and hydro, to enhance energy generation. Such integration would aggregate value by storing excess energy when demand is low and mitigating fluctuations during long periods of low wind, thereby improving the overall efficiency and reliability of the energy system.

6.4. SOCIETY IMPACT

The research findings presented in this thesis carry significant implications for society, both scientifically and practically, by addressing key challenges in wind energy generation and its integration into the power grid.

Scientific Importance:

- The study contributes to advancing wind farm control technologies, enhancing the reliability and efficiency of wind energy generation. With high penetration levels of wind energy, a paradigm shift is foreseen towards on-demand energy generation. By exploring wind farm control strategies, the research demonstrates how wind farms can adapt to the volatile nature of wind sources and extend their durability by accounting for current structural loads. This fosters a more sustainable and cost-effective approach to wind energy generation.
- An achievement is the development of load-limiting controllers, which effectively restrict structural loads within safe thresholds in real time. These controllers ensure the continued operation of wind turbines under adverse conditions, promoting energy safety and reliability.
- Additionally, this research explores the frontier of distributed wind farm control technologies, focusing on the potential of multi-rate systems and consensus theory. The insights gained from the proposed novel distributed controller pave the way for their widespread adoption in renewable energy and other controlled systems.
- Through high-fidelity simulations and experimental testing, the research validates the efficacy of wind farm control strategies, providing valuable insights into their practical implementation. These findings serve as a foundation for future research and development in on-demand wind energy generation.

Practical Applications:

- Wind farm control technologies offer tangible benefits for practical application, including increased energy generation, improved turbine lifespan, and enhanced grid integration. By ensuring power output and balancing structural loads, wind farms can operate more efficiently, contributing to a cleaner and lower-cost energy future.
- The research highlights the importance of considering structural degradation and environmental factors in wind turbine operation, emphasizing the need for self-aware

controllers and monitoring practices. By addressing these challenges, wind energy projects can ensure long-term viability and minimize environmental impact.

- Furthermore, the implementation of distributed control frameworks facilitates the deployment of wind farm controllers in large-scale wind farms, minimizing costs and resource requirements. The distributed approach enhances the accessibility and scalability of wind energy solutions, making them more attainable for manufacturers and generation owners.

In conclusion, the societal impact of this research is to provide solutions to current and future challenges in wind energy generation. By advancing wind farm control technologies and advocating structural load-oriented practices, the study contributes to a greener and more resilient energy infrastructure. With the proposed controllers, we enhance flexibility and reliability in wind energy, bringing benefits to wind power plant owners, system operators, and society at large.

BIBLIOGRAPHY

- [1] Irene Eguinoa et al. “Wind farm flow control oriented to electricity markets and grid integration: Initial perspective analysis”. In: *Advanced Control for Applications* 3.3 (2021), pp. 1–28. ISSN: 2578-0727. DOI: [10.1002/adc2.80](https://doi.org/10.1002/adc2.80).
- [2] Paul Veers et al. “Grand challenges in the science of wind energy”. In: *Science* 366.6464 (2019). ISSN: 0036-8075. DOI: [10.1126/science.aau2027](https://doi.org/10.1126/science.aau2027).
- [3] United Nations Framework Convention on Climate Change. *Adoption of the Paris Agreement*. Dec. 2015.
- [4] IEA. *Net Zero by 2050*. Accessed: 2023-11-07. 2021. URL: <https://www.iea.org/reports/net-zero-by-2050>.
- [5] Global Wind Energy Council. *Global Wind Report 2022*. Accessed: 2024-01-15. 2022. URL: <https://gwec.net/global-wind-report-2022/>.
- [6] Global Wind Energy Council. *Global Wind Report 2023*. Accessed: 2024-01-15. 2023. URL: <https://gwec.net/global-wind-report-2023/>.
- [7] Trinomics. *Final Report Cost of Energy (LCOE)*. Accessed: 2023-11-07. URL: <https://trinomics.eu/wp-content/uploads/2020/11/Final-Report-Cost-of-Energy-LCOE.pdf>.
- [8] International Renewable Energy Agency (IRENA). *Renewable Power Generation Costs in 2022*. Accessed: 2023-09-20. 2022. URL: <https://www.irena.org/Publications/2023/Aug/Renewable-Power-Generation-Costs-in-2022>.
- [9] J.G Manwell J.F; MCGowan and A.L Rogers. *Wind energy explained : theory, design and application*. 2nd ed. United Kingdom, John Wiley and Sons Ltd., 2010.
- [10] Eric Lantz, Ryan Wiser, and Mohammed Hand. *IEA Wind Task 26 - The Past and Future Cost of Wind Energy*. Jan. 2012.
- [11] IRENA. *Renewable power generation costs in 2022*. Accessed: 2024-07-16. 2023. URL: www.irena.org/Publications/2023/Aug/Renewable-Power-Generation-Costs-in-2022.
- [12] Paul Fleming et al. “Computational fluid dynamics simulation study of active power control in wind plants”. In: *2016 American Control Conference (ACC)* (2016), pp. 1413–1420. DOI: [10.1109/ACC.2016.7525115](https://doi.org/10.1109/ACC.2016.7525115).
- [13] Poul Sørensen et al. *Wind farm models and control strategies*. Tech. rep. 1464(EN). Denmark. Forskningscenter Risoe., 2005.
- [14] Torben Knudsen, Thomas Bak, and Mikael Svenstrup. “Survey of wind farm control—power and fatigue optimization”. In: *Wind Energy* 18.8 (2015), pp. 1333–1351. DOI: [10.1002/we.1760](https://doi.org/10.1002/we.1760).

- [15] S. Boersma et al. “A tutorial on control-oriented modeling and control of wind farms”. In: *2017 American Control Conference (ACC)* (2017), pp. 1–18. DOI: [10.23919/ACC.2017.7962923](https://doi.org/10.23919/ACC.2017.7962923).
- [16] EirGrid. *EirGrid grid code version 10.0*. Accessed: 2022-08-17. 2021. URL: <https://www.eirgridgroup.com/customer-and-industry/general-customer-information/grid-code-info/>.
- [17] National Grid Electricity System Operator Limited. *The Grid Code*. Issue 6, Revision 13. Accessed: 2022-08-17. 2021. URL: <https://www.nationalgrideso.com/electricity-transmission/industry-information/codes/grid-code/code-documents>.
- [18] Jan Willem van Wingerden et al. “Active Power Control of Waked Wind Farms”. In: *IFAC-PapersOnLine* 50.1 (2017). 20th IFAC World Congress, pp. 4484–4491. ISSN: 2405-8963. DOI: [10.1016/j.ifacol.2017.08.378](https://doi.org/10.1016/j.ifacol.2017.08.378).
- [19] Kuichao Ma et al. “Wind turbine down-regulation strategy for minimum wake deficit”. In: *2017 11th Asian Control Conference (ASCC)*. 2017, pp. 2652–2656. DOI: [10.1109/ASCC.2017.8287595](https://doi.org/10.1109/ASCC.2017.8287595).
- [20] Daan van der Hoek, Stoyan Kanev, and Wouter Engels. “Comparison of Down-Regulation Strategies for Wind Farm Control and their Effects on Fatigue Loads”. In: *2018 American Control Conference (ACC)* (2018), pp. 3116–3121. DOI: [10.23919/ACC.2018.8431162](https://doi.org/10.23919/ACC.2018.8431162).
- [21] E Uzunoglu, D Karmakar, and C Guedes Soares. “Floating offshore wind platforms”. In: *Floating offshore wind farms* (2016), pp. 53–76.
- [22] Allan May, David McMillan, and Sebastian Thöns. “Economic analysis of condition monitoring systems for offshore wind turbine sub-systems”. In: *IET Renewable Power Generation* 9.8 (2015), pp. 900–907. DOI: [10.1049/iet-rpg.2015.0019](https://doi.org/10.1049/iet-rpg.2015.0019).
- [23] *WATEREYE project*. Accessed: 2023-09-20. 2022. URL: <https://watereye-project.eu/>.
- [24] Upeksha Chaturani Thibbotuwa, Ainhoa Cortés, and Andoni Irizar. “Ultrasound-Based Smart Corrosion Monitoring System for Offshore Wind Turbines”. In: *Applied Sciences* 12.2 (2022). ISSN: 2076-3417. DOI: [10.3390/app12020808](https://doi.org/10.3390/app12020808). URL: <https://www.mdpi.com/2076-3417/12/2/808>.
- [25] M.H. Hansen et al. *Control design for a pitch-regulated, variable speed wind turbine*. English. Denmark. Forskningscenter Risoe. Risoe-R 1500(EN). 2005. ISBN: 87-550-3409-8.
- [26] Wai Hou Lio, Mahmood Mirzaei, and Gunner Chr. Larsen. “On wind turbine down-regulation control strategies and rotor speed set-point”. In: *Journal of Physics: Conference Series* 1037 (June 2018), p. 032040. DOI: [10.1088/1742-6596/1037/3/032040](https://doi.org/10.1088/1742-6596/1037/3/032040).

- [27] Jan Willem van Wingerden et al. “Expert Elicitation on Wind Farm Control”. In: *Journal of Physics: Conference Series* 1618.2 (2020), p. 022025. DOI: [10.1088/1742-6596/1618/2/022025](https://doi.org/10.1088/1742-6596/1618/2/022025). URL: <https://dx.doi.org/10.1088/1742-6596/1618/2/022025>.
- [28] Daan van der Hoek et al. “Effects of axial induction control on wind farm energy production - A field test”. In: *Renewable Energy* 140 (2019), pp. 994–1003. ISSN: 0960-1481. DOI: <https://doi.org/10.1016/j.renene.2019.03.117>.
- [29] Michael F. Howland, Sanjiva K. Lele, and John O. Dabiri. “Wind farm power optimization through wake steering”. In: *Proceedings of the National Academy of Sciences* 116.29 (2019), pp. 14495–14500. DOI: [10.1073/pnas.1903680116](https://doi.org/10.1073/pnas.1903680116). eprint: <https://www.pnas.org/doi/pdf/10.1073/pnas.1903680116>. URL: <https://www.pnas.org/doi/abs/10.1073/pnas.1903680116>.
- [30] P. Fleming et al. “Continued results from a field campaign of wake steering applied at a commercial wind farm – Part 2”. In: *Wind Energy Science* 5.3 (2020), pp. 945–958. DOI: [10.5194/wes-5-945-2020](https://doi.org/10.5194/wes-5-945-2020). URL: <https://wes.copernicus.org/articles/5/945/2020/>.
- [31] Joeri A. Frederik et al. “The helix approach: Using dynamic individual pitch control to enhance wake mixing in wind farms”. In: *Wind Energy* 23.8 (2020), pp. 1739–1751. DOI: <https://doi.org/10.1002/we.2513>. eprint: <https://onlinelibrary.wiley.com/doi/pdf/10.1002/we.2513>. URL: <https://onlinelibrary.wiley.com/doi/abs/10.1002/we.2513>.
- [32] Daan van der Hoek. “Advances in actuation techniques for wind farm flow control”. English. Dissertation (TU Delft). Delft University of Technology, 2023. ISBN: 978-94-6366-765-4. DOI: [10.4233/uuid:56cadf8e-cc7f-4f7b-b6b0-696dd4ecb65d](https://doi.org/10.4233/uuid:56cadf8e-cc7f-4f7b-b6b0-696dd4ecb65d).
- [33] ENTSO-E. *ENTSO-E Network Code for Requirements for Grid Connection Applicable to all Generators*. Accessed: 2022-08-17. 2016. URL: https://www.entsoe.eu/network_codes/.
- [34] E Ela et al. *Active Power Controls from Wind Power : Bridging the Gaps*. Tech. rep. National Renewable Energy Laboratory (NREL), 2014. DOI: [10.2172/1117060](https://doi.org/10.2172/1117060).
- [35] Konstanze Kölle et al. “Towards integrated wind farm control: Interfacing farm flow and power plant controls”. In: *Advanced Control for Applications* 4.2 (2022), pp. 1–11. ISSN: 2578-0727. DOI: [10.1002/adc2.105](https://doi.org/10.1002/adc2.105).
- [36] Jacob Aho, Paul Fleming, and Lucy Y. Pao. “Active power control of wind turbines for ancillary services: A comparison of pitch and torque control methodologies”. In: *American Control Conference (ACC)* (2016), pp. 1407–1412. DOI: [10.1109/ACC.2016.7525114](https://doi.org/10.1109/ACC.2016.7525114).
- [37] M. Tsili and S. Papathanassiou. “A review of grid code technical requirements for wind farms”. In: *IET Renewable Power Generation* 3.3 (2009), pp. 308–332. ISSN: 17521416. DOI: [10.1049/iet-rpg.2008.0070](https://doi.org/10.1049/iet-rpg.2008.0070).

- [38] S.K. Kanev, F.J. Savenije, and W.P. Engels. “Active wake control: An approach to optimize the lifetime operation of wind farms”. In: *Wind Energy* 21.7 (2018), pp. 488–501. ISSN: 10991824. DOI: [10.1002/we.2173](https://doi.org/10.1002/we.2173).
- [39] M. Vali et al. “An active power control approach for wake-induced load alleviation in a fully developed wind farm boundary layer”. In: *Wind Energy Science* 4.1 (2019), pp. 139–161. DOI: [10.5194/wes-4-139-2019](https://doi.org/10.5194/wes-4-139-2019).
- [40] Vasilis Pettas and Po Wen Cheng. “Down-regulation and individual blade control as lifetime extension enablers”. In: *Journal of Physics: Conference Series* 1102.1 (2018). ISSN: 17426596. DOI: [10.1088/1742-6596/1102/1/012026](https://doi.org/10.1088/1742-6596/1102/1/012026).
- [41] D Astrain Juangarcia, I Eguinoa, and T Knudsen. “Derating a single wind farm turbine for reducing its wake and fatigue”. In: *Journal of Physics: Conference Series* 1037 (June 2018), p. 032039. DOI: [10.1088/1742-6596/1037/3/032039](https://doi.org/10.1088/1742-6596/1037/3/032039).
- [42] V. Spudić et al. “Cooperative distributed model predictive control for wind farms”. In: *Optimal Control Applications and Methods* 36.3 (2015), pp. 333–352. DOI: <https://doi.org/10.1002/oca.2136>.
- [43] Stefanos Baros and Anuradha M. Annaswamy. “Distributed optimal wind farm control for fatigue load minimization: A consensus approach”. In: *International Journal of Electrical Power and Energy Systems* 112 (2019), pp. 452–459. ISSN: 01420615. DOI: [10.1016/j.ijepes.2019.04.003](https://doi.org/10.1016/j.ijepes.2019.04.003).
- [44] Sara Siniscalchi-Minna et al. “A non-centralized predictive control strategy for wind farm active power control: A wake-based partitioning approach”. In: *Renewable Energy* 150 (2020), pp. 656–669. ISSN: 0960-1481. DOI: <https://doi.org/10.1016/j.renene.2019.12.139>.
- [45] *FLORIS, version 3.2*. Accessed: 2022-08-17. 2022. URL: <https://www.nrel.gov/wind/floris.html>.
- [46] P. Bauweraerts and J. Meyers. “On the Feasibility of Using Large-Eddy Simulations for Real-Time Turbulent-Flow Forecasting in the Atmospheric Boundary Layer.” In: *Boundary-Layer Meteorol* 171 (2019), pp. 213–235. DOI: [10.1007/s10546-019-00428-5](https://doi.org/10.1007/s10546-019-00428-5).
- [47] *OpenFAST*. Accessed: 2022-08-17. 2022. URL: <https://github.com/OpenFAST/openfast>.
- [48] Jason M. Jonkman et al. “Development of FAST.Farm: A New Multi-Physics Engineering Tool for Wind-Farm Design and Analysis”. In: *35th Wind Energy Symposium*. 2017. DOI: [10.2514/6.2017-0454](https://doi.org/10.2514/6.2017-0454). eprint: <https://arc.aiaa.org/doi/pdf/10.2514/6.2017-0454>. URL: <https://arc.aiaa.org/doi/abs/10.2514/6.2017-0454>.
- [49] M. Kretschmer et al. “FAST.Farm load validation for single wake situations at alpha ventus”. In: *Wind Energy Science* 6.5 (2021), pp. 1247–1262. DOI: [10.5194/wes-6-1247-2021](https://doi.org/10.5194/wes-6-1247-2021). URL: <https://wes.copernicus.org/articles/6/1247/2021/>.

- [50] Coen-Jan Smits. “A FAST.Farm and MATLAB/Simulink Interface for Wind Farm Control Design”. PhD thesis. 2023, p. 88. URL: <https://repository.tudelft.nl/islandora/object/uuid:99b76099-cb4f-49e9-aa0a-95c9af01e0ea>.
- [51] Paul Fleming et al. “The SOWFA super-controller: A high-fidelity tool for evaluating wind plant control approaches”. In: *EWEC, Procs. of 3* (2013), pp. 1561–1570.
- [52] *OpenFOAM*. Accessed: 2022-08-17. 2022. URL: <https://openfoam.org/>.
- [53] Matthew J. Churchfield et al. “A numerical study of the effects of atmospheric and wake turbulence on wind turbine dynamics”. In: *Journal of Turbulence* 13 (2012), N14. DOI: [10.1080/14685248.2012.668191](https://doi.org/10.1080/14685248.2012.668191).
- [54] Jean Gonzalez Silva, Riccardo Ferrari, and Jan-Willem van Wingerden. “Wind farm control for wake-loss compensation, thrust balancing and load-limiting of turbines”. In: *Renewable Energy* 203 (2023), pp. 421–433. ISSN: 0960-1481. DOI: <https://doi.org/10.1016/j.renene.2022.11.113>.
- [55] Francisco Díaz-González et al. “Participation of wind power plants in system frequency control: Review of grid code requirements and control methods”. In: *Renewable and Sustainable Energy Reviews* 34 (2014), pp. 551–564. ISSN: 13640321. DOI: [10.1016/j.rser.2014.03.040](https://doi.org/10.1016/j.rser.2014.03.040).
- [56] Müfit Altin et al. “Wind Power Plant Control - An Overview”. In: *9th International Workshop on Large-Scale Integration of Wind Power into Power Systems*. Energy-nautics GmbH. 2010.
- [57] BEIS. *Digest of UK Energy Statistics (DUKES) 2021*. Accessed: 2022-08-17. 2021. URL: <https://gwec.net/global-wind-report-2022/>.
- [58] Alan G. Isemonger. “The evolving design of RTO ancillary service markets”. In: *Energy Policy* 37.1 (2009), pp. 150–157. ISSN: 03014215. DOI: [10.1016/j.enpol.2008.06.033](https://doi.org/10.1016/j.enpol.2008.06.033).
- [59] Carl R. Shapiro et al. “Model-based receding horizon control of wind farms for secondary frequency regulation”. In: *Wind Energy* 20.7 (2017), pp. 1261–1275. DOI: [10.1002/we.2093](https://doi.org/10.1002/we.2093).
- [60] A. S. Ahmadyar and G. Verbič. “Coordinated Operation Strategy of Wind Farms for Frequency Control by Exploring Wake Interaction”. In: *IEEE Trans. on Sustainable Energy* 8.1 (2017), pp. 230–238. DOI: [10.1109/TSTE.2016.2593910](https://doi.org/10.1109/TSTE.2016.2593910).
- [61] S. Boersma et al. “A constrained wind farm controller providing secondary frequency regulation: An LES study”. In: *Renewable Energy* 134 (2019), pp. 639–652. ISSN: 0960-1481. DOI: [10.1016/j.renene.2018.11.031](https://doi.org/10.1016/j.renene.2018.11.031).
- [62] Jiangsheng Zhu et al. “Comparison of loads for wind turbine down-regulation strategies”. In: *2017 11th Asian Control Conference (ASCC)* (2017), pp. 2784–2789. DOI: [10.1109/ASCC.2017.8287618](https://doi.org/10.1109/ASCC.2017.8287618).
- [63] Kwansoo Kim et al. “Design and Validation of Demanded Power Point Tracking Control Algorithm of Wind Turbine”. In: *Int. J. of Precision Engineering and Manufacturing-Green Technology* 5 (July 2018), pp. 387–400. DOI: [10.1007/s40684-018-0041-6](https://doi.org/10.1007/s40684-018-0041-6).

- [64] Daria Madjidian. “Scalable minimum fatigue control of dispatchable wind farms”. In: *Wind Energy* 19.10 (2016), pp. 1933–1944. DOI: <https://doi.org/10.1002/we.1960>. eprint: <https://onlinelibrary.wiley.com/doi/pdf/10.1002/we.1960>. URL: <https://onlinelibrary.wiley.com/doi/abs/10.1002/we.1960>.
- [65] Adam Stock et al. “Distributed Control of Wind Farm Power Set Points to Minimise Fatigue Loads”. In: *2020 American Control Conference (ACC)* (2020), pp. 4843–4848. ISSN: 07431619. DOI: [10.23919/ACC45564.2020.9147732](https://doi.org/10.23919/ACC45564.2020.9147732).
- [66] Phillip W. Richards, D. Todd Griffith, and Dewey H. Hodges. “Smart Loads Management for Damaged Offshore Wind Turbine Blades”. In: *Wind Engineering* 39.4 (2015), pp. 419–436. DOI: [10.1260/0309-524X.39.4.419](https://doi.org/10.1260/0309-524X.39.4.419).
- [67] Paul A. Fleming et al. “Effects of power reserve control on wind turbine structural loading”. In: *Wind Energy* 19.3 (2016), pp. 453–469. DOI: <https://doi.org/10.1002/we.1844>.
- [68] Seth J. Price and Rita B. Figueira. “Corrosion Protection Systems and Fatigue Corrosion in Offshore Wind Structures: Current Status and Future Perspectives”. In: *Coatings* 7.2 (2017). ISSN: 2079-6412. DOI: [10.3390/coatings7020025](https://doi.org/10.3390/coatings7020025).
- [69] D. Todd Griffith et al. “Structural health and prognostics management for the enhancement of offshore wind turbine operations and maintenance strategies”. In: *Wind Energy* 17.11 (2014), pp. 1737–1751. DOI: [10.1002/we.1665](https://doi.org/10.1002/we.1665).
- [70] Jean Gonzalez Silva et al. “A Switching Thrust Tracking Controller for Load Constrained Wind Turbines”. In: *2022 American Control Conference (ACC)*. 2022, pp. 4230–4235. DOI: [10.23919/ACC53348.2022.9867888](https://doi.org/10.23919/ACC53348.2022.9867888).
- [71] Yichao Liu, R. Ferrari, and J.-W. van Wingerden. “Load reduction for wind turbines: an output-constrained, subspace predictive repetitive control approach”. In: *Wind Energy Science* 7.2 (2022), pp. 523–537. DOI: [10.5194/wes-7-523-2022](https://doi.org/10.5194/wes-7-523-2022). URL: <https://wes.copernicus.org/articles/7/523/2022/>.
- [72] Jean Gonzalez Silva et al. “Active Power Control of Waked Wind Farms: Compensation of Turbine Saturation and Thrust Force Balance”. In: *2021 European Control Conference (ECC)*. 2021, pp. 1223–1228. DOI: [10.23919/ECC54610.2021.9655154](https://doi.org/10.23919/ECC54610.2021.9655154).
- [73] Adrian Gambier. “Pitch control of three bladed large wind energy converters— a review”. In: *Energies* 14.23 (2021), pp. 1–24. ISSN: 19961073. DOI: [10.3390/en14238083](https://doi.org/10.3390/en14238083).
- [74] Ameet S. Deshpande and Rhonda R. Peters. “Wind turbine controller design considerations for improved wind farm level curtailment tracking”. In: *2012 IEEE Power and Energy Society General Meeting* (2012), pp. 1–6. DOI: [10.1109/PESGM.2012.6343975](https://doi.org/10.1109/PESGM.2012.6343975).
- [75] NREL. *ROSCO. Version 2.3.0*. Accessed: 2022-08-17. 2021. URL: <https://github.com/NREL/rosco>.

- [76] Lucy Y. Pao and Kathryn E. Johnson. “A tutorial on the dynamics and control of wind turbines and wind farms”. In: *2009 American Control Conference (2009)*, pp. 2076–2089. DOI: [10.1109/ACC.2009.5160195](https://doi.org/10.1109/ACC.2009.5160195).
- [77] J. Jonkman et al. “Definition of a 5MW Reference Wind Turbine for Offshore System Development”. In: *National Renewable Energy Laboratory (NREL)* (Jan. 2009). DOI: [10.2172/947422](https://doi.org/10.2172/947422).
- [78] S P Mulders et al. “Wind turbine control: open-source software for control education, standardization and compilation”. In: *Journal of Physics: Conference Series* 1452 (Jan. 2020), p. 012010. DOI: [10.1088/1742-6596/1452/1/012010](https://doi.org/10.1088/1742-6596/1452/1/012010).
- [79] Jean Gonzalez Silva et al. “Active power control of wind farms: an instantaneous approach on waked conditions”. In: *Journal of Physics: Conference Series* 2265.2 (2022), p. 022056. ISSN: 1742-6588. DOI: [10.1088/1742-6596/2265/2/022056](https://doi.org/10.1088/1742-6596/2265/2/022056). eprint: [2204.05417](https://arxiv.org/abs/2204.05417).
- [80] M. N. Soltani et al. “Estimation of Rotor Effective Wind Speed: A Comparison”. In: *IEEE Trans. on Control Systems Technology* 21.4 (2013), pp. 1155–1167. DOI: [10.1109/TCST.2013.2260751](https://doi.org/10.1109/TCST.2013.2260751).
- [81] Yichao Liu et al. “The Immersion and Invariance Wind Speed Estimator Revisited and New Results”. In: *IEEE Control Systems Letters* 6 (2022), pp. 361–366. DOI: [10.1109/LCSYS.2021.3076040](https://doi.org/10.1109/LCSYS.2021.3076040).
- [82] Yichao Liu et al. “Fault diagnosis of the 10MW Floating Offshore Wind Turbine Benchmark: A mixed model and signal-based approach”. In: *Renewable Energy* 164 (2021), pp. 391–406. ISSN: 0960-1481. DOI: [10.1016/j.renene.2020.06.130](https://doi.org/10.1016/j.renene.2020.06.130).
- [83] Salah Laghrouche, Franck Plestan, and Alain Glumineau. “Higher order sliding mode control based on integral sliding mode”. In: *Automatica* 43.3 (2007), pp. 531–537. DOI: [10.1016/j.automatica.2006.09.017](https://doi.org/10.1016/j.automatica.2006.09.017).
- [84] Data-Driven Control (TU Delft). *SOWFA*. Accessed: 2022-08-17. 2020. URL: <https://github.com/TUdelft-DataDrivenControl/SOWFA>.
- [85] Yu Ting Wu and Fernando Porté-Agel. “Large-Eddy Simulation of Wind-Turbine Wakes: Evaluation of Turbine Parametrisations”. In: *Boundary-Layer Meteorology* 138.3 (2011), pp. 345–366. ISSN: 00068314. DOI: [10.1007/s10546-010-9569-x](https://doi.org/10.1007/s10546-010-9569-x).
- [86] Matthew Churchfield et al. “A Large-Eddy Simulation of Wind-Plant Aerodynamics”. In: *50th AIAA Aerospace Sciences Meeting including the New Horizons Forum and Aerospace Exposition* (Jan. 2012). DOI: [10.2514/6.2012-537](https://doi.org/10.2514/6.2012-537).
- [87] Søren Juhl Andersen et al. *Reference Wind Power Plant*. <https://orbit.dtu.dk/en/publications/reference-wind-power-plant-d103>. Tech. Rep. TotalControl Deliverable D1.3. Accessed: 2022-08-17. 2018.
- [88] Christian Bak et al. “Description of the DTU 10 MW Reference Wind Turbine”. In: *European Wind Energy Conference and Exhibition (EWEC)* (2013), p. 138.
- [89] C Pilong. *PJM Manual 12: Balancing Operations*. 30th. Audubon, PA, USA: PJM, 2013.

- [90] *MLife*. Accessed: 2022-08-17. 2012. URL: <https://www.nrel.gov/wind/nwtc/mlife.html>.
- [91] T. Ashuri et al. “Multidisciplinary design optimization of offshore wind turbines for minimum levelized cost of energy”. In: *Renewable Energy* 68 (2014), pp. 893–905. ISSN: 09601481. DOI: [10.1016/j.renene.2014.02.045](https://doi.org/10.1016/j.renene.2014.02.045). URL: <http://dx.doi.org/10.1016/j.renene.2014.02.045>.
- [92] Jean Gonzalez Silva, Riccardo Ferrari, and Jan-Willem van Wingerden. “Convex Model Predictive Control for Down-regulation Strategies in Wind Turbines”. In: *2022 IEEE 61st Conference on Decision and Control (CDC)*. 2022, pp. 3110–3115. DOI: [10.1109/CDC51059.2022.9993421](https://doi.org/10.1109/CDC51059.2022.9993421).
- [93] Herbert J Sutherland. “On the Fatigue Analysis of Wind Turbines”. In: *Tech. Rep.* (1999). DOI: [10.2172/9460](https://doi.org/10.2172/9460).
- [94] E. A. Bossanyi. “Wind Turbine Control for Load Reduction”. In: *Wind Energy* 6.3 (2003), pp. 229–244. DOI: [10.1002/we.95](https://doi.org/10.1002/we.95).
- [95] Mahmood Mirzaei et al. “Model based active power control of a wind turbine”. In: *2014 American Control Conference*. 2014, pp. 5037–5042. DOI: [10.1109/ACC.2014.6859055](https://doi.org/10.1109/ACC.2014.6859055).
- [96] Christian Santoni et al. “Development of a high fidelity CFD code for wind farm control”. In: *2015 American Control Conference (ACC)*. 2015, pp. 1715–1720. DOI: [10.1109/ACC.2015.7170980](https://doi.org/10.1109/ACC.2015.7170980).
- [97] Emanuele Garone, Stefano Di Cairano, and Ilya Kolmanovsky. “Reference and command governors for systems with constraints: A survey on theory and applications”. In: *Automatica* 75 (2017), pp. 306–328.
- [98] Yichao Liu et al. “The Immersion and Invariance Wind Speed Estimator Revisited and New Results”. In: *IEEE Control Systems Letters* 6 (2022), pp. 361–366. DOI: [10.1109/LCSYS.2021.3076040](https://doi.org/10.1109/LCSYS.2021.3076040).
- [99] Sigurd Skogestad and Ian Postlethwaite. *Multivariable feedback control: Analysis and Design*. Hoboken, NJ, USA: John Wiley, 2005.
- [100] M. Miller et al. *Res-e-next: Next generation of res-e policy instruments*. Tech. Rep. IEA-RETD, 2013.
- [101] Stefano Rivero et al. “Model predictive controllers for reduction of mechanical fatigue in wind farms”. In: *IEEE Transactions on Control Systems Technology* 25.2 (2016), pp. 535–549.
- [102] Tobias Gybel Hovgaard, Stephen Boyd, and John Bagterp Jørgensen. “Model predictive control for wind power gradients”. In: *Wind Energy* 18.6 (2015), pp. 991–1006. DOI: <https://doi.org/10.1002/we.1742>.
- [103] Mohamed L. Shaltout, Mohamed M. Alhneish, and Sayed M. Metwalli. “An Economic Model Predictive Control Approach for Wind Power Smoothing and Tower Load Mitigation”. In: *Journal of Dynamic Systems, Measurement, and Control* 142.6 (Mar. 2020). 061005. ISSN: 0022-0434. DOI: [10.1115/1.4046278](https://doi.org/10.1115/1.4046278).

- [104] Tushar Jain and Joseph Yamé. “Health-aware fault-tolerant receding horizon control of wind turbines”. In: *Control Engineering Practice* 95 (2020), p. 104236. ISSN: 0967-0661. DOI: <https://doi.org/10.1016/j.conengprac.2019.104236>.
- [105] Pieter Tielens and Dirk Van Hertem. “Receding Horizon Control of Wind Power to Provide Frequency Regulation”. In: *IEEE Transactions on Power Systems* 32.4 (2017), pp. 2663–2672. DOI: [10.1109/TPWRS.2016.2626118](https://doi.org/10.1109/TPWRS.2016.2626118).
- [106] Peter Fogh Odgaard, Tobias Gybel Hovgaard, and Rafael Wiesniewski. “Model predictive control for wind turbine power boosting”. In: *2016 European Control Conference (ECC)*. 2016, pp. 1457–1462. DOI: [10.1109/ECC.2016.7810495](https://doi.org/10.1109/ECC.2016.7810495).
- [107] Stephen Boyd and Lieven Vandenbergh. *Convex Optimization*. Cambridge University Press, 2004. DOI: [10.1017/CBO9780511804441](https://doi.org/10.1017/CBO9780511804441).
- [108] Alessandro Magnani and Stephen P. Boyd. “Convex piecewise-linear fitting”. In: *Optimization and Engineering* 10.1 (2009), pp. 1–17. ISSN: 13894420. DOI: [10.1007/s11081-008-9045-3](https://doi.org/10.1007/s11081-008-9045-3).
- [109] Jacob Aho et al. “A tutorial of wind turbine control for supporting grid frequency through active power control”. In: *2012 American Control Conference (ACC)*. 2012, pp. 3120–3131. DOI: [10.1109/ACC.2012.6315180](https://doi.org/10.1109/ACC.2012.6315180).
- [110] Joachim C. Heinz et al. “Vortex-induced vibrations on a modern wind turbine blade”. In: *Wind Energy* 19.11 (2016), pp. 2041–2051.
- [111] P. Novak et al. “Modeling and control of variable-speed wind-turbine drive-system dynamics”. In: *IEEE Control Systems Magazine* 15.4 (1995), pp. 28–38. DOI: [10.1109/37.408463](https://doi.org/10.1109/37.408463).
- [112] Amanullah Choudhry, Maziar Arjomandi, and Richard Kelso. “Methods to control dynamic stall for wind turbine applications”. In: *Renewable Energy* 86 (2016), pp. 26–37. ISSN: 0960-1481.
- [113] ENTSO-E Technical Group HPOPEIPS. *High Penetration of Power Electronic Interfaced Power Sources and the Potential Contribution of Grid Forming Converters*. Accessed: 2023-04-18. 2019. URL: <https://www.entsoe.eu/publications/system-operations-reports/>.
- [114] National Grid Electricity System Operator Limited. *The Grid Code*. Issue 6, Revision 16. Accessed: 2023-04-18. 2021. URL: <https://www.nationalgrideso.com/industry-information/codes/grid-code-gc/grid-code-documents>.
- [115] J. Meyers et al. “Wind farm flow control: prospects and challenges”. In: *Wind Energy Science* 7.6 (2022), pp. 2271–2306. DOI: [10.5194/wes-7-2271-2022](https://doi.org/10.5194/wes-7-2271-2022). URL: <https://wes.copernicus.org/articles/7/2271/2022/>.
- [116] E. Barklund et al. “Energy Management in Autonomous Microgrid Using Stability-Constrained Droop Control of Inverters”. In: *IEEE Transactions on Power Electronics* 23.5 (2008), pp. 2346–2352. DOI: [10.1109/TPEL.2008.2001910](https://doi.org/10.1109/TPEL.2008.2001910).

- [117] Yuan-Kang Wu et al. “Frequency Regulation at a Wind Farm Using Time-Varying Inertia and Droop Controls”. In: *IEEE Transactions on Industry Applications* 55.1 (2019), pp. 213–224. DOI: [10.1109/TIA.2018.2868644](https://doi.org/10.1109/TIA.2018.2868644).
- [118] Dylan Wald et al. “Integration of distributed controllers: Power reference tracking through charging station and building coordination”. In: *Applied Energy* 314 (2022), p. 118753. ISSN: 0306-2619. DOI: <https://doi.org/10.1016/j.apenergy.2022.118753>.
- [119] Jennifer Annoni et al. “Analysis of axial-induction-based wind plant control using an engineering and a high-order wind plant model”. In: *Wind Energy* 19.6 (2016), pp. 1135–1150. DOI: <https://doi.org/10.1002/we.1891>.
- [120] Simone Tamaro and Carlo L. Bottasso. “A New Wind Farm Active Power Control Strategy to Boost Tracking Margins in High-demand Scenarios”. In: *2023 American Control Conference (ACC)*. 2023, pp. 192–197. DOI: [10.23919/ACC55779.2023.10156275](https://doi.org/10.23919/ACC55779.2023.10156275).
- [121] A. Croce, S. Cacciola, and F. Isella. “Combining wake redirection and derating strategies in a load-constrained wind farm power maximization”. In: *Wind Energy Science* 9.5 (2024), pp. 1211–1227. DOI: [10.5194/wes-9-1211-2024](https://doi.org/10.5194/wes-9-1211-2024). URL: <https://wes.copernicus.org/articles/9/1211/2024/>.
- [122] Filiberto Fele, Jose M. Maestre, and Eduardo F. Camacho. “Coalitional Control: Cooperative Game Theory and Control”. In: *IEEE Control Systems Magazine* 37.1 (2017), pp. 53–69. DOI: [10.1109/MCS.2016.2621465](https://doi.org/10.1109/MCS.2016.2621465).
- [123] Vitor N. Coelho et al. “Multi-agent systems applied for energy systems integration: State-of-the-art applications and trends in microgrids”. In: *Applied Energy* 187 (2017), pp. 820–832. ISSN: 0306-2619. DOI: <https://doi.org/10.1016/j.apenergy.2016.10.056>.
- [124] Mojtaba Jabbari Ghadi et al. “From active distribution systems to decentralized microgrids: A review on regulations and planning approaches based on operational factors”. In: *Applied Energy* 253 (2019), p. 113543. ISSN: 0306-2619. DOI: <https://doi.org/10.1016/j.apenergy.2019.113543>.
- [125] Alejandro D. Dominguez-Garcia and Christoforos N. Hadjicostis. “Coordination and Control of Distributed Energy Resources for Provision of Ancillary Services”. In: *2010 First IEEE International Conference on Smart Grid Communications*. 2010, pp. 537–542. DOI: [10.1109/SMARTGRID.2010.5621991](https://doi.org/10.1109/SMARTGRID.2010.5621991).
- [126] Hao Liang et al. “Stability Enhancement of Decentralized Inverter Control Through Wireless Communications in Microgrids”. In: *IEEE Transactions on Smart Grid* 4.1 (2013), pp. 321–331. DOI: [10.1109/TSG.2012.2226064](https://doi.org/10.1109/TSG.2012.2226064).
- [127] Florian Dörfler, John W. Simpson-Porco, and Francesco Bullo. “Breaking the Hierarchy: Distributed Control and Economic Optimality in Microgrids”. In: *IEEE Transactions on Control of Network Systems* 3.3 (2016), pp. 241–253. DOI: [10.1109/TCNS.2015.2459391](https://doi.org/10.1109/TCNS.2015.2459391).

- [128] Christopher J. Bay et al. “Distributed model predictive control for coordinated, grid-interactive buildings”. In: *Applied Energy* 312 (2022), p. 118612. ISSN: 0306-2619. DOI: <https://doi.org/10.1016/j.apenergy.2022.118612>.
- [129] Florian Dörfler et al. “Sparsity-Promoting Optimal Wide-Area Control of Power Networks”. In: *IEEE Transactions on Power Systems* 29.5 (2014), pp. 2281–2291. DOI: [10.1109/TPWRS.2014.2304465](https://doi.org/10.1109/TPWRS.2014.2304465).
- [130] Yaser E. Hawas and Hani S. Mahmassani. “Comparative Analysis of Robustness of Centralized and Distributed Network Route Control Systems in Incident Situations”. In: *Transportation Research Record* 1537.1 (1996), pp. 83–90. DOI: [10.1177/0361198196153700112](https://doi.org/10.1177/0361198196153700112).
- [131] Twan Keijzer and Riccardo M.G. Ferrari. “Threshold design for fault detection with first order sliding mode observers”. In: *Automatica* 146 (2022), p. 110600. ISSN: 0005-1098. DOI: <https://doi.org/10.1016/j.automatica.2022.110600>.
- [132] Jason R. Marden, Shalom D. Ruben, and Lucy Y. Pao. “A Model-Free Approach to Wind Farm Control Using Game Theoretic Methods”. In: *IEEE Transactions on Control Systems Technology* 21.4 (2013), pp. 1207–1214. DOI: [10.1109/TCST.2013.2257780](https://doi.org/10.1109/TCST.2013.2257780).
- [133] P. M. O. Gebraad and J. W. van Wingerden. “Maximum power-point tracking control for wind farms”. In: *Wind Energy* 18.3 (2015), pp. 429–447. DOI: <https://doi.org/10.1002/we.1706>.
- [134] Jinkyoo Park and Kincho H. Law. “A data-driven, cooperative wind farm control to maximize the total power production”. In: *Applied Energy* 165 (2016), pp. 151–165. ISSN: 0306-2619. DOI: <https://doi.org/10.1016/j.apenergy.2015.11.064>.
- [135] Zhen Dong et al. “Distributed neural network enhanced power generation strategy of large-scale wind power plant for power expansion”. In: *Applied Energy* 303 (2021), p. 117622. ISSN: 0306-2619. DOI: <https://doi.org/10.1016/j.apenergy.2021.117622>.
- [136] Jennifer Annoni et al. “A Framework for Autonomous Wind Farms: wind Direction Consensus”. In: *Wind Energy Science Discussions* (Oct. 2018), pp. 1–17. DOI: [10.5194/wes-2018-60](https://doi.org/10.5194/wes-2018-60).
- [137] Federico Bernardoni et al. “Identification of wind turbine clusters for effective real time yaw control optimization”. In: *Journal of Renewable and Sustainable Energy* 13.4 (July 2021). ISSN: 1941-7012. DOI: [10.1063/5.0036640](https://doi.org/10.1063/5.0036640). URL: <https://doi.org/10.1063/5.0036640>.
- [138] Hamed M. Al-Rahmani and Gene F. Franklin. “Multirate control: A new approach”. In: *Automatica* 28.1 (1992), pp. 35–44. ISSN: 0005-1098. DOI: [https://doi.org/10.1016/0005-1098\(92\)90005-Z](https://doi.org/10.1016/0005-1098(92)90005-Z).
- [139] M. Tomizuka. “Multi-rate control for motion control applications”. In: *The 8th IEEE International Workshop on Advanced Motion Control, 2004. AMC '04*. 2004, pp. 21–29. DOI: [10.1109/AMC.2004.1297635](https://doi.org/10.1109/AMC.2004.1297635).

- [140] Reza Olfati-Saber, J. Alex Fax, and Richard M. Murray. “Consensus and Cooperation in Networked Multi-Agent Systems”. In: *Proceedings of the IEEE* 95.1 (2007), pp. 215–233. DOI: [10.1109/JPROC.2006.887293](https://doi.org/10.1109/JPROC.2006.887293).
- [141] A. Jadbabaie, Jie Lin, and A.S. Morse. “Coordination of groups of mobile autonomous agents using nearest neighbor rules”. In: *IEEE Transactions on Automatic Control* 48.6 (2003), pp. 988–1001. DOI: [10.1109/TAC.2003.812781](https://doi.org/10.1109/TAC.2003.812781).
- [142] Prodromos Daoutidis, Masoud Soroush, and Costas Kravaris. “Feedforward/feedback control of multivariable nonlinear processes”. In: *AIChE Journal* 36.10 (1990), pp. 1471–1484. DOI: <https://doi.org/10.1002/aic.690361003>.
- [143] Jose Alvarez-Ramirez, America Morales, and Ilse Cervantes. “Robust proportional-integral control”. In: *Industrial & engineering chemistry research* 37.12 (1998), pp. 4740–4747.
- [144] Zhong-Ping Jiang and I. Marcel. “Robust nonlinear integral control”. In: *IEEE Transactions on Automatic Control* 46.8 (2001), pp. 1336–1342. DOI: [10.1109/9.940947](https://doi.org/10.1109/9.940947).
- [145] Wei Ren et al. “Experimental Validation of Consensus Algorithms for Multivehicle Cooperative Control”. In: *IEEE Transactions on Control Systems Technology* 16.4 (2008), pp. 745–752. DOI: [10.1109/TCST.2007.912239](https://doi.org/10.1109/TCST.2007.912239).
- [146] Lin Xiao and Stephen Boyd. “Fast linear iterations for distributed averaging”. In: *Systems & Control Letters* 53.1 (2004), pp. 65–78. ISSN: 0167-6911. DOI: <https://doi.org/10.1016/j.sysconle.2004.02.022>.
- [147] E.I. Jury. *Theory and Applications of the Z-Transform Method*. New York, 1964.
- [148] E. I. Jury. “A Simplified Stability Criterion for Linear Discrete Systems”. In: *Proceedings of the IRE* 50.6 (1962), pp. 1493–1500. DOI: [10.1109/JRPROC.1962.288193](https://doi.org/10.1109/JRPROC.1962.288193).
- [149] Martin Andreasson et al. “Distributed Control of Networked Dynamical Systems: Static Feedback, Integral Action and Consensus”. In: *IEEE Transactions on Automatic Control* 59.7 (2014), pp. 1750–1764. DOI: [10.1109/TAC.2014.2309281](https://doi.org/10.1109/TAC.2014.2309281).
- [150] J.C. Doyle, B.A. Francis, and A. Tannenbaum. *Feedback Control Theory*. Macmillan Publishing Company, 1992. ISBN: 9780023300110.
- [151] P.J. Antsaklis and A.N. Michel. *Linear Systems*. Birkhäuser Boston, 2006. ISBN: 9780817644352.
- [152] C. B. Moler and G. W. Stewart. “An Algorithm for Generalized Matrix Eigenvalue Problems”. In: *SIAM Journal on Numerical Analysis* 10.2 (1973), pp. 241–256. ISSN: 00361429. URL: <http://www.jstor.org/stable/2156353> (visited on 08/26/2024).
- [153] Jean Gonzalez Silva et al. “Wind Tunnel Testing of Wind Turbine and Wind Farm Control Strategies for Active Power Regulation”. In: *Journal of Renewable and Sustainable Energy* (2024). DOI: [10.1063/5.0215493](https://doi.org/10.1063/5.0215493).

- [154] WindEurope. *Future system needs and the role of grid-forming converters*. 2019. URL: <https://windeurope.org/policy/position-papers/future-system-needs-and-role-of-grid-forming-converters/> (visited on 09/12/2023).
- [155] J.M. Morales et al. *Integrating Renewables in Electricity Markets: Operational Problems*. International Series in Operations Research & Management Science. Springer US, 2013. ISBN: 9781461494119. URL: <https://books.google.nl/books?id=QF24BAAAQBAJ>.
- [156] E.D. Castronuovo and J.A.P. Lopes. “On the optimization of the daily operation of a wind-hydro power plant”. In: *IEEE Transactions on Power Systems* 19.3 (2004), pp. 1599–1606. DOI: [10.1109/TPWRS.2004.831707](https://doi.org/10.1109/TPWRS.2004.831707).
- [157] Lori Bird et al. “Wind and solar energy curtailment: A review of international experience”. In: *Renewable and Sustainable Energy Reviews* 65 (2016), pp. 577–586. ISSN: 1364-0321. DOI: <https://doi.org/10.1016/j.rser.2016.06.082>. URL: <https://www.sciencedirect.com/science/article/pii/S1364032116303161>.
- [158] J.D. Jenkins et al. “The benefits of nuclear flexibility in power system operations with renewable energy”. In: *Applied Energy* 222 (2018), pp. 872–884. ISSN: 0306-2619. DOI: <https://doi.org/10.1016/j.apenergy.2018.03.002>. URL: <https://www.sciencedirect.com/science/article/pii/S0306261918303180>.
- [159] Jean Gonzalez Silva et al. “UKF-based Wind Estimation and Sub-optimal Turbine Control under Waked Conditions”. In: *IFAC-PapersOnLine* (2023).
- [160] Filippo Campagnolo et al. “Wind tunnel testing of a closed-loop wake deflection controller for wind farm power maximization”. In: *Journal of Physics: Conference Series* 753.3 (2016), p. 032006. DOI: [10.1088/1742-6596/753/3/032006](https://doi.org/10.1088/1742-6596/753/3/032006). URL: <https://dx.doi.org/10.1088/1742-6596/753/3/032006>.
- [161] V Petrović et al. “Wind tunnel validation of a closed loop active power control for wind farms”. In: *Journal of Physics: Conference Series* 1037.3 (2018), p. 032020. DOI: [10.1088/1742-6596/1037/3/032020](https://doi.org/10.1088/1742-6596/1037/3/032020). URL: <https://dx.doi.org/10.1088/1742-6596/1037/3/032020>.
- [162] Flavio Noca et al. “Wind and Weather Facility for Testing Free-Flying Drones”. In: *AIAA Aviation 2019 Forum* (2019). DOI: [10.2514/6.2019-2861](https://doi.org/10.2514/6.2019-2861). eprint: <https://arc.aiaa.org/doi/pdf/10.2514/6.2019-2861>. URL: <https://arc.aiaa.org/doi/abs/10.2514/6.2019-2861>.
- [163] J Schottler et al. “Design and implementation of a controllable model wind turbine for experimental studies”. In: *Journal of Physics: Conference Series* 753.7 (2016), p. 072030. DOI: [10.1088/1742-6596/753/7/072030](https://doi.org/10.1088/1742-6596/753/7/072030). URL: <https://dx.doi.org/10.1088/1742-6596/753/7/072030>.

- [164] Per-Åge Krogstad and Pål Egil Eriksen. ““Blind test” calculations of the performance and wake development for a model wind turbine”. In: *Renewable Energy* 50 (2013), pp. 325–333. ISSN: 0960-1481. DOI: <https://doi.org/10.1016/j.renene.2012.06.044>. URL: <https://www.sciencedirect.com/science/article/pii/S0960148112003953>.
- [165] AAW van Vondelen et al. “Synchronized Dynamic Induction Control: An Experimental Investigation”. In: *Journal of Physics: Conference Series* 2767.3 (2024), p. 032027. DOI: [10.1088/1742-6596/2767/3/032027](https://doi.org/10.1088/1742-6596/2767/3/032027). URL: <https://dx.doi.org/10.1088/1742-6596/2767/3/032027>.
- [166] S. J. Julier, J. K. Uhlmann, and H. F. Durrant-Whyte. “A new approach for filtering nonlinear systems”. In: *American Control Conf.* 1995, 1628–1632 vol.3.
- [167] ASTM E1049-85. *Standard Practices for Cycle Counting in Fatigue Analysis*. 2017.
- [168] Richard Budynas and Keith Nisbett. *Shigley’s Mechanical Engineering Design, 11th edition*. McGraw-Hill Higher Education, 2020. ISBN: 9781259986246.

CURRICULUM VITÆ

Jean GONZALEZ SILVA



02-04-1993 Born in Macaé, Brazil.

EDUCATION

2012–2016 Bachelor of Engineering, Mechanical Engineering
Universidade Federal do Rio de Janeiro

2014–2015 Exchange Bachelor Student, Mechanical Engineering
The University of Texas at Austin

2017–2019 Master in Mechatronic Systems
Universidade de Brasília

2020–2024 Doctoral degree in Mechanical Engineering
Delft University of Technology
Thesis: Wind farm control strategies for structural load
management and energy efficiency
Promotors: Prof. dr. R. Ferrari and Prof. dr. J.-W. van Wingerden

EXPERIENCE

2018–2019 Mechanical Designer
Indústrias Rossi Eletromecânica
Fabbrica Automatismi Apertura Cancelli (FAAC) Group

2024 Mechanical Equipment Engineer
Petróleo Brasileiro S.A. (Petrobras)

LIST OF PUBLICATIONS

JOURNAL PAPERS

- **J. G. Silva**, T. Keijzer, A. J. Gallo, R. Ferrari, and J.-W. van Wingerden, *Multi-rate consensus-based distributed control for large-scale wind farms*, IEEE Transactions on Control System Technology (2025).
- **J. G. Silva**, D. van der Hoek, R. Ferrari, and J.-W. van Wingerden, *Wind Tunnel Testing of Wind Turbine and Wind Farm Control Strategies for Active Power Regulation*, *Journal of Renewable and Sustainable Energy* **16**, 053302 (2024).
- **J. G. Silva**, R. Ferrari, and J.-W. van Wingerden, *Wind farm control for wake-loss compensation, thrust balancing and load-limiting of turbines*, *Renewable Energy* **203**, 421-433 (2023).

BOOK CHAPTER

- **J. G. Silva**, R. Ferrari, and J.-W. van Wingerden, 'Towards control of large-scale wind farms: a multi-rate distributed control approach', in C. Ocampo-Martinez and N. Quijano *Towards Energy Systems Integration for Multi-Energy Systems: From Operation to Planing in the Green Energy Context*, Springer 265-298 (2024).

CONFERENCE PAPERS

- **J. G. Silva**, R. Ferrari, and J.-W. van Wingerden, *Convex Model Predictive Control for Down-regulation Strategies in Wind Turbines*, *IEEE 61st Conference on Decision and Control (CDC)* 3110-3115 (2023).
- C.-J. Smits, **J. G. Silva**, V. Chabaud, and R. Ferrari, *A FAST.Farm and MATLAB/Simulink interface for wind farm control design*, *Journal of Physics: Conference Series* **2626**, 012069 (2023).
- **J. G. Silva**, Y. Liu, R. Ferrari, and J.-W. van Wingerden, *UKF-based Wind Estimation and Sub-optimal Turbine Control under Waked Conditions*, *IFAC-PapersOnLine: 22nd IFAC World Congress* **56**, 2, 7662-7667 (2023).
- **J. G. Silva**, D. van der Hoek, S. P. Mulders, R. Ferrari, and J.-W. van Wingerden, *A Switching Thrust Tracking Controller for Load Constrained Wind Turbines*, *American Control Conference (ACC)* 4230-4235 (2022).
- **J. G. Silva**, B. M. Doekemeijer, R. Ferrari, and J.-W. van Wingerden, *Active power control of wind farms: an instantaneous approach on waked conditions*, *Journal of Physics: Conference Series* **2265**, 022056 (2022).

- D. Ratering, , W. B. Kleijn, **J. G. Silva**, and R. Ferrari, *Wave-Domain Approach for Cancelling Noise Entering Open Windows*, [IEEE International Conference on Acoustics, Speech and Signal Processing \(ICASSP\) 9110915 \(2022\)](#).
- **J. G. Silva**, B. M. Doekemeijer, R. Ferrari, and J.-W. van Wingerden, *Active Power Control of Waked Wind Farms: Compensation of Turbine Saturation and Thrust Force Balance*, [European Control Conference \(ECC\) 1223-1228 \(2021\)](#).